Republic of Iraq
Ministry of Higher Education & Scientific Research
University of Babylon
College of Science for Women
Laser Physics Department

Synthesis and Characterization of $Ga_2O_{3\ (1-X)}\ CdO_{(X)}$ Nanostructure by Pulse Laser Deposition for Sensing Applications

A Thesis
Submitted to the Council of the College of Sciences for Women,
University of Babylon
In Partial Fulfillment of the Requirements for the Degree of
Doctor of Philosophy in Laser Physics and its Applications
By

Aqeel Ibrahim Faris
B.Sc. Physics, University of Babylon (2009)
M.Sc. Physics, University of Babylon (2017)

Supervised by
Assist. Professor Jinan Ali Abd, Ph.D.
University of Babylon
College of Science for Women
Laser Physics Department
Professor Faisal Ali Mustafa, Ph.D.
Hilla University College
Department of Radiology

2021 A.D. **1442 A.H**

بِسْمِ اللّهِ الرَّحْمنِ الرَّحِيمِ

﴿ يَوْمَ تَرَى الْمُؤْمِنِينَ وَالْمُؤْمِنَاتِ يَسْعَى نُورُهُم بَيْنَ أَيْدِيهِمْ وَبِأَيْمَانِهِم بُشْرَاكُمُ الْيَوْمَ جَنَّاتٌ تَجْرِي مِن تَحْتِهَا الْأَنْهَارُ خَالِدِينَ فِيهَا ذَلِكَ هُوَ الْفَوْزُ الْعَظِيمُ ﴾

صَدَق الله العليّ العَظيم

سورة الحديد الآية(12)

Supervisor's certificate

We certify that this thesis entitled **"Synthesis and Characterization of $Ga_2O_{3\ (1-X)}$ $CdO_{(X)}$ Nanostructure by Pulse Laser Deposition for Sensing Applications "** was prepared by the student **(Aqeel Ibrahim Faris)** under our supervision at the department of Laser physics, College of Science for Women, University of Babylon, as a partial fulfillment of the requirements of the degree of Doctorate of philosophy in laser physics and its applications.

Signature:

Name: Jinan Ali Abd

Title: **Assistant Professor**

(Supervisor)

Date: / / 2021

Signature:

Name: Faisal Ali Mustafa

Title: **Professor**

(Supervisor)

Date: / / 2021

Head of the Department Certificate

In view of the available recommendations, I forward this dissertation for debate by the examining committee.

Signature:

Name: Jinan Ali Abd

Title: Assistant Professor

(Head of Laser Physics Department)

Examination Committee Certification

We certify that after reading this thesis, entitled: "**Synthesis and Characterization of Ga_2O_3 $_{(1-X)}$ $CdO_{(X)}$ Nanostructure by Pulse Laser Deposition for Sensing Applications**", and as committee, examined the student "**Aqeel Ibrahim Faris**" its contents and that in our opinion it meets the standards of a thesis for the Degree of Philosophy of Doctorate in Laser Physics and its Application.

Signature:
Name:**Dr. Aliyah Abdul Mohsin Shihab**
Title: Professor
Date: / / 2021
(Chairman)

Signature:
Name: **Dr. Sahib Neamh Abdulwahid**
Title: Professor
Date: / / 2021
(Member)

Signature:
Name: **Dr. Qussay Mohammed Salman**
Title: Assistant Professor
Date: / / 2021
(Member)

Signature:
Name: **Dr. Zainab Jassim Shanan**
Title:
Date: / / 2021
(Member)

Signature:
Name: **Dr. AMER K. H. AL-NAFIEY**
Title: Assistant Professor
Date: / / 2021
(Member)

Signature:
Name: **Dr. Jinan Ali Abd**
Title: Assistant Professor
Date: / / 2021
(Member/Supervisor)

Signature:
Name: **Dr. Faisal Ali Mustafa**
Title: Professor
Date: / / 2021
(Member/ Supervisor)

Approved by the Dean of College

Signature:
Name: **Dr. Faez Ali Rashid AL-Maamori**
Title: Professor
Address: Dean of the College of Science for Women.
Date: / /2021

Dedication

To

My Family

Acknowledgement

First of all, Praise is to Allah, mercy and peace are to the Prophet Mohammed and his relatives and companions.

I would like to sincerely thank my supervisors, Assistant Professor Dr. Jinan Ali Abd and Prof. Dr. Faisal Ali Mustafa, for their direction, assistance, guidance, and their recommendations and suggestions for this work.

I am deeply indebted to the Head of the Laser Physics Department, the staff and the dean of the College of Science for Women for the support that provided.

I wish to express my thanks to all my friends, especially the (Ph.D) group, for their kind assistance and support during our course studies and thesis work.

Aqeel

Abstract

The compounds Ga_2O_3, CdO and $CdGa_2O_4$ thin films were prepared using a pulsed laser deposition technique, it is a method that has proven its efficiency in preparing thin films. Nd-YAG laser were used with laser energies 500 mJ, pulses number (1000pulses), frequency (6Hz), wavelength (1064nm) and pressure ($\geq 10^{-4}$mbar) to depositionon onto substrates quartz.

X-ray diffraction(XRD) was used to analyze the crystal structure of the produced films and the results showed that all the prepared films are polycrystalline in the cubic phase for CdO and $CdGa_2O_4$ and monoclinic for Ga_2O_3. There is a decrease in the crystallite size of the nanoparticles, decrease in the strain and the dislocation density when increasing CdO concentration. This is an indication of improved properties of the prepared films .The surface topography of the prepared films using atomic force microscopy (AFM) has been studied. It has been observed that the grain size decreases with increasing CdO concentration. There is also an decreases in the surface roughness rate and the square root rate (RMS) by increasing the CdO concentration . As for the results of the Field Emission Scan Electronic Microscope (FESEM) and energy dispersion of X-ray spectroscopy (EDX), the images show the grain shape are semi spherical for all films. While the films of 0% ,25% wt and 50%wt are a semi spherical shape with a hole with the increase in the concentration of cadmium oxide, it can be observed that the holes in the grains disappear and it clusters to make the grains more dense.

The optical properties of prepared films with thickness (205± 5) nm were studied using optical transmittance measurements in the spectral region (200-900) nm. It was noted that direct allowed transition and the increase in CdO concentration leads to a decrease in the optical energy gap of the Ga_2O_3

Abstract

$_{(1-X)}CdO_{(X)}$ films from 4.65eV to 4.19eV. The optical constants such as refractive index, extinction coefficient and dielectric constant have been calculated for all prepared films.

The electrical properties include D.C conductivity and Hall effect were studied. The results show that the prepared films were p-type for Ga_2O_3 and 25%wt it becomes n-type when the CdO is increased. It is found that the resistance and the resistivity increase with the increase of the temperature for the films 0%wt and 25%wt and vice versa for the other films also the conductivity decreases with increasing temperature for 0%wt and 25%wt films and vice versa for other films.

From the sensing properties measurements of thin films for NO_2 and NH_3 gases showed that all samples are working at room operating temperature when CdO is added to Ga_2O_3.The maximum sensitivity of tested gas sensor to 60 ppm of NO_2 about 61.7% at around 300°C for 75%wt composite , while the 50%wt composite have 0.8% lowest sensitivity to NO_2. When NH_3 is used as the probing gas, the maximum sensitivity of samples gas sensor to 200 ppm of NH_3 can reach 48.2% for pure Ga_2O_3, and the optimum sensing temperature of composite sensor is at around (200 - 300) °C

As well the response time and recovery time decrease to increase the temperature, in other words, the fast response speed for NO_2 gas (10.8 s) for 75% wt sample at 250^oC and (9s) for pure Ga_2O_3 at 250^oC for NH_3 gas.

TABLE OF CONTENTS

Table of Contents

Table of Contents

Table of Contents

Table of Contents

List of Symbols

Symbol	Physical meaning
A	Absorptance
α	Absorption Coefficient
D	Average Crystallite Size
k_B	Boltzmann's Constant
n_e	Carrier Concentration
n*	Complex Refractive Index
E_c	Conduction Band energy
J	Current density
ρ	Density of material
δ	Dislocation Density
V_d	Drift velocity
m*	Effective mass of the carrier
G_g	Electrical conductance of the film in presence of a gas
G_a	Electrical conductance of the film in the air
σ	Electrical Conductivity
E_e	Electrical Field
ℓ	Electrode spacing distance
q	Electric charge
μ_ν	Electron Mobility
ν	Frequency
R_H	Hall Coefficient
E_H	Hall Electric Field

List of Symbols

V_H	Hall Voltage
μ_H	Hole Mobility
Io	Incident Intensity of Light
T0	Initial temperature
B	Magnetic Field
T_c	Mean free time (the collision time)
ε'	Micro strain
hkl	Miller indices
σ_o	Minimum Electrical Conductivity
μ	Mobility of the carriers
E_g	Optical band gap
h	Plank Constant
τ_{las}	Pulse laser time
N	Refractive Index
R_g	Resistance of the film in presence of a gas
R_i	Resistance of the film in the air
I_a	Sample current measured at ambient environment
I_g	Sample current measured under the test gas
S	Sensitivity
C_p	Specific Heat Capacity
T_{vap}	Temperature of evaporation
T_s	Temperature of the substrate
R_a	The actual deposition rate
R_e	The deposition rate of the thin film
Ɓ	The full width at half maximum
D	The Inter Planar Distance

List of Symbols

X	The laser spot dimension
τ_{res}	The response time
D_m	The supersaturation of laser plasma
L	Thermal diffusion depth
N	Thermal diffusivity of the material
T	Transmission
I_T	Transmitting rays
EV	Valence Band energy
I^*_{vap}	Vaporize the material
λ	Wavelength

List of Abbreviations

Symbol	Physical meaning
AFM	Atomic Force Microscope
CL	Cathodoluminescence
CBD	Chemical Bath Deposition
CSP	Chemical Spray Pyrolysis
C.B	Conduction Band
CPS	Counts per second
CCP	Cubic Close Packed Structure
SGD	Deposition using Sol-Gel
DSC	Differential Scanning Calorimetry
EL	Electroluminescent
EDX	Energy-dispersive X-ray spectroscopy
FCC	Faced Centered Cubic
FET	Field effect transistors
FESEM	Field Emission Scanning Electron Microscope
FWHM	Full Width at Half Maximum
HCP	Hexagonal Close Packed Structure
IR	Infrared
ICDD	International Center of Diffraction Data
LED	Light Emitting Diode
LPG	liquid petroleum gas
MOCVD	Metal organic chemical vapor deposition
MEMS	Micro-Electro-Mechanical Systems
NS	Nanostructures
NWs	Nanowires
Nd:YAG	Neodymium-doped yttrium aluminium garnet
1D	One-dimensional

List of Abbreviation

PPM	Parts per million
PL	Photo Luminescence spectroscopy
PCD	Photochemical Deposition
PVD	Physical vapor deposition
PLD	Pulse Laser Deposition
RT	Room temperature
R.M.S.	Root Mean Square
SEM	Scanning Electron Microscope
SIS	Semiconductor - Insulator - Semiconductor
SPT	Spray Pyrolysis Technique
FWHM	The full width at half maximum
TF	Thin film
TCOs	Transparent Conducting Oxides
TMA	Trimethylamine
2-D	Two-dimensional
UV	Ultra Violet Spectrum
V.B	Valence Band
VIS	Visible Spectrum
XRD	X-Ray Diffraction

List of Tables

List of Figures

List of Figures

List of Figures

List of Figures

List of Figures

Chapter One

General Introduction

1.1 Thin Film

The research material is a thin film (TF) which is an important subject in solid-state physics has contributed to TF technology a major contribution to the semiconductors study and many of the chemical and physical properties have been identified in order to determine the use in a wide range applications. The term thin film is a description of one or many layers of atoms that are currently less than one micro, which can be defined as "thin material layers ranging from fractions of a nanometer (monolayer) to less than about ($1\mu m$) one micrometers in thickness.". A suitable difference between thick film and thin film deposition should be based in mind. TF deposition include deposition of individual atoms, while the latter concerned with the particles deposition, as an example, painting is thick film method [1, 2]. Normally, one classifies TF (arbitrarily) into: thin films (D < 1 micrometer, D : film thickness) or thick films (D > 1 micrometer) [3].

The importance of thin film coating swells lead to a breakthrough in microelectronics, nanotechnology and optics. Thin film manufacturing was created mainly to meet the requirements of the integrated circuit industry. The thin films production for purposes of devices have been developed for more than 50 years ago. TF as a 2-D system are of great importance of solving many real-world problems, their material costs very small compared to the corresponding bulk materials and when it comes to surface processes, they have the same purpose. Thus, knowledge and identification of the nature, new properties and functions of TF can be used to improvement of new technologies such as solar cells, and other optical applications,

electronic engineering etc. Thin films as compared with bulk material, thin films physical properties on substrate may radically different, especially depending on improvement of structure and morphology [4]. The layer of film deposits onto a selection of substrates based on the nature of the scientific need or the study. Such substrates could be silicon wafers ,glass, quartz and aluminum [5]. Applications involve wide range electronic packaging manufacturing, integrated circuits, gas sensor, optical films and devices also decorative coatings and protective. At nowadays, the enormous opportunities and quickly changing needs for thin film and it devices are opening up new horizons for the improvement of new processes, technologies and materials [6-8]. The development of high performance solid state chemical sensors is currently of paramount importance in many advanced technological fields. Many research has shown that the characteristic of solid gas sensors is the reverse reaction of gas with the surface of solid state material. The deposition of thick film usually does not give a great deal of control over the quality of films and is relatively inexpensive for the deposition of TF. Behave of thin films differently of bulk materials from the same chemical composition in many ways. As example, thin films are sensitive to surface properties while bulk materials generally are not. Thin films are also relatively more sensitive for thermo -mechanical stresses. The TF technology itself is today a separate a division of materials science and has evolved into a range of technologies used to manufacture many products[9]. As mentioned above the thin films have enormous importance today duo to its application industries, these film has been used in different fields as rectifiers, ordinary and thermally, anti-reflected and reflected coating, photograph, integrated circuits, and optical

communications such as light emitting diodes, detectors, solar cells, and of gas sensor,.... etc.[10].

1.2 Semiconductor gas sensors

A Sensor is device that changes its output in response to a specified input stimulus [11] . This stimulus can be a physical stimulus as pressure and temperature or a concentration of a specific chemical or biochemical material. The signal which output from sensor is usually an electrical signal relative to the input variable. All three phases of material sensors can be used, although liquid and gas sensors are the most popular[12] .

Gas-sensing devices have gained importance as interest in areas such as pollution management, hazardous gas detection, and combustion monitoring processes has grown .Because of their mobility and simplicity, solid state gas sensors based on thin metal oxide films have become popular. A metal oxide layer over an insulating substrate is generally used, together with two metal electrodes. When a change in the surrounding environment occurs, these films indicate a change in electrical conductivity, which is the basis for gas detection[13]. The conductivity change can be due to either direct transmission of electrons from the adsorbed gas to the oxide semiconductor [14] or because of an interaction of the adsorbed gas with previously chemisorbed surface oxygen [15, 16]. The response time and the sensitivity of these devices are found depend strongly on the conditions of film deposition [17].

In the last years, a number of researches have been focused on improving gas sensors based on nanostructures and/or nanomaterials. Metal oxides are the most common sensor material and a variety of researches have been carried out to enhance the response of these gas sensors

[18-21].Both the two types of semiconductor (p-type) and (n-type) are used on gas sensors but n-type is preferred on the p-type because it gives a resistance change from the highest value to the lowest value in the case of gas while the p-type the change of resistance is vice versa (from the lowest value to the highest value). The type-n crystalline structure such as SnO_2 , Ga_2O_3 and CdO contains a small increase of electrons[22].

The mechanism causing the change in resistance is thought to be due to reactions at the boundaries of grain. In many cases, the sensitivity can be shown to improve with the size of smaller grains for higher grain-boundary density. A few models were suggested to change resistance when exposed to gas elements. Here are the two most common theories, it will be mentioned. The first theory is related to conduction across boundaries of grain. These grain boundaries are rich in oxygen, and potential barriers are formed that surrounding vectors and block the flow of current through them figure (1.1). The gas to be detected has the ability to neutralize the pre-absorbed oxygen, reduce the barrier, and the resistance will be reduced.

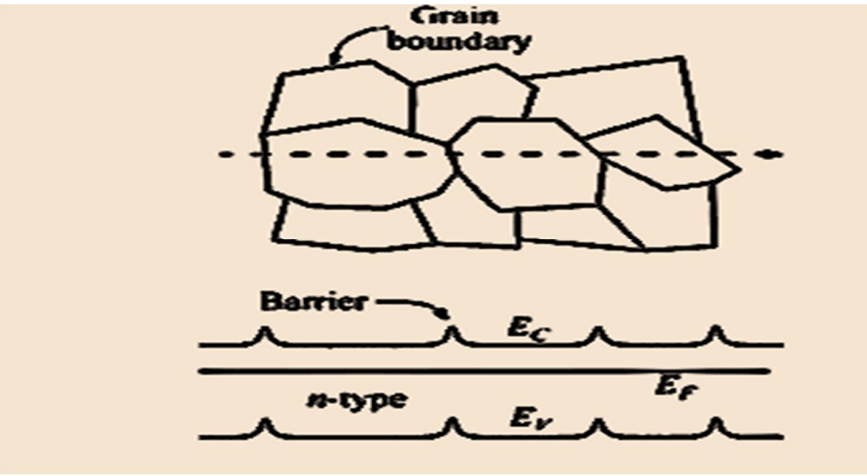

Figure(1.1):The grain boundaries give rise to potential barriers in a metal oxide semiconductor sensor[23].

A bulk effect is another possible process. Here the molecule of gas reacts with the absorbed oxygen at the boundary of grain, and emitting a free electron or neutralized, depending on the reaction type. This method changes the bulk's net carrier concentration and resistance [23].

The semiconductor gas sensor has become important in recent years and has many applications that can be seen in the figure (1.2) that shows the most important applications of the semiconductor gas sensor.

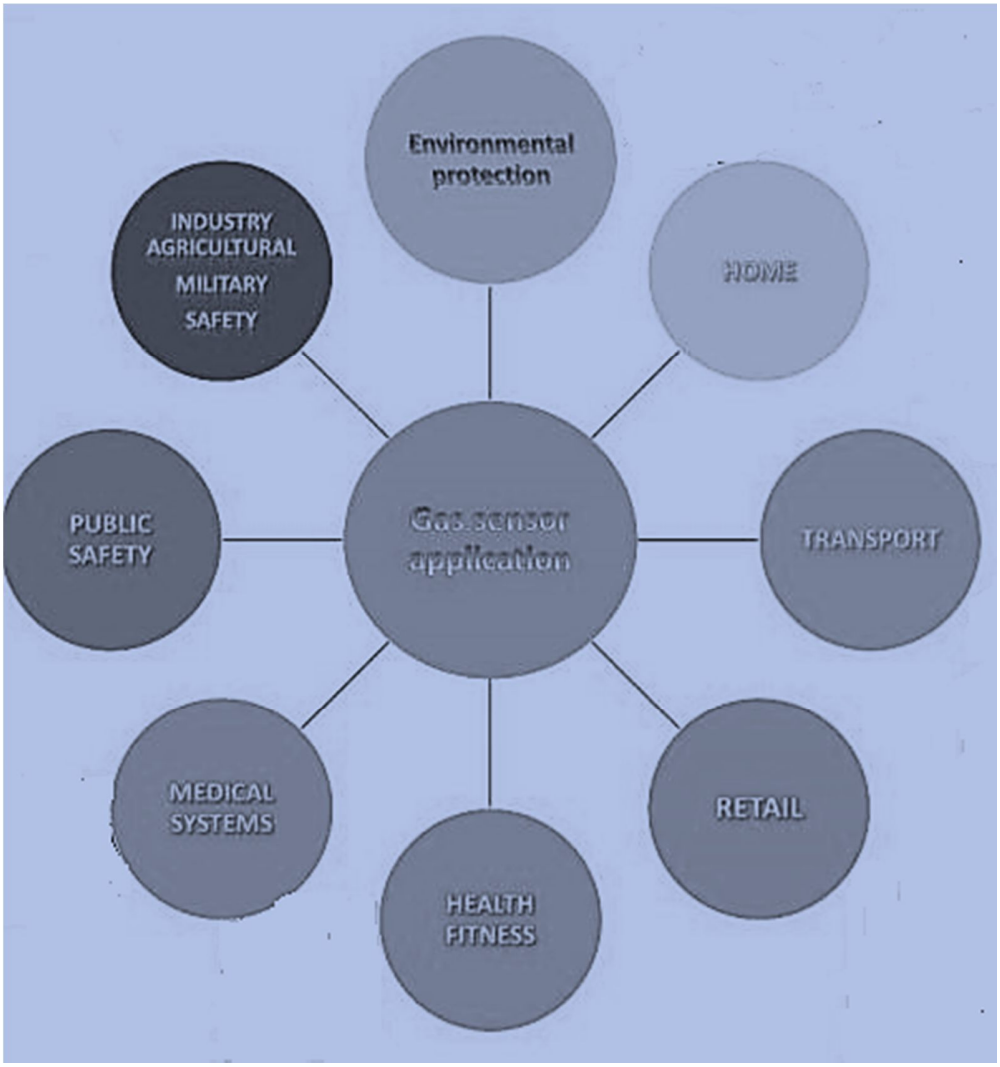

Figure(1.2):Scheme showing semiconductor gas-sensor applications[24].

1.3 Nanoparticles and Nanostructured Materials

Nanoparticles (NPs) and nanostructured materials (NSMs) represent an active area of research and a techno-economic sector with full expansion in many application domains. NPs and NSMs have gained prominence in technological advancements due to their tunable physicochemical characteristics such as melting point, wettability, electrical and thermal conductivity, catalytic activity, light absorption and scattering resulting in enhanced performance over their bulk counterparts. A nanometer (nm) is an International System of Units that represents 10^{-9} meter in length. In principle, NMs are described as materials with length of 1–1000 nm in at least one dimension; however, they are commonly defined to be of diameter in the range of 1 to 100 nm[25].

1.3.1 Synthesis of Nanoparticles

The nanoparticles are synthesised by various methods that are categorised into bottom-up or top-down method. A simplified representation of the process is presented in figure (1.3).

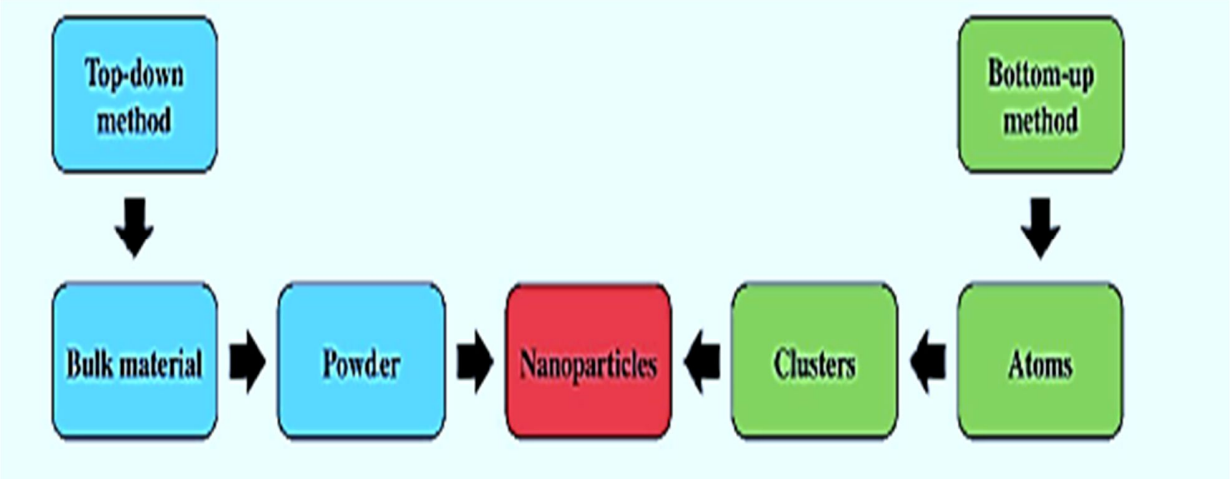

Figure (1.3): Scheme of Synthesis of nanoparticles process[26].

1.3.2 Properties of Nanoparticles

The properties of nanoparticles are generally categorised into physical and chemical as shown below:

1.3.2.1 Physical properties

The physical properties include optical such as the color of the nanoparticle, its light penetration, absorption and reflection capabilities, and UV absorption and reflection abilities in a solution or when coated onto a surface. It also includes the mechanical properties such as elastic, ductile, tensile strengths and flexibility that play a significant factor in their application. Other properties like hydrophobicity, hydrophobicity, suspension, diffusion and settling characteristics has found its way in many modern everyday things. Magnetic and electrical properties such as conductivity, semi conductivity and resistivity has led a path for the nanoparticles to be used in modern electronics thermal conductivity in renewable energy applications[26, 27].

1.3.2.2 Chemical properties

The chemical properties such as the reactivity of the nanoparticles with the target and stability and sensitivity to factors such as moisture, atmosphere, heat and light determine its applications. The antibacterial, anti-fungal, disinfection, and toxicity, properties of the nanoparticles are ideal for biomedical and environmental applications. Corrosive, anti-corrosive, oxidation, reduction and flammability characteristics of the nanoparticles determine their respective usage[26, 28].

1.4 Transparent Conducting Oxides (TCOs)

1.4.1 Introduction to Transparent Conducting Oxides

In the last years, Transparent conducting oxides, later referred to as TCOs, which for more than a century ago, it has been well-known. It prepared in the thin films form are the focus of attention of researchers, because of their distinctive and unique properties of transparency and conductivity. TCOs are electrically conductive compounds with a poor light absorption compared to other materials.

TCOs are ordinarily prepared with TF technologies and used in opto-electrical devices for example a displays, solar cells, opto-electrical interfaces and circuitries. Glass fibers almost lossless light conductors, but it is an electrical insulators; silicon and compound semiconductors are optical resistances based on wavelength (generating mobile electrons), but dopant dependent electrical conductors. TCOs are highly flexible intermediate states with both these characteristics. Its conductivity can be adjusted from semiconductor insulation to conductivity as well as its transparency. Because it can be produced as n-type and p-type conductives, it opens up a wide range of optical circuits and energy-saving technological applications[29] .

A Transparent conducting oxides is wide band gap semiconductor with a relatively high concentration of free electrons in the conduction band. These arise either from extrinsic dopants or from defects in the material, levels of impurities that act as a shallow donor level. Electromagnetic radiation is caused by a high carrier concentration which absorbed in both infrared and visible parts of the spectrum [30] . A TCOs must always be a

compromise between the optical transmittance and electrical conductivity; a careful balance between both above properties are required. Reducing resistance involves either increasing concentration of carrier or in the mobility. The rise in the first will improve absorption in the visible region while the increases in mobility has no adverse effect on optical properties. Therefore, the search for new TCOs materials is focused on the production of materials with a higher electronic mobility capability.

The following are the most important uses of thin layer TCOs[31, 32] :

1- Solar Cells: These are utilized in a variety of solar cell kinds, including Hetrojunction solar cells (Semiconductor Insulator Semiconductor) (SIS) and transparent electrical electrodes (ITO).
2- The manufacture of the thermal mirror, which has many advantages, it is used to control the temperature in a device exposed to space as the uncovered sections of solar cells exposed to solar radiation, to protect the energy required for curl heating in the radiant lamp, and to decrease unwanted heat in the lamp's shining region
3- Opto-Electronic Devices: Thin film transparent conductors oxides (TCOs). It has a wide range of uses in electronic equipment, and it is utilized in a variety of gadgets such as (hot crystals, photodiode, and others), as well as in thin films in photographic detector, in high conductivity connectors, and in visible photographic devices… etc.
4- Thin film resistors are resistors with a thin resistive layer deposited onto ceramic basis.
5- Gas sensors (sometimes referred to as gas detectors) are electrical devices that detect and identify various gases.

6- Semiconductor lasers are solid-state lasers that use semiconductor gain media as their gain medium.
7- TCOs are used in a variety of applications, including ship coatings to resist ice and fog, and to eliminate electronic charges that collect on glass windows in various devices, as well as transparent heating metals on aircraft and automobile windows [33] .

1.4.2 Classification of TCOs

Beta-Gallium(III) Oxide (β-Ga_2O_3) is a n-type which is the most stable crystalline modification where the oxide ions are in a distorted cubic closest packing arrangement, and the gallium (III) ions occupy distorted tetrahedral and octahedral sites, with Ga-O bond distances of 1.83 and 2.00Å ,respectively[34] . Ingram et al [35]has classified the TCO structural into four major families which are listed in the table (1.1). The first family has cations tetrahedrally coordinated by O_2, and is a type n in character. Zinc oxide is the only known oxide to exclusively have this coordination. The cations in the second family are in octahedral coordination, and is also n-type in character. This is the most extensive TCOs family, involving CdO, SnO_2, $CdIn_2O_4$, In_2O_3, Cd_2SnO_4, and most of the best n-type complex oxide materials. The cations in the third family of TCOs are in linear coordination with oxygen, and is p-type in character. This family involves $CuAlO_2$, related Cu- and Ag-based delafossites and $SrCu_2O_2$. The last family, the cage-structure oxide, $12CaO{\cdot}7Al_2O_3$, is outlined as the initial member of a prospective new TCO family with an n-type in character.

Table(1.1): Classification of TCOs[35]

Carrier type	Structural feature	Examples
n-type	Tetrahedrally-coordinated cations	ZnO
n-type	Octahedrally - coordinated cations	CdO, In_2O_3, SnO_2, Cd_2SnO_4
p-type	Linearly-coordinated cations	$CuAlO_2$, $SrCu_2O_2$
n-type	Cage framework	$12CaO{\cdot}7Al_2O_3$

1.5 Characteristic of Gallium oxide

Gallium(III) oxide (Ga_2O_3) has a long history, and the phase equilibria of the Al_2O_3-Ga_2O_3-H_2O system ,which first reported in 1952[36], in which the polymorphs (i.e., crystal structures or viruses forms) of gallium(III) oxide and their regions of stability were also identified. There are 5 known specific polymorphs or forms of gallium oxide, it's called α, β, γ, δ, and ε [37-45] . These are referred to as (α), (β), (γ) and (ε) corundum, monoclinic, defective spinel and orthorhombic, respectively, with the beta- phase commonly

accepted as being a form of the orthorhombic phase[36, 42, 46] . Among these several phases of Gallium oxide, the orthorhombic β -Gallia structure (β -Ga_2O_3or β -phase) is the most stable crystal structure and it has attracted most of the recent attention. The various polymorphs may be either conductors or insulators, depending onto the conditions of growth [36, 42].The second form, beta-Ga_2O_3 has monoclinic structure and belongs to space group C2/m. This Ga_2O_3 form can be obtained by baking every other Ga_2O_3 polymorph in air at a high enough temperature. The -type of β -Ga_2O_3 are the most widespread and well-studied polymorph. Beta Ga_2O_3 is only polymorph that remains intact across the entire temperature spectrum until it melts, all other polymorphs, on the other hand, are metastable and transform into the beta gallium oxide at 750 C° to 900 C°[47].As a compared with other semiconductors, beta gallium oxide has poor thermal conductor. It has a thermal conductivity that is half that of sapphire and one order of magnitude lower than that of GaN. The thermal conductivity of beta gallium oxide varies greatly depending on the crystal orientation due to crystalline anisotropy. The highest thermal conductivity along the length of the direction [010], and lowest along the direction [100] at all used temperatures in the measurements. Methods for measuring thermal conductivity is laser flash is 13W/m.K along the direction [100] [48] and 21 W/m.K along the [010] direction[49] The asymmetric unit of beta gallium oxide includes two crystallographically different Ga atoms, one with tetrahedral coordination geometry and the other with octahedral coordination geometry. The distances of Ga-O are in the range 1.833 -1.8630A, within the tetrahedra, but are longer within the octahedra 1.935 -2.074A. There is a distorted cubic close packing of the O atoms [50].

Different techniques have been used to deposition of Ga_2O_3 films, such as sol–gel[51]spray pyrolysis[52], pulsed laser deposition[53] , sputtering[54] , chemical vapor deposition[55] , thermal evaporation [56] , and magnetron sputtering [57].The β -Ga_2O_3 structure is shown in figure 1.4 a and b.

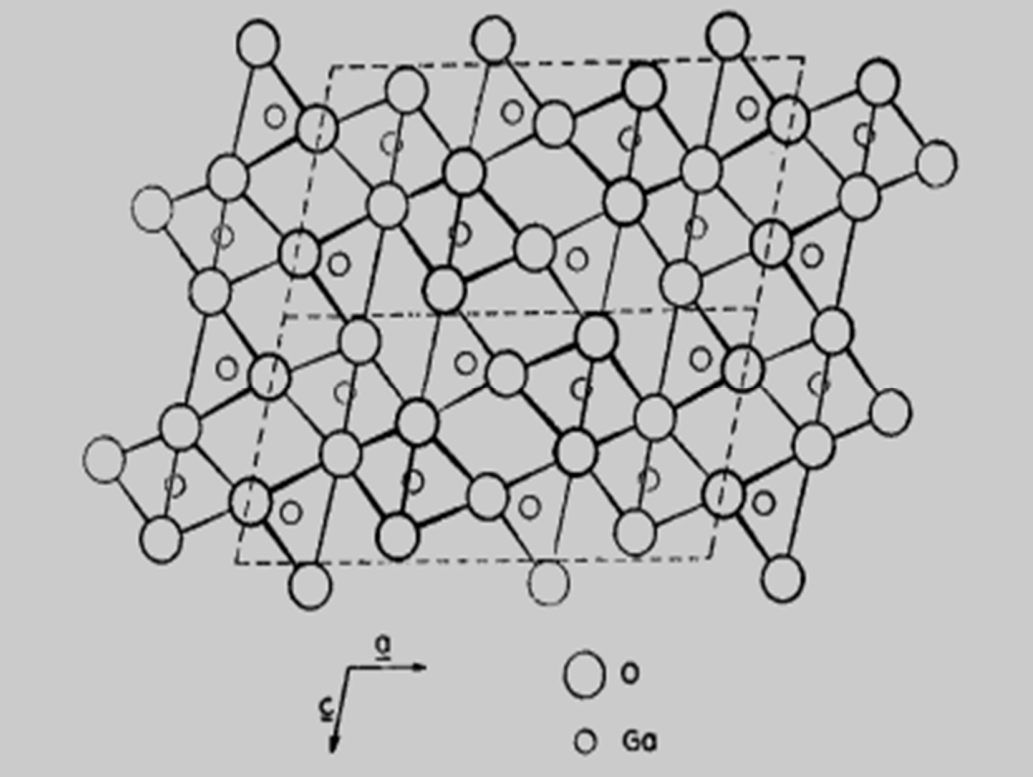

Figure (1.4a): The beta gallium oxide structure in plan. The tetrahedra and octahedra are built from and connected by oxygen atoms in three successive symmetry planes, as indicated by the lines linking atoms [58].

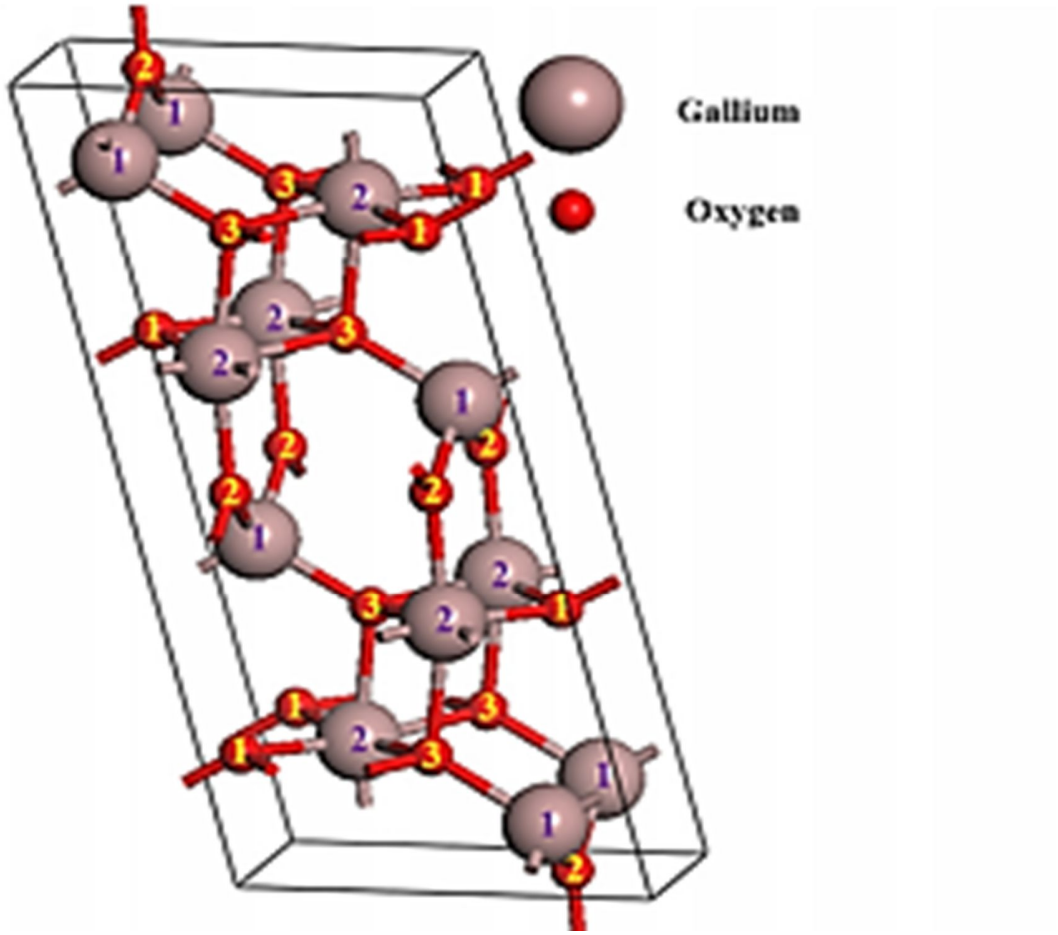

Figure(1.4b): Beta gallium oxide crystal structure[46].

Gallium (III) oxide belongs to a transparent semiconducting oxide conducting family. Although Ga_2O_3has been recognized for decades, it has remained on the fringe of mainstream science. The background of Ga_2O_3 dates back to 1875 when Lecoq de Boisbaudran described newly discovered element Ga and its compounds. The early publications concentrated on

fundamental research on the material as such. Subsequently, new applications have been created and from the point of view of microwave and optical maser experiments, gallium oxide was studied as a material for phosphors and electroluminescent instruments, for chemical sensing and catalysis, as transparent conductive coatings ……etc. [37].

Beta Ga_2O_3 is a semiconductor with a wide optical band gap of 4.80 eV at 300 K[59] . It has been varied studied for high-temperature gas sensors applications [60] , deep ultraviolet (UV) photodetectors[61, 62] and as a transparent dielectric substrate[63] . Its high electron mobility (200 cm^2/Vs for Si-doped gallium (III) oxide with a carrier density of (10^{17} cm^{-3}). Devices with a wide band gap have a high breakdown voltage, making gallium oxide an attractive material for high-power electronic applications [63-66] . Metal oxide semiconductor(MOS)-based resistive gas sensors have a long history and because of its high melting point (approximately at 1800 °C), gallium oxide is one of the finest materials for gas detection at high temperatures [67, 68]. Gas sensors made of semiconducting materials, most often polycrystalline, gallium oxide thin films can be used either for reducing gases (T<900 C) or sensing oxygen (T > 900 °C), depending on the temperature of operating [69-78] Another benefit of gallium oxide is that it has only one stable structural adjustment, monoclinic, that can be very easily obtained by thermal annealing at temperatures (800 - 900 C). [72-75]. There are many properties of Ga_2O_3, which are tabulated in table (1.2):

Table (1. 2): Special properties of Ga_2O_3

Molecular Formula	Ga_2O_3
Molar mass	187.444 [79]
Appearance	white odourless powder
Melting point	1900 ˚C [34]
Density	5.95 g/cm3 [80]
refractive index	1.9 [81]
Stability	Stable. Incompatible with magnesium.
Thermal conductivity	10.9±0.1W/mK for [100] [82]
Electron mobility	300 (cm^2 /Vs)[46]
Solubility in water	Insoluble
Solubility in acid	soluble in most acids
Lattice constant	a=11.83 ± 0.02, b=2.92 ± 0.01, c=5.64 ± 0.01 Å, and β= 104.0 ± 0.5°. [83]

1.6 Characteristic of Cadmium Oxide

Cadmium oxide (CdO) was synthesized and characterized in bulk form as early as 1902[84] , in 1907 the first thin film work after five years later [85]. CdO is a type -n semiconductor with a rock-salt crystal structure (FCC) and presents an optical bangap of about 2.2 eV[86] . The crystal structure of CdO can be seen in figure (1.5). Cadmium oxide's strong electrical conductivity, as well as its high optical transmittance in the visible part of the solar spectrum and moderate reflecting index, make it suitable for a broad range of applications, including photodiodes and gas sensors.[87, 88], windows, solar cells, photo transistors, flat panel display etc. [89, 90] . Undoped, monodoped and dual doped cadmium oxide thin films have been deposited by many techniques for example spray pyrolysis[91-94] , dc magnetron reactive sputtering[95] , r.f.sputtering[96], mechanochemical method[97] , sol-gel [98] and pulsed laser deposition[99], …etc. The temperature is a significant factor for gas sensing materials and the sensor designing. To achieve the appropriate electrical characteristics required for gas sensor application, a suitable crystallization degree is required. Cadmium oxide thin films show high optical transmittance in ranges of visible and have good conductivity.

Cadmium oxide usually exists in nonstoichiometric with pronounced cation interstitials or anion vacancies, resulting in a free electron concentration of (10^{19} to 10^{21}) cm^{-3}. Depending upon processing or preparation condition, it is either a non-degenerate or degenerate type-n semiconductor[100]. There are many properties of cadmium oxide, which are listed in table (1.3).

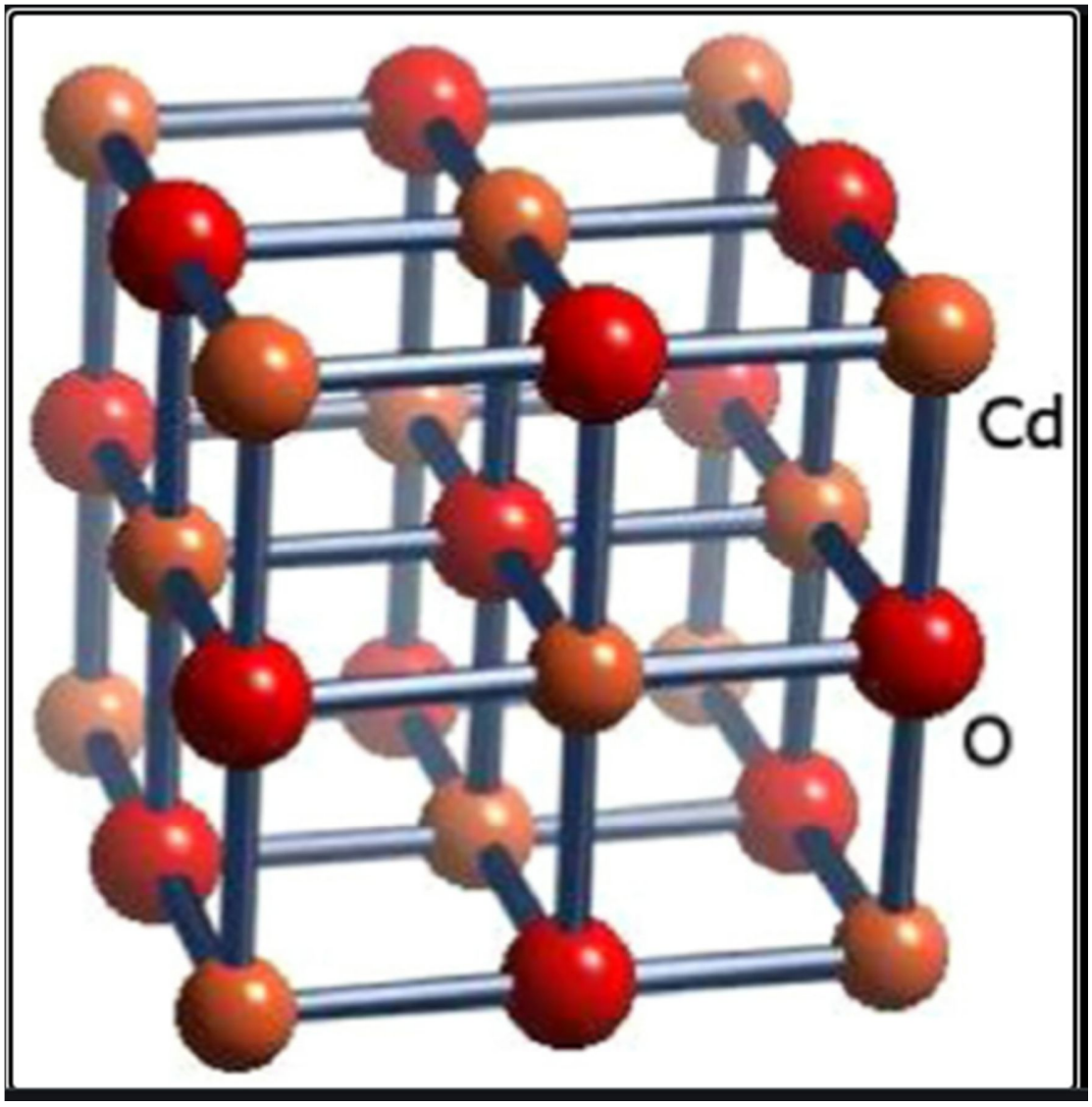

Figure(1.5): The crystal structure of CdO[101].

Table (1. 3): Special properties of CdO

Molecular formula	CdO
Molar mass	128.41 g/mol[101]
Appearance	Colorless powder (alpha form) Red-brown crystal (beta form)[102]
Density	8.15g/cm³(crystalline) 6.95g/cm³(amorphous)
Melting point	(900-1000˚C) (decomposition of amorphous form)[103]
Boiling point	1559˚C (sublimation)[103]
Solubility in water	Insoluble
Solubility in acid and alkaline	Degrades
Electron mobility	531cm²/V.s
Magnetic susceptibility	3×10^{-5}cm³/mol
Thermal conductivity	0.7 W/m.K
Lattice constant	4.6958Å
Refractive index	2.49[101]

1.7 Literature Survey

Synthesis and characterization of gallium oxide and cadmium oxide for the gas sensitivity had an interest during the past century and one can review them as related to the present work as follows:

Between 1991 and 2000[104-120] there are many important studies that dealt with gallium oxide and cadmium oxide and their deposition in the form of thin films and studied some properties such as structural , electrical properties and sensitivity to different gases with various temperatures degrees of operation using various methods of deposition process.

Ogita, *et al*. in 2001 studied the resistivity of gallium oxide which changes with the O_2 concentration in the thin film, where an O_2 sensor was made on the basis of this principle. Thin film of Ga_2O_3 was deposited onto the silicon substrate from a sintered powder target by a radio frequency magnetron sputtering using argon as the sputtering gas. The TF's gas sensitivity, electrical conductivity, and increasing response time are all affected by the argon sputtering pressure used during the deposition procedure. It's already been established that Ga_2O_3 thin film deposited at lower sputtering pressure demonstrates electrical conductivity is improved and high response time, whereas the TF deposited at high sputtering pressure demonstrates greater gas sensitivity[121].

High temperature gallium oxide gas sensors exhibit some variations between this sensor and others based on different metal oxides such as SnO_2. Among the advantages of gallium oxide based sensors good long term stability, fast recovery and response times, good reproducibility, It is important to note low cross-sensitivity to moisture and brief pre-aging periods. In the contrary, the operation temperature started from 600°C to 800°C which means

that power consumption is comparably about (<1 W). The sensitivity of gallium oxide sensors to NO_2 and CO is lower as compared to other MO based sensors, which studied by Hoefer, *et al*. in 2001 [122].

Weh, *et al*. in 2001 studied the detection mechanisms inside a high temperature metal oxide sensor with gallium oxide as its sensitive material and a silicon dioxide top layer to increasing the sensitivity of hydrogen where the sensor is exposed to dry and O_2 free gas mixtures. While the absence of oxygen significantly reduces sensor selectivity, dry air has little effect on selectivity. Hydrogen detection is possible in all cases. For further investigation, an electrode was installed directly above the sensor affecting space charges within the sensor, which appears to be the main detection mechanism[123].

Li, *et al*. in 2003 studied the O_2 gas sensing performance of gallium oxide thin films doped with Sb, Ce, Zn and W have been investigated. Where the TF has been deposited by the sol–gel process and it deposited onto sapphire transducers with interdigital electrodes and a platinum heater integrated. Sensors were exposed to different concentrations of O_2 gas in an ocean of nitrogen and the performance of the gas sensor was examined. The sensors responses doped with Sb, Ce, Zn and W were stable and reproducible at their respective operating temperatures. It was observed that gallium oxide films doped with W, Ce and Zn are promising for applications of oxygen gas sensing [124].

The preparation of $CdGa_2O_4$ and its gas-sensing properties are described by Xiangfeng, *et al.* in 2004. The sol–gel process was used to extract $CdGa_2O_4$ raw powders. XRD was used to characterize the influence

of the calcining temperature on the process constituents, and SEM was used to characterize the microstructure. $CdGa_2O_4$ was studied for its conductance–temperature and gas-sensing properties [125].

The development of miniaturized gas-sensing devices, particularly for pollution monitoring and for toxic gas detection. Though different method are available for gas detection, solid state metal oxides show wide range of materials and their sensitivities for different gaseous species, making. It is a superior solution to the alternatives, where a critical parameters analysis of various metal oxides ,which known to be sensitive for the oxide, operating temperature range, sensing gaseous species, and physical form of the material for the improvement of integrated gas sensors. The oxides that are covered in their studies include oxides of aluminum, cadmium, cerium, bismuth, cobalt, chromium, gallium, copper, iron, indium, molybdenum, manganese, niobium, nickel, tantalum, ruthenium, tin, titanium, vanadium, tungsten, zirconium, zinc, and the mixed or multi-component metal oxides. They cover gases for example CO_2, CO, C_2H_5OH, CH_4, C_3H_8, H_2S, H_2, NO, NH_3, NO_2, O_3, SO_2, O_2, acetone, dimethylamine (DMA), liquid petroleum gas (LPG), humidity, trimethylamine (TMA), smoke, petrol, and many others. Both undoped and doped oxides are studied by Eranna, *et al.* in 2004 [126].

O_2 sensor based on Ga_2O_3 thin films have been analyzed by Baban , *et al.* in 2005 , where the Ga_2O_3 thin films were deposited using radio frequency magnetron sputtering from a powder target with argon as the sputtering gas. The sensing characteristics (sensitivity, stability and response time) of the O_2 sensor were investigated at a 1K °C. At high temperatures Ga_2O_3 thin films behaves as a type-n semiconductor because of O_2 defect.

Because of the greater O_2 vacancy concentration, the thin films produced using the aforesaid technique have a better electrical conductivity. Two sensors with different shapes were investigated: one with interdigital electrodes and the other with a sandwich structure on top with a mesh type electrode. For low O_2 concentrations, the first type sensor has a response time of around 14 seconds while the second type has a response time of about 27 seconds. In sputtered Ga_2O_3 films, the O_2 process is also explored[127].

In 2008 Liu, *et al.* prepared Ga_2O_3 nanowires (NWs) were synthesized using a chemical thermal evaporation technique with gallium metal as a source material. Scanning electron microscopy (SEM), XRD, and TEM characterizations indicate that the gathered (NWs) are well-crystallized single phase monoclinic gallium oxide. Multiple nano-wire gas sensors were prepared by dispensing the gallium oxide nano-wires on an interdigitated Pt-electrode. The gallium oxide nanowire gas sensors exhibit reversible response to oxygen and carbon monoxide gases in operating temperature range of 100°C to 500 °C. A peak response appears at 300 °C for oxygen gas and the peak response at 200 °C for Carbon monoxide gas [56].

The effect of [Ga]/ [Cd] ratio on the structural, morphological, electrical and optical properties of chemically sprayed Ga-doped CdO thin films are investigated it has been studied by Deokate, *et al.* in 2010. The films are polycrystalline with a cubic structure and (200) preferred orientation, according to X-ray diffraction investigations. It is concluded that the Ga^{3+} ions interstitial locations at high concentrations and replace the lattice sites at lower concentrations. There is a considerable broadening of (2 0 0) peak and shift of Bragg's angle with respect to [Ga]/ [Cd] ratio. The

electrical studies confirm degenerate, a n- type semiconductor nature of Ga-doped CdO thin films with minimum resistivity of $3.7 \times 10^{-4}\ \Omega\,\text{cm}$. The optical gap ranges from 2.27 to 2.44 eV because of Moss–Burstein effect. The highest value of merit observed in the present study is $1.69 \times 10^{-4}\ \Omega^{-1}$. Intensity of PL for green emission around 470 nm ,which found to be increased with increasing [Ga]/[Cd] ratio [128].

Isai, *et al.* in 2011 have been started from a point of environmental problems, O_2 gas sensors attract attention of controlling the exhaust gas. The gallium oxide has an O_2 detection characteristic at temperatures higher than 900℃, also this material attracts higher attention as an O_2 device sensor at high temperature. The beta-Ga_2O_3 films were deposited using the RF magnetron sputtering technique. The influence of Ar: O_2 flow ratio, thickness of films, and RF power on the crystal also O_2 sensing properties have been studied. Consequently, the superior crystal properties were obtained at the Ar: O_2 flow ratio of (5:1). It was found that the sensitivity of O_2 depended on the thickness of film[129].

In 2012, One-dimensional (1D) nanostructures (NS) of gallium oxide were created by Kim, *et al.* by evaporation method. The crystal structure, morphology and improved sensing properties for the gallium oxide NS functionalized with Pt to CO gas at 100 °C were tested. The length and diameter of the one-dimensional NS ranged from a few hundreds of micrometers and (10 to 100) nm, respectively. Pt nanoparticles with diameters of a few tens of nm were distributed over the gallium oxide (NWs). Multiple networked gas sensors prepared from these Pt-functionalized gallium oxide NWs showed improved electrical responses to CO gas. The NWs responses were enhanced 27.8, 26.1, 22.0 and 16.9 fold at

CO concentrations of 10, 25, 50, and 100 ppm, respectively, as compared to the bare gallium oxide NWs. The mechanism responsible for the improved gas sensing properties of the Pt-functionalized gallium oxide NWs is discussed[130].

Kumar and Singh in 2013 reviewed a briefly study on β-Ga_2O_3 nanowires NWs and nanostructures NS . Beta gallium oxide is a wide-bandgap (4.9 eV) semiconductor and can be doped with both n- type and p-type dopants. This might lead to applications in a variety of different devices. They have been discussing briefly the properties of beta gallium oxide in bulk form and showed the growth of beta gallium oxide NWs/NS using variety techniques such as thermal CVD, metal organic chemical vapor deposition MOCVD and laser ablation. They were showen that the luminescence properties of beta gallium oxide NWs like photoluminescence (PL) and cathodoluminescence (CL). The origin of different peaks in the CL and PL spectra of beta gallium oxide NWs/ NS will be presented, with reference to different experimental studies carried out recently. Also described different applications of beta gallium oxide NWs in nanodevices for example field effect transistors , deep-UV photodetectors and gas sensors [131].

In 2013, Chandiramouli and Jeyaprakash have been reviewed the cadmium oxide thin film and the various method for preparing it. CdO TF is one of the first TCO semiconductors. And have excellent electronic and optical properties have made cadmium oxide a promising material of flat panel displays[132].

In 2013 field-effect H_2 gas sensor devices with self-temperature compensation based on beta gallium oxide thin films were deposited by Nakagomi and Kokubun. A beta gallium oxide TF was deposited onto a sapphire substrate by Ga evaporation in O_2 plasma. The resistance between 2 ohmic electrodes on thin film of beta gallium oxide with a Pt gate was decreased in H_2 atmosphere. The sensor can detect 100 ppm H_2 in 20% O_2/N_2 at 400 °C. The device resistance without the Pt gate electrode didn't change significantly with differentiating of the atmospheric composition. A sensor device with self-temperature compensation was constructed using the in-series connection of devices without and with gate electrodes. Even when temperatures fluctuated by more than 100°C in the range of (400 - 550) °C, the sensor device's output remained constant. [133].

In 2014 β-Ga_2O_3 thin films were deposited on a quartz substrate using spray pyrolysis method with gallium acetylacetonate as precursor salt. Which prepared by Pandeeswari and Jeyaprakash where the XRD pattern of the annealed film at 900 °C indicated the formation of monoclinic beta gallium oxide phase with polycrystalline nature. FESEM exhibited nano crystallites on the surface of film. The ammonia (NH_3) sensing property of the film at (~30 °C) was deposited using chemi-resistive method. Influencing factors such as relative humidity, vapor concentration and film thickness in NH_3 sensing performance were studied and reported [134].

In 2014 polycrystalline beta gallium oxide thin films were deposited onto sapphire substrate (0001) were prepared by Goyal, *et al.* using PLD technique. The optical band gap crystalline structure and were studied as a function of growth temperature, annealing temperature laser beam energy, and time. To tailor the band gap of beta gallium oxide thin films by Al

diffusion from the sapphire substrate the films were annealed for 24 hour at various temperatures. The magnitude of Al diffusion was various for various annealing temperatures which resulted in the increase of band gap in addition, the shift of various peaks to higher angles with increasing temperature. The annealed films exhibited high transparency in the deep UV spectrum [135].

In 2015, thin films have been grown under different deposition conditions in order to understand the processing effect on the film properties and to specify the optimum condition by Yousif and Hasan. Various ($In_2 O_3$) contents (0, 1%, 3%, 5% and 7%) using double frequency pulse laser beam to deposit ($CdO:In_2O_3$) films on quartz and aluminum oxide (sapphire α-Al_2O_3 (006)) substrates. The surface morphology of the deposited materials was examined in order to assess the sample structural characteristics (AFM). The samples have a granular texture to them. The lowest grain size equals (79.11 nm) and (82.99 nm) for quartz and sapphire-Al_2O_3 substrates, respectively, as the doping concentration ratio increases. The sensitivity of doped and undoped CdO samples toward (NO_2) gas in the surrounding air was measured in the home building system. All films were examined at mixing ratio (3% NO_2: air). The optimum operating temperature is (200 to 225)°C for pure CdO and decreases to (175-200)°C for samples. At a doping concentration of 3%, maximum sensitivity(263.97%), reaction time (13.5 s), and recovery time (15.5 s) are attained for sapphire-Al_2O_3 substrate [99].

In 2016 cadmium oxide thin films with low concentrations of Ga doping were deposited onto low-cost glass substrates using PLD were prepared by Li, *et al.* The influence of Ga doping concentration on cadmium

oxide thin films' structural, optical, and electrical characteristics was investigated. The Ga-doped cadmium oxide thin films exhibit decreasing wavelength of plasma and resistivity when rising the doping concentration, and the widening optical gap differs from 2.49 eV to 2.85 eV with the Ga doping concentration rising from 0.2% to 1.2 at % because of Moss–Burstein effect. When Ga doping concentration in cadmium oxide thin films was controlled at low level from 0.6% to 1.0 at%, the films reached both high conductivity ($\sim 10^{-4}\ \Omega \cdot cm$) and high transmittance up to the IR region (>1600 nm), which demonstrates good potential as an ideal transparent conductor of full-spectrum photovoltaic devices[136].

Ramizy and Ibrahim in 2017, studied the structure and optical characteristics of pure CdO films doped with Ga_2O_3 were produced using the spray pyrolysis technique with 300 °C as the substrate temperature. The films were made with varied ratios (1, 3, 5 and 7) % on silicon and glass substrates. According to XRD results, all generated samples showed a cubic polycrystalline structure with a favored orientation of (111) for CdO. The thin films grain size is approximately (105.42-69.07) nm, the surface roughness is about (3.32-0.901) nm, and the root mean square (RMS) is about (3.97-1.05) nm for CdO films. The optical properties of the films were investigated using UV-VIS spectroscopy at wavelengths ranging from 300 to 1100 nm. It was discovered that the transmittance value increases as the gallium doping level increases, and that the films have a direct energy gap of about (2.3-4.0) eV, which increases as the Ga concentration rises. At various operation temperatures, the sensitivity characteristics of pure CdO films and films doped with Ga_2O_3 were deposited onto silicon substrates for NO_2 gas. It was discovered that the films of CdO doped with Ga_2O_3 on Si substrate

have greater sensitivity than the films that are not doped, and that The films' sensitivity has enhanced as a result of the doping CdO [137].

In 2017, the In_2O_3:Ga_2O_3 mixed oxide polycrystalline thin films with different components ratios were obtained by PLD, which prepared by Demin and Kozlov. The films composition effect onto surface morphology, electro physical and gas sensing properties, adsorption energies and desorption of combustible gases was studied. The films with 50% In_2O_3 and the same ratio for Ga_2O_3 composition exhibited maximum gas response (~25 times) combined with minimum optimal operation temperature (530 °C) as compared with the other films. The optical transmittance films were investigated in visible range. For 50% Ga_2O_3–50% In_2O_3 films, the transmittance is higher as comparison with the other films. The Ga_2O_3–In_2O_3films had been assumed to have perspectives as gas sensing material for semiconducting gas sensors [138].

Demin and Kozlov in 2018 studied the gas sensor based on the sensitive layer 50% Ga_2O_3 –50% In_2O_3 thin films. Dependences on concentration and temperature were examined for the resistance response caused by the gas to this sensor and the dynamic reliance of its resistance response to test gases in the air. Ethanol, ammonia, acetone, and liquefied petroleum gas were used as test gases. To increase selectivity, sensor information parameters were evaluated in dynamic operation mode. The results provided show that sensor selectivity can be improved in this mode using the following information parameters: gas-induced resistance response in a stable state, activation energy of the response and the pre-exponential factor of temperature dependence for constant response time [139].

A tweaked epoxide gel process was used to make stoichiometric and non-stoichiometric cadmium gallate (gallium rich) samples. Powder X-ray diffraction study revealed a cubic spinel structure for stoichiometric and gallium-rich compositions. To determine the intricate variations between these two samples, a complete structural analysis using Raman spectroscopy was performed. Microscopy techniques and EDX processing were used to gather additional evidence for the cubic symmetry and elemental ratio of all samples. This study was carried out in 2018 by Gupta, *et al.* [140].

In 2019, Kumar, *et al.,* described (NS) of beta gallium oxide, demonstrating their potential for high-performance nanoscale devices. Several growth methods for beta gallium oxide nanostructures are outlined, including most widely used CVD. Their properties, for instance structural, morphological, and optical. It's also discussed. Nanowires are one of the most important nanostructures with a promising component in nanoscale device applications. different applications of beta gallium oxide nanostructures such as gas sensors, photo-detectors, and field effect transistors have been identified and discussed [141].

Guo, *et al.* in 2019 studied Ga_2O_3, with an ultra-wide bandgap 4.9 eV, has recently attracted a lot of scientific and technological attention because of its many uses in the future applications in power electronics (Schottky barrier diodes, field effect transistors), optoelectronics (electroluminescent (EL) devices, solar-blind photodetectors), memory (resistance random access memory devices, spintronic devices), sensing systems (nuclear radiation detectors, gas sensors), and so on. gallium oxide has six various polymorphs, known as α, β, γ, δ, ε, and κ. Each of these polymorphs has

unique physical properties and can be used in different fields of devices[142].

In 2019 a series of gallium oxide films grown onto sapphire substrates which prepared by Yang, *et al.* using PLD with various temperature of growth (400 - 1000 °C) and various thickness from 69 nm to 332 nm were studied by XRD, optical transmittance and spectroscopic ellipsometry. With increasing growth temperature, the phase transitioned from amorphous to polycrystalline beta gallium oxide structure. In the transparent area, refractive indices rise when film thickness or growth temperature increases, with the film thickness effect being considerably more important than the growth temperature influence. Urbach's tail is observed in edge of absorption by measuring ellipse along with the transmittance spectra and the XRD intensities showing that higher growth temperature or thicker thickness can develop the films crystal quality. The temperature dependent Eg was quantitatively analyzed using the Varshni equation as the gallium oxide band gap films increases with decreasing growth film thickness and elevated experimental temperature from 25 °C to 600 °C[143].

In 2020, Shen *et al*., describe employing PLD technology to fabricate high-performance solar blind photodetectors utilizing gallium oxide thin films with different thicknesses produced onto single crystal (0001) Sapphire substrate. The number of ablating laser pulses were changed from (1k to 15k) shots to change the thickness of the gallium oxide films. XRD, Raman spectroscopy, SEM, AFM, and UV–Vis spectroscopy were used to evaluate the effect of thickness on the structure, surface morphology, and optical characteristics of the films. All of the thin films were discovered to be phase-pure gallium oxide with excellent crystal quality[144].

In 2021, Zade, *et al* investigated the relationship between the composition, surface/interface morphology, and mechanical properties of gallium oxide films onto quartz substrates using PLD with 200 nm thick gallium oxide films of variable microstructure and amorphous-to nanocrystalline composition onto quartz substrates by varying the deposition temperature from RT to 700 °C. At RT, gallium oxide films were amorphous; at 700 °C, nanocrystalline gallium oxide thin films were formed[145].

In 2021, the solvothermal-calcination technique was used to make a series of $CdGa_2O_4$ nanospheres prepared by Huirong , *et al*. . The crystal structure, morphology, specific surface area, and elemental content of the prepared materials were studied using a variety of characterization methods. The performance of $CdGa_2O_4$ nanospheres as gas sensors was studied. The effect of calcining temperature on $CdGa_2O_4$ nanospheres' gas sensing abilities was investigated. The $CdGa_2O_4$ material with the maximum sensitivity of 99 to 100 ppm formaldehyde at 140°C was produced at a calcination temperature of 700°C. It also had an ultra-low detection limit of 0.1 ppb[146].

1.8 Aim of the Present Work

The aims of the present work are:

1. Synthesis $CdGa_2O_4$ nanostructure films deposited onto quartz substrates using the PLD technique.
2. Studying the effect of the different mixing ratios of CdO on the optical, electrical and structural properties of the prepared films.
3. Studying the sensing properties of all the prepared samples for gas sensor application.

Chapter Two

Theoretical Part

2.1 Introduction

This chapter gives a general description of PLD technique and the theoretical part containing the characteristics. Structural, optical, electrical, optoelectronic, and sensing properties of $Ga_2O_{3\ (1-X)}$ $CdO_{(X)}$, thin films deposited onto quartz substrates. Finally, this chapter provides a theoretical summary with all relations, scientific explanations, and also the equations which can be used on this work.

2.2 Laser-Material Interaction

The laser beam provides the capacity to accurately transfer large energy amounts to confined areas of a material in order to achieve the required response[147]. The material must be absorption of the laser beam to have an effect on it. This absorption is remarkable of the process for laser-material interaction. This absorption process is a major source of energy within the material, this main source, rather, shows that the beam of laser released from the source determines what occurs to the laser irradiated material[148] .In figure 2.1, the incident pulse of laser heats the material target quickly, lead to shifting in phase and generating stress waves in the irradiated target. Then the material begin to melt and turns to a gaseous state , this happens in a very short time and plasma is created .The beam of laser will be absorbed by the plasma flame, resulting in the attenuation of the light intensity falling on the target, also due to the excitation and ionization of the

plasma field, the plasma extends and moves away from the zone of reaction to reach the base (substrate) and form a thin film layer [149] .

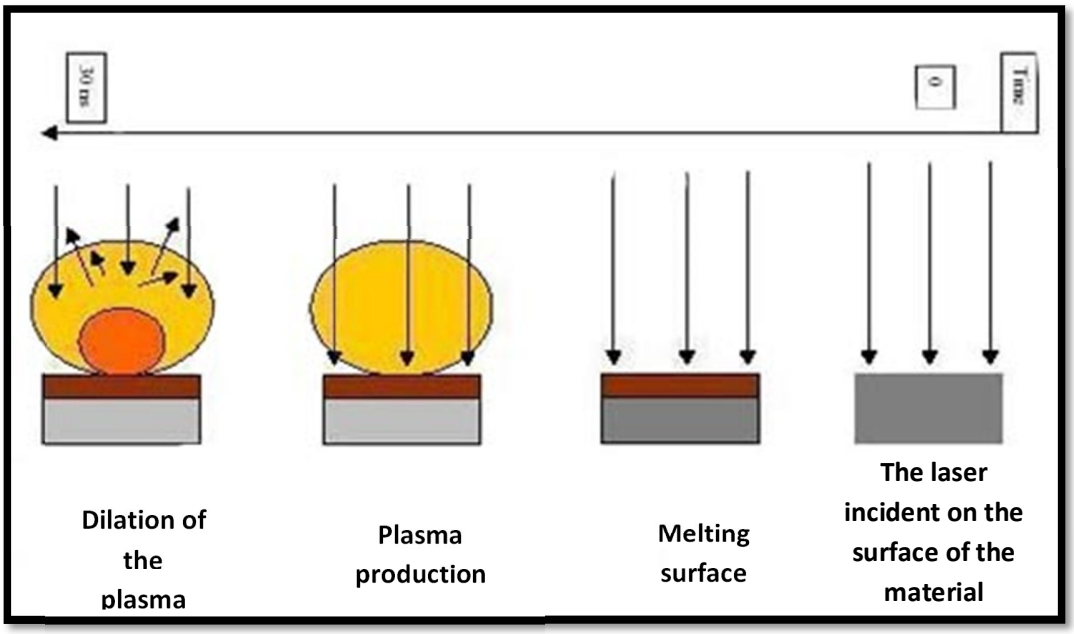

Figure(2.1): Pulsed Laser Ablation [150].

In process of the laser evaporation, the beam of laser incident on the target and the material evaporates from the target surface and the evaporated material transfer to the substrate and deposition on the substrate. The thermal propagation depth of the laser pulse(L) can be found it using the following equation [150] :

$$L = \sqrt{4N\tau_{las}} \quad \ldots\ldots\ldots\ldots\ldots\ldots\ldots\ldots\ldots\ldots\ldots\ldots\ldots\ldots\ldots\ldots \quad (2.1)$$

Where N and τ_{las} are thermal diffusivity of the material and pulse laser time respectively.

To determine the intensity threshold of the laser beam required to vaporize the material (I^*_{vap}), the following eq.(2.2) can be applied[150] :

$$I^{*}_{vap} = \frac{C_p \rho \sqrt{\pi x} \left(T_{vap} - T_o \right)}{2 \left(1-R \right) \sqrt{\tau_{las}}} \quad \ldots\ldots\ldots\ldots\ldots\ldots\ldots\ldots\ldots\ldots\ldots\ldots\ldots\ldots\ldots\ldots \quad (2.2)$$

Where C_p is the target material specific heat capacity, R represents the target surface reflectivity, T_{vap} temperature of evaporation, T_0 initial temperature, ρ density of material, x the laser spot dimension. When the laser beam intensity of close to the evaporation threshold of material. At the surface of the target, the proportion of vacuum-induced materials would have a low evaporation density, when the beam of laser becomes high intense, the vaporized material proportion will be large, generating a layer which called the Knudsen layer[151]. Rising the laser beam intensity increases the atoms density and heat in the Knudsen layer and their ionization will be grow. When the laser beam intensity is greater than the threshold limit for the plasma flame, the vapor of plasma will be fully ionized. In the technique of laser deposition, energies of laser are responsible for generating the plasma flames of the target material which is often in disk shape, in this way can be vaporize and grow materials thin films or compounds and several layers. The wavelength range of commonly used lasers is often located between (200nm – 1100nm), in order that, most materials have an absorption coefficient that decreasing with increases the laser wavelength. Materials show strong light absorption in the spectrum range of Ultraviolet and visible range, moreover, the high absorption from the spectrum lowers the target material's ablation threshold limit[152] .

2.3 Dynamic and Plasma Engineering

One benefit of pulse laser deposition mechanism is that it is possible to fill up the vacuum chamber with or without inert gas that reacts with the

plume of plasma before it reaches to the substrate .It can be seen in figure (2.2). When the chamber pressure increases, it changes the spatial distribution of the plasma plume and reduces the ions number reaching to the substrate. Therefore, the atoms kinetic energy in the plasma plume decreases as a consequence of collision with atoms of gas. This will change the pattern of film growth, the crystal structure and the film deposition direction [153].

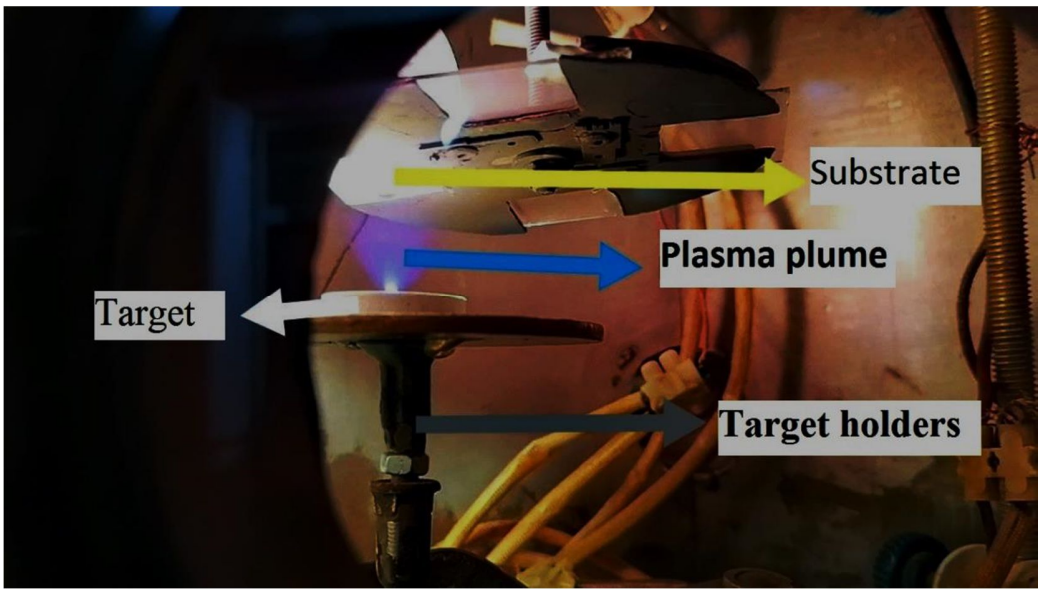

Figure (2.2): Plasma plume generated by laser incident.

2.4 Nd-YAG Laser

Nd-YAG laser is one of many types solid-state lasers that are extensively utilized in a whole lot of applications such as material processing such as drilling and welding, medical applications, laser ranging, in particular for laser rangefinders and target designators used in a military contest and scientific applications. The term solid state laser is generally used for lasers containing active species ions that are introduced as

impurities in a transparent host material (in crystalline or glass form)[154]. These lasers are had designed to work for short time periods and the Pockel cell is often used as a laser pulse control switch. Gold plating is used on a single linear flashing lamp and an elliptical cavity. This laser system is cooled either by air or by a closed system of liquid cooling with a liquid air heat exchanger and fan. As mention above Nd-YAG pulsed laser is most popular used in applications of material processing as (laser welding, punching and scratching). Variable pulse repetition rate rang (1 to 100 pulse /s) and varies power rate $(1-4)\times 10^{2}$ watt[155] . Nd-YAG lasers was selected in applications of materials processing for several reasons in addition to high pulse repetition rate and the power supply can produce the maximum power rate, so that the pulse energy is inversely proportional to the pulse repetition rate, but the same capacity.

2.4.1 Nd-YAG- Laser System Components

The Nd-YAG laser is made up of a YAG crystal rod that acts as an effective medium which is an yttrium oxide aluminum doped with ions of neodymium .The crystal color is purple. It features a YAG crystal with high damage resistance, high optical quality and hardness against breakage, also other materials can be used as effective medium. Nd-YAG laser works in four levels system and by using a flashlight, the optical medium is pumped visually. By the pump chamber, the light is concentrated to the active medium. The optical chamber components are two types flat mirrors, one of which is 100% reflective, which is the input mirror, and the other is 99%, which is know the output mirror.

2.5 Laser ablation

Solid thin films have been successfully produced using a variety of processes. Based on the nature of the deposition process, the methods used for thin oxide film deposition may be classified into two groups: physical methods and chemical methods. In which chemical deposition methods includes gas phase such as (chemical vapor deposition) CVD & atomic layer epitaxy (ALE) and solution spray pyrolysis for example (sol-gel, dip coating and spin coating). Physical vapor deposition (PVD), molecular beam epitaxy (MBE), sputtering, and pulsed laser deposition (PLD) are examples of physical techniques. PLD is a thin-film deposition technology that employs brief and intense laser pulses to evaporate target material, as illustrated in the figure (2.3). The ablated particles escape and condense on the substrate after being ejected from the target. To reduce particle dispersion, the deposition procedure takes place in a vacuum chamber. However, in other circumstances, reactive gases are employed to change the deposit's stoichiometry[156] .

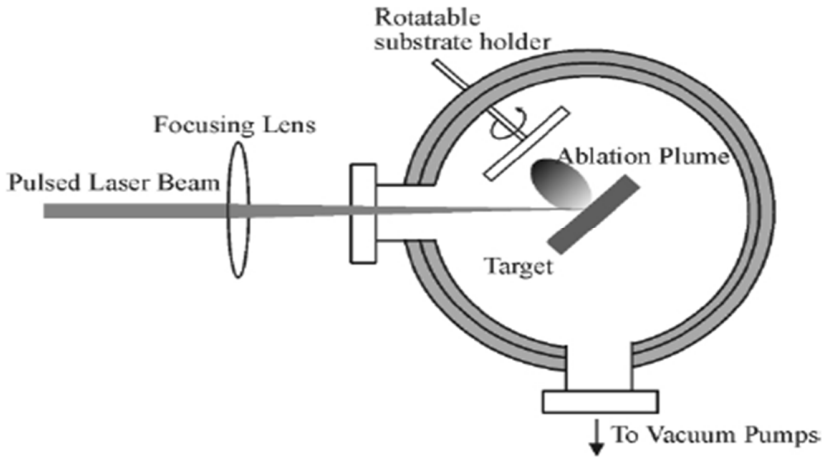

Figure(2.3): An apparatus schematic diagram for PLD of a solid target with deposition on an on-axis mounted substrate[149].

2.5.1 Laser ablation mechanisms

Outside the chamber, a laser source, as well as optical instruments like as lenses, apertures, and mirrors, are built with the goal of concentrating and directing the laser beam, which is put in front of the deposition chamber's port. The laser beam is aimed at the surface target in the chamber. To ensure that the target is worn in a uniform, target surface can be restored by the beam of laser, or it can be transfer and/or rotated, where the beam of laser remains stationary[157]. The PLD mechanism, despite the ease of the setup, it is a very complicated physical phenomenon. It not only include the physical process of laser-material reaction under the influence of high-power pulsed irradiation on the surface of solid target, but also the creation of a plasma plume containing high-energy species, as well as the transfer of ablated material from the plasma plume to the heated substrate surface. Thus the TF formation process in PLD generally can be listed into typically four the following stages[158]:

1. Interaction of laser irradiation with the solid target

2. The ablated materials dynamics.

3. The ablation materials deposition on the substrate.

4. Growth and nucleation of a thin film onto the substrate surface.

Each stage of the PLD process is crucial to the creation of a homogenous thin layer.

The laser beam is focused onto the target surface in the first stage. All elements in the solid target are easily heated up to their evaporation

temperature at relatively high flux densities and short pulse duration. Materials are separated from the surface of target and ablated out with stoichiometry as in the target[159]. The instantaneous ablation rate is strongly influenced by the laser fluences shining on the target. The mechanisms of ablation include many complex physical phenomena such as thermal, collisional, exfoliation, electronic excitation and hydrodynamics[160].

Through the 2nd stage, according to the principles of gas mechanics, the released materials appear to shift towards the substrate. The laser spot size and the temperature of plasma has significant influence on the deposited film uniformity. Another element that affects the angular dispersion of the ablated materials is the distance between the target and the substrate. A mask put near to the substrate might sometimes help to minimize the spreading.

The thin film quality must be determined at the third stage. The high-energy ejected species impact on the substrate surface and can produce various types of damage into the substrates. These energetic ejected species spewed some of the surface atoms, resulting in the formation of a collision zone between the sputtered atoms and the incident flow After a thermalized region is formed The grows of film. The thermalized region acts as a condensation source for particles. Thermal equilibrium is quickly attained when the rate of particles evaporated by sputtering is smaller than the condensation rate, and layer forms over the substrate surface[161].

Increasing the energy of the adatoms has the same effect on film growth as increasing the temperature of the substrate[152]. Typical power densities included in PLD are approximately 50 MW/cm^2 for a reasonable

growth rate (> 1 A°/shot). Initially the plasma is formed during laser interaction with target in vacuum or in air and then again an explicit laser plasma reaction occurs. The ions in the plasma are accelerated to(100–1000) eV as a result of this [152]. The density, ionization degree, energy, and type of condensing material, as well as the physico-chemical characteristics and temperature of the substrate, all influence the growth and nucleation of crystalline films. The growth mechanism's two key thermodynamic parameters are the supersaturation D_m of laser plasma and the substrate temperature. They can be written as the following equation[152]:

$$D_m = kT_s \ln(R_a/Re) \qquad \text{(2.3)}$$

Where k, R_a, R_e and T_s are the Boltzmann constant, the actual deposition rate, the thin film deposition rate and the substrate temperature respectively.

The interfacial energies between the three phases present in the condensing material determine the nucleation mechanism, the substrate and the vapor. The nucleus critical size depends on the substrate temperature and the driving force, i.e. the deposition rate. Large nuclei, which are a hallmark of small supersaturation, produce isolated patches (islands) of film onto the substrate, which expand and coalesce together. The vital nucleus shrinks as supersaturation grows, until its height exceeds an atomic diameter and its form is that of a 2-D layer. Layer-by-layer nucleation will occur for incompletely wetted foreign substrates when supersaturation is high. The growth of crystalline film depends on the adatom surface mobility (vapors atoms). Normally, until adhesion on the stable location within the newly created film, the substance can disperse over many atomic distances. The temperature of surface the substrate determines the adatoms surface diffusion ability. Crystal development at low temperatures or with high

supersaturations can be stifled by energetic particle impingement, resulting in disorganized or even amorphous formations, while high temperature or large supersaturation crystal growth prefers fast and defect-free crystal growth. The average thickness (N_{th}) at which a thin, discontinuous film is expanding and achieving continuity, which given by[152] :

$$N_{th} = A(\frac{1}{R})^{(\frac{1}{3})} e^{(-\frac{1}{T_s})} \quad \text{..... (2.4)}$$

Where T_s, R and A are the temperature of the substrate, the deposition rate (supersaturation related) and a constant related to the materials respectively.

2.5.2 Advantage and Disadvantages of PLD

Pulsed laser deposition (PLD) has been evaluated at various research institutes since the invention of the laser, it has recently attracted considerable attention TCOs thin film growth. This section briefly introduces disadvantages and advantage of PLD.

As the sophistication of devices based on transparent conducting oxide materials increases, improved optical and electrical properties of the transparent conducting oxide films are required. Hence, many TF preparation methods have been used to enhance optical and electrical properties of these films, and the preparation parameters play an important role in controlling these. These methods involve vacuum evaporation, CVD, sputtering, and spray pyrolysis [162].However, these techniques require either a high substrate temperature during deposition (300°C –500°C) or a post deposition anneal of the films at temperature (400°C –700°C). These high temperature process mostly damage surfaces of both the thin film and/or the substrate. Some efforts have been made to make high-quality

films on low-temperature substrates by using electron beam evaporation and sputtering, which often leading to amorphous films with poor electrical properties.

PLD has been used for grow high performance TCOs films, and pulse laser deposition offers many advantages as compared to other methods. The composition of the films grown using pulse laser deposition is very close to that of the target, even for a multicomponent target. Pulse laser deposition films crystallize at lower temperatures of substrate relative to other (PVD) method because of high kinetic energy (>1 eV) of the ionized species and ejected atoms in the laser-produced plasma [155]. Because of the low crystallization temperature, Pulse laser deposition can be used for grow TCOs films especially on substrates made of plastic, which is essential for prepared of flexible flat-panel displays. Adurodija et al. in 2000[163] reported that crystalline, low resistivity, and highly transparent films have been fabrication from In_2O_3 and ITO targets at a low substrate deposition temperature (Ts) of 100°C by pulse laser deposition coupled with in situ pulsed laser radiation. The films deposited at RT yielded a low resistivity of $(2.0 \times 10^{-4})\Omega$-cm despite the fact that they were amorphous. The lowest resistivity of $(94 \times 10^{-6})\Omega$-cm was achieved at 300°C. Another advantage of pulse laser deposition for the growth of TCO films is an extremely smooth film surface as compared to films grown using other PVD methods Suzuki et al. in 2001[164] reported the production of ITO films with low resistivity and flat surface morphology by a magnetic field applied perpendicular to the plume produced by pulse laser deposition . Magnetic fields act on charged particles in laser produced plumes and affect the ionization of species such as molecules and atoms [165].

The main disadvantages of pulse laser deposition are creation of particulates, target degradation, small area deposition and narrow angle of stoichiometric transfer of target material. Among the disadvantages of the pulse laser deposition technique, the particulates creation are the major drawback to attain a high-quality thin film which makes it unsuitable for many applications, predominantly microelectronics, Micro-Electro-Mechanical Systems (MEMS) and photonics devices. However ultrafast lasers as femtosecond lasers, it provides a considerable advantages in film quality and deposition rate over traditional nanosecond lasers because the unique laser-material interactions associated with them.

2.6 Structural Properties

The structural properties are important tool for study the thin films crystallographic structure.

2.6.1 The X-ray diffraction (XRD)

One of the most important methods for qualitative study of crystalline compounds is X-ray diffraction (XRD). XRD is a commonly used experimental method for deciding crystal lattice parameters and desired orientation. The XRD mechanism is simple. If the Bragg's law is satisfied, constructive diffractions (or interference) from parallel planes of atoms with inter-planar spacing (d) occur when a monochromatic X-ray beam is incident onto a crystal sample [166-168].

$$2d \sin\theta = n\lambda \quad \ldots\ldots\ldots\ldots\ldots\ldots\ldots\ldots\ldots\ldots\ldots\ldots\ldots\ldots\ldots\ldots \quad (2.5)$$

Where:

n, θ and λ are integer that indicates the order of the reflection, Bragg diffraction angle of the XRD peak (degree) and the wavelength of the X-ray beam.

If the wavelength of the X-ray beam is known by measuring the Bragg angle (θ), the interplanar distance (d) can be obtained. These specific directions appear as spots on the diffraction pattern which called reflections, as shown in figure (2.4).

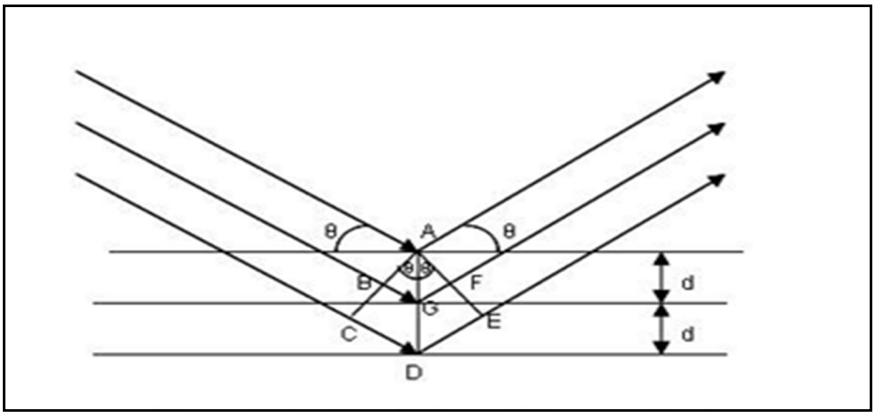

Figure(2.4): X-rays diffraction[168].

2.6.2 Parameters Calculation

XRD is commonly used to determine various parameters and to elucidate the investigations of deposited films.

A. Full Width at Half Maximum (FWHM)

The preferred orientation's FWHM (peak) may be estimated since it is equal to the width of the line profile at half the maximum intensity (in degrees)[169].

B. Average Crystallite Size (D)

The single line method is one of the many line profile analysis methods that use a Voigt function to calculate the average grain size (D) and the size-strain parameters (micro-strains and crystallite sizes), which can be calculated using the Scherer's eq.[170]:

$$D = \frac{0.94\,\lambda}{\acute{B}\cos\theta} \qquad \ldots\ldots\ldots\ldots\ldots\ldots\ldots\ldots\ldots\ldots\ldots\ldots\ldots\ldots \quad (2.6)$$

Where: Ɓ is FWHM by (radian).

C. Micro Strains (ε')

The crystal defects leads to a change in the space between the interlayers (d) or, to put it another way, a change in the spacing between the atomic surfaces causes a deformation in the crystal, which means that (d) is not equal in any point of the crystal, causing all parts of the crystal to reflects X-rays at angles different from the other parts, resulting in different angles of reflection from different parts of the crystal micro strain (**ε'**) occurs during film development as a result of expansion or compression of the lattice, and it is determined using the following equation[171]:

$$\varepsilon' = \frac{\beta\cos\theta}{4} \qquad \ldots\ldots\ldots\ldots\ldots\ldots\ldots\ldots\ldots\ldots\ldots\ldots\ldots\ldots \quad (2.7)$$

D. Dislocation Density (δ)

It refers to the number of dislocation lines that divide a unit area in a crystal, and it helps in crystallite size estimation (D), it can account for dislocation density (δ) arising from crystallite size in the Williamson and Smallmans equation[172]:

$$\delta \approx \frac{1}{D^2} \quad \ldots\ldots\ldots\ldots\ldots\ldots\ldots\ldots\ldots\ldots\ldots\ldots\ldots\ldots\ldots\ldots \quad (2.8)$$

2.7 Atomic Force Microscope AFM

Atomic force microscopy (AFM) is a widely used technique for quantifies surface topography and investigating the surface microstructure. The picture of a thin film surface may be zoomed using current and extremely sophisticated technological methods in the aforementioned approach. Its benefits include a large analysis capacity of up to (5×10^2 - 10^8) and the ability to operate it under ordinary barometric pressure without the need for high vacuum. As a result of the varying conditions and film processing process sand impurities used in the films, a strong distinction can be seen with the film surfaces under inspection. The end probe of the microscope has an arm (Cantilever) with a sharp tip (Tip) that is used to scan the sample surface. This arm is generally constructed of silicon nitride (Si_3N_4) and has a few nanometers in radius[173] . It's usually used to determine the surface area of insulators, conductive materials, and semiconductors. Atomic force microscopy was used to determine the average grain size and surface topography of the samples on an atomic scale[174]. It also provides us with extremely detailed statistics on roughness and grain size[175].

2.8 Field Emission Scanning Electron Microscope (FESEM)

Field Emission Scanning Electron Microscope (FE-SEM) offers ultra-high resolution imaging with low accelerating voltages and small distances working. It is one of the commonly used instruments in laboratories of material research. In this technique, instead of light waves, electrons are

used to see the microstructure of the sample surface. However since excited electrons to high energy (keV), so electron waves wavelength are quite small also resolution is quite high[176].

The electromagnetic lenses which are used in them are not part of the system of image composition, but only help to concentrate the electron beam on the sample surface. This provides SEM with two key advantages: the zoom range and field depth in the image, giving the image three-dimensional detail .Electrons are thermionically emitted from a cathode of tungsten or lanthanum hexaboride (LaB_6) in a typical SEM[177] and are accelerated to an anode; electrons may alternatively be emitted as field emission(FE). Tungsten is utilized because it has the greatest melting point and lowest vapor pressure of all metals, allowing it to be heated for electron emission. Through one or two condenser lenses, an electron beam with an energy spectrum ranging from a few hundred eV to 100 keV is condensed into a beam with an extremely small focus point of 1 nm to 5 nm. In the objective lens, the beam passes through pairs of scanning coils, which deflect the beam vertically and horizontally to scan over a rectangular region of the sample surface in a raster fashion. When the interacts happens between primary electron beam and the sample, the electrons lose energy inside a teardrop-shaped volume of the sample known as the volume of interaction, which ranges from less than 100 nm to around 5 μm into the surface through repeated scattering and absorption. The amount of the interaction depends on the accelerating voltage of the beam, the atomic number of the specimen and the density of the specimen. As mentioned below, the energy exchange between the beam of electron and the sample results in the emission of electrons and electromagnetic radiation that can be detected to create an

image. Low energy (<50eV) secondary electrons are controlled by the most common imaging mode because of their low energy, these electrons originate within a few nanometers from the surface. A scintillator-photomultiplier system senses the electrons and renders the resulting signal into a two-dimensional distribution of strength that can be displayed and processed as a digital image. This method is based on a primary beam raster-scanned. The signal brightness depends on the amount of secondary electrons that enter the detector. If the beam reaches the sample perpendicular to the surface, the triggered area will be uniform along the beam axis and a certain amount of electrons will escape from inside the sample. As the angle of incidence increases, the "escape" distance from one side of the beam decreases, and more secondary electrons are emitted. Therefore, steep surfaces and edges appear to be lighter than flat surfaces, resulting in well-defined, three-dimensional images. Resolutions of 1 nm are possible with this technique[178, 179].

2.9 Optical Properties of TCOs

2.9.1 Optical Absorption

The optical properties of TCOs such as T and A, transmission, and absorption, respectively also, band gap E_g and geometry are calculated. Geometry include film thickness and surface roughness of film. T and A, are intrinsic, depending on the solid structure and chemical composition of the material. The geometry, on the other hand, is extrinsic. There is a negative relationship between carrier density and the location of the infrared absorption edge, as well as a positive relationship between carrier density and the position of the UV absorption edge, with Eg increases at a large

carrier density (Moss-Burstein effect)[180, 181] . As a consequence, the conductivity and transmission boundaries of the TCO are related.

An important method for measuring the E_g of semiconductors is to measure the absorption (or transmission) of incident photons by the material. In this case, selected wave length photons are directed at the sample, and can observed the relative transmission of the various photons. Since photons with energies less than the band gap are transmitted while photons with energies equal or greater than the band gap energy ($h\nu \geq Eg$) are absorbed, the measurement of absorbed (or transmitted) photon can give the semiconductor band gap energy. Optical radiation is absorbed in semiconductors by causing excitation from one level to a higher one, provided that the radiation frequency ν is such that ($h\nu$) equal or greater than the energy difference between the two levels. The Lamberts equation, which is given by equation (2.9), has a dependency on the radiation intensity I in (W/cm^2) transmitted through the semiconductor with thickness t [182-184]:

$$I=I_o \exp(-\alpha t) \quad \ldots\ldots\ldots\ldots\ldots\ldots\ldots\ldots\ldots\ldots\ldots\ldots\ldots\ldots \quad (2.9)$$

where I_o, α are the initial intensity of radiation in (W/cm^2) and the absorption coefficient, respectively where the absorption coefficient have been defined as the amount of photons absorbed per unit distance of semiconductor. There are four major kinds of transition which can be brought by radiation: (a) intrinsic absorption, (b) Absorption of free carrier, (c) Localized states absorption and (d) Lattice absorption, (α) also absorption coefficient can be given by equation (2.16):

The laws for the conservation of energy and momentum, which are given as the following, include four transformation forms [185]:

a) Allowed direct transitions

The transformation occurs at the same wave vector from the top points of the valance band(V.B) and the bottom points of the conduction band(C.B), where (K=0) for conservation of momentum, as seen in figure (2.5.a). The following relationship describes the above transition[186, 187] :

$$\alpha h\nu = B'(h\nu - E_g)^{1/2} \quad \text{.....} \quad (2.10)$$

Where:

ν and B' are frequency in (Hz) and the constant (B') varied depending on the form of material (is inversely proportional to amorphousity) and 1/2 for Allowed direct transitions.

b) Forbidden direct transitions

If the transformation happens between states with the same wave vector that are not equal to zero ($\Delta K \neq 0$), it will occur near the top points in V.B and the bottom points in C.B, which can be seen in figure (2.5.b). This form of transformation is known as a forbidden direct transition, and its absorption coefficient is given by the equation below[185]:

$$\alpha h\nu = B'(h\nu - E_g)^{3/2} \quad \text{.....} \quad (2.11)$$

Two ways of transformation also have indirect transition.

c) Allowed indirect transitions

In this case, for the indirect transition the bottom of C.B is not over the top of V.B in curve of Energy-wave vector (E-K). The electron transits from V.B to C.B is not vertically where the wave vector value of electron

after and before the transition is equal not zero ($\Delta K \neq 0$). This transition type occur with helpful of particle which called as "Phonon", In order to maintain the law of energy and momentum, a phonon is then required to preserve the momentum, so[188]:

$$h\nu = E_g \pm E_p \quad \ldots\ldots\ldots\ldots\ldots\ldots\ldots\ldots\ldots\ldots\ldots\ldots\ldots\ldots \quad (2.12)$$

Where:

E_p is the absorbed energy or phonon emitted, where the negative sign when phonon absorption, and the positive signal when phonon emission. For an allowed indirect transition, the transition happen from the top of V.B to the bottom of the C.B, which can be seen in (2.5.c), so that[188] :

$$\alpha h\nu = B'(h\nu - E_g)^2 \quad \ldots\ldots\ldots\ldots\ldots\ldots\ldots\ldots\ldots\ldots\ldots\ldots\ldots\ldots \quad (2.13)$$

(d) Forbidden indirect transitions

The forbidden indirect transitions happens from any point near the top of valance band to any point other than the bottom of the conduction band, as figure (2.5.d). The absorption coefficient of transition with a phonon absorption can be given as[188] :

$$\alpha h\nu = B'(h\nu - E_g)^3 \ldots\ldots\ldots\ldots\ldots\ldots\ldots\ldots\ldots\ldots\ldots\ldots\ldots\ldots \quad (2.14)$$

Experimentally, the degree of the absorption coefficient can be separated between direct and indirect processes; α values can be taken $\geq 10^4$ cm^{-1} for direct transitions and $< 10^4$ cm^{-1} for indirect transitions at the absorption edge.

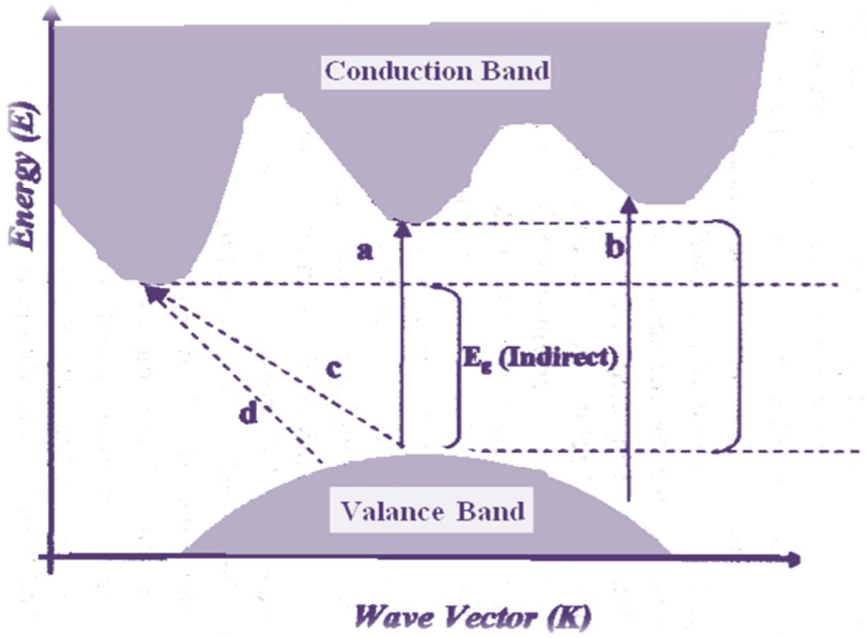

Figure(2.5): Types of the transition [169, 183] .

(a) Allowed direct transition. **(c) Allowed indirect transition.**

(b) Forbidden direct transition. **(d) Forbidden indirect transition.**

2.9.2 Optical Constants

Optical constants are very significant parameters when they describe the optical behavior of the material and optical constants list below:

2.9.2.1 Absorption Coefficient (α)

The absorption coefficient is defined as the ratio of incoming ray energy flux to the unit of distance in the direction of incident wave diffusion. Absorption coefficient (α) is determined by incident photon energy (hυ) and

semiconductor properties (p or n), with electronic transitions of type (p) or (n) and forbidden energy gap. According to Beer Lambert low[184] :

$$\alpha = \frac{1}{I}\frac{d[I]}{dt} \quad \ldots\ldots\ldots\ldots\ldots\ldots\ldots\ldots\ldots\ldots\ldots\ldots\ldots\ldots \quad (2.15)$$

α Also can be written as by:

$$\alpha = \frac{2.303 \times A}{t} \quad \ldots\ldots\ldots\ldots\ldots\ldots\ldots\ldots\ldots\ldots\ldots\ldots\ldots\ldots \quad (2.16)$$

Where (A) is absorbance and (t) is thickness of thin film.

For semiconductors, the coefficient of absorption is a strong related to the wavelength or photon energy. Photon energy can be written as:

$$E = h\upsilon \quad \ldots\ldots\ldots\ldots\ldots\ldots\ldots\ldots\ldots\ldots\ldots\ldots\ldots\ldots \quad (2.17)$$

Where h is Planck constant and υ is the frequency of the electron.

2.9.3 Absorbance (A)

Absorption can be defined as the ratio between the intensity (I_A) of absorbed light by material and the incident light intensity (I_o)[189] :

$$A = \frac{I_A}{I_o} \quad \ldots\ldots\ldots\ldots\ldots\ldots\ldots\ldots\ldots\ldots\ldots\ldots\ldots\ldots \quad (2.18)$$

2.9.4 Transmittance (T)

Transmittance is given by the ratio between the transmitting rays (I_T) intensity through the film to the incident rays intensity (I_o) on it as the relationship below[190] :

$$T = \frac{I_T}{I_o} \quad \ldots\ldots\ldots\ldots\ldots\ldots\ldots\ldots\ldots\ldots\ldots\ldots\ldots\ldots \quad (2.19)$$

Also can be find a transmittance as a function of wavelength through the exponential relationship for both transmittance and absorbance which [190]:

$$A = \log\left(\frac{1}{T}\right) \quad \ldots\ldots\ldots\ldots\ldots\ldots\ldots\ldots\ldots\ldots\ldots\ldots\ldots\ldots \quad (2.20)$$

2.10 Electrical properties of TCOs:

TCOs have found applications in a number of optoelectronic devices such as solar cells, light emitting diodes LEDs, and flat panels additionally, flexible displays[191]. It also plays an important role in gas sensors, solid state gas sensors by demonstrating gas response in terms of changing electrical characteristics. The semiconductors electrical properties depend upon the semiconductors nature, they being pure or doped, amorphous or crystalline. The chemical composition of a material is controlled not only by its chemical composition, but also by the arrangement of its atoms in the solid, and the existence of defects causes electron states to develop in the energy gap, affecting the material's electrical characteristics this defect can be minimized by a variety of methods, such as the annealing process [23].

2.10.1 D.C. Electrical Conductivity

In crystalline semiconductors, the D.C conductivity depends on both of the presence of positive holes and free electrons. At absolute zero, the V.B is regarded as filled and the C.B is empty. As the temperature is increased, the bonds break and the influence, is that free electrons are excited into the C.B, and this leaves behind holes in the V.B.

Electrical conductivity(σ) which define as the relative factor between the current density and the electric field, and the equation gives it [23, 192, 193]:

$$J = \sigma E_e \quad \ldots\ldots\ldots\ldots\ldots\ldots\ldots\ldots\ldots\ldots\ldots\ldots\ldots\ldots \quad (2.21)$$

Where: ($J = I / A$) and $E_e = V / \ell$

J, Ee, V and ℓ: are the current density, the electric field, the bias voltage and the electrode spacing distance (conductor length), respectively.

So

$$\sigma = n_e q \mu \quad \ldots\ldots\ldots\ldots\ldots\ldots\ldots\ldots\ldots\ldots\ldots\ldots\ldots\ldots \quad (2.22)$$

or

$$\sigma = \frac{(n_e q\, 2\tau)}{m^*} \quad \ldots\ldots\ldots\ldots\ldots\ldots\ldots\ldots\ldots\ldots\ldots\ldots\ldots\ldots \quad (2.23)$$

Where:

μ, τ, n_e , m* and q are the mobility of the carriers, the carrier's life time, the carrier's concentration, the effective mass of the carrier and the electron charge, respectively.

For semiconductors, the relation between the current density and electric field is written as [194] :

$$J = q\left(n\mu_n + p\mu_p\right)E_e \quad \ldots\ldots\ldots\ldots\ldots\ldots\ldots\ldots\ldots\ldots\ldots\ldots\ldots \quad (2.24)$$

Where:

The hole and electron concentrations are denoted by p and n, respectively.

μ_p andμ_n are the mobility of hole and electron, respectively.

The mobility is related to drift velocity (v_d) which given by the following equation [194]:

$$\mu = \frac{v_d}{E_e} \quad \ldots\ldots\ldots\ldots\ldots\ldots\ldots\ldots\ldots\ldots\ldots\ldots\ldots\ldots \quad (2.25)$$

By using eq. (2.23) so, that we have[195] :

$$\sigma = q(n\mu_n + p\mu_p) \quad \ldots\ldots\ldots\ldots\ldots\ldots\ldots\ldots\ldots\ldots\ldots\ldots\ldots\ldots \quad (2.26)$$

This essential association combines conductivity with the concentration and mobility of the electron and hole. [194] . For most instances of intrinsic semiconductors, the change of electrical conductivity with temperature is provided by [23, 194, 196, 197] :

$$\sigma = \sigma_o \exp\left(\frac{-E_a}{k_B T}\right) \quad \ldots\ldots\ldots\ldots\ldots\ldots\ldots\ldots\ldots\ldots\ldots\ldots\ldots\ldots \quad (2.27)$$

Where:

E_a , T and σ_o are the activation energy, the absolute temperature and the minimum electrical conductivity at 0K, respectively.

2.10.2 Hall Effect

Hall measurements are widely used in the initial semiconductors characterization to measure the mobility and carrier concentration, It's also used to tell if a semiconductor is p or n – type.

A continuous current (I) flows from left to right down the x–axis in the presence of a z–directional magnetic field (B). Initially, electrons are exposed to the Lorentz force, which causes them to drift toward the negative

y–axis, resulting in an excess surface electrical charge on the sample side and a transverse voltage. This voltage of transverse is referred to the Hall voltage (V_H), it can be seen in figure (2.6). The Hall coefficient (R_H) is calculated by measuring the Hall voltage that generates the Hall field across the sample with thickness (t),which given by[198] :

$$R_H = \frac{V_H}{I} \cdot \frac{t}{B} \quad \ldots\ldots\ldots\ldots\ldots\ldots\ldots\ldots\ldots\ldots\ldots\ldots\ldots\ldots\ldots\ldots \quad (2.28)$$

The carrier concentration of the semiconductor can be determined from the Hall coefficient equation as well as the carrier type, as R_H is negative and positive for the n-and p-type, respectively:

$$R_H = \frac{-1}{n.e} \quad \text{for n-type} \quad \ldots\ldots\ldots\ldots\ldots\ldots\ldots\ldots\ldots\ldots\ldots\ldots\ldots\ldots \quad (2.29)$$

$$R_H = \frac{1}{p.e} \quad \text{for p-type} \quad \ldots\ldots\ldots\ldots\ldots\ldots\ldots\ldots\ldots\ldots\ldots\ldots\ldots\ldots \quad (2.30)$$

Where: (e) is the electron charge. If the conduction is due to a single form of carrier:

$\sigma_H = e\, n_H\, \mu_n$ for n-type …… (2.31)

$\sigma_H = e\, p_H\, \mu_p$ for p-type …… (2.32)

Also can calculate the Hall mobility as[197]:

$$\mu_H = \frac{\sigma}{n.e} \quad \ldots\ldots\ldots\ldots\ldots\ldots\ldots\ldots\ldots\ldots\ldots\ldots\ldots\ldots\ldots\ldots \quad (2.33)$$

$$\mu_H = \sigma |R_H| \quad \ldots\ldots\ldots\ldots\ldots\ldots\ldots\ldots\ldots\ldots\ldots\ldots\ldots\ldots\ldots\ldots \quad (2.34)$$

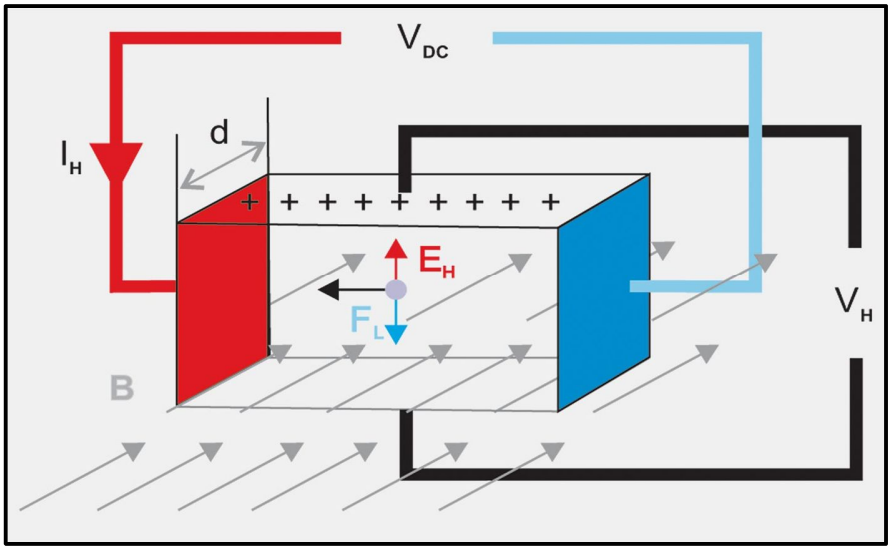

Figure (2.6): Hall effect schematic diagram [198].

2.10.3 Resistivity (ρ)

The semiconducting material conductivity, additionally it dependent on hole and/or electron concentration, is also a function of the mobility of the charge carriers. Any conductor's (film's) resistivity can be measured using this formula:

$$\rho = R_e \times A^* / L \quad \ldots\ldots\ldots\ldots\ldots\ldots\ldots\ldots\ldots\ldots\ldots\ldots\ldots\ldots \quad (2.35)$$

where (A*) is the area of the cross section (film sheet) and (L) is the conductor length (inter electrode spacing). The resistivity of a film is proportional to the electric field (E) and the current density flowing through it:

$$\rho = E / J \quad \ldots\ldots\ldots\ldots\ldots\ldots\ldots\ldots\ldots\ldots\ldots\ldots\ldots\ldots\ldots\ldots \quad (2.36)$$

where the electric field equals to (V/d), d is the electrode spacing distance ,V is the applied voltage, and the current density equals to (I/A*), it depends on the conductivity (or resistivity), that is on the carrier concentration (holes

or electrons). In specific, doping, temperature and deposition methods are influenced by too many parameters or conditions [199].

2.10.4 Mobility (μ)

For any application in photovoltaic , mobility is an important parameter for transport of carrier since it explains how strongly the electron motion is affected by an applied electric field [23].

$$\upsilon_n = -\mu_n \ E \qquad \ldots\ldots\ldots\ldots\ldots\ldots\ldots\ldots\ldots\ldots\ldots\ldots\ldots\ldots \quad (2.37)$$

In the conduction band, electrons have a comparable expression, while holes have a similar expression in the V.B:

$$\upsilon_p = \mu_p E \qquad \ldots\ldots\ldots\ldots\ldots\ldots\ldots\ldots\ldots\ldots\ldots\ldots\ldots\ldots \quad (2.38)$$

Where:

μ_n , μ_p , E, v_n and v_p are the electrons mobility , holes mobility electric field, the electron drift velocity and the hole drift velocity, respectively.

The holes in eq. (2.38) drift in the same direction as the electric field, so the negative sign was removed.

The mobility is directly connected to the mean free time between collisions in equation (2.39), which is determined by various scattering processes. Impurity scattering and lattice scattering are the two most important processes[23].

$$\mu = \left(\frac{q}{m_e^*}\right)\tau_c \qquad \ldots\ldots\ldots\ldots\ldots\ldots\ldots\ldots\ldots\ldots\ldots\ldots\ldots\ldots \quad (2.39)$$

Where:

τ_c: is mean free time (the collision time) .

Thermal vibration of the lattice atoms causes lattice scattering at any temperature above absolute zero (0K).These vibrations cause a disruption in the periodic potential of the lattice, allowing energy to be passed between the lattice and the carriers. Since vibration of lattice increasing with increase temperature, at high temperature the scattering of lattice becomes dominant, hence the mobility increasing with decrease temperature.

When a charge carrier passes through an ionized dopant impurity, it scatters (acceptor or donor).Due to Coulomb force interaction, the charging carrier direction would be deflected. The probability of impurity scattering depends on the overall concentration of ionized impurities, i.e. the sum of the concentration of ions charged negatively and positively. However, unlike lattice scattering, impurity scattering becomes less significant at higher temperatures. At higher temperatures , the carriers move faster, they remain near the impurity atom for a shorter time and are therefore less effectively scattered [23]. Electrical measurements of the films for CdO have resistivity, carrier concentration, and mobility in the range (2.65 to 6.64)× 10^{-6} Ω m, (1.60 to 2.35) × 10^{26} m^{-3}, and (57.65 to 100.48) × 10^{-4} m^2 v^{-1} s^{-1} respectively[118]. Kang et al. using the Boltzmann transport equation and the relaxation time approach, we computed the room-temperature mobility of Ga_2O_3 for carrier densities ranging from 10^{17} to 10^{20} cm^{-3}. For carrier densities of up to 10^{19} cm^{-3}, the electron-phonon interaction also dominates the mobility[200].

2.11 Sensing Properties

The identification of toxic gases has always been a challenging problem which finds a difficult to choose an effective gas-sensing metal oxide. Several gas-sensitive metal oxides have been documented and used in air quality control and industrial protection. But there are no such gas sensors exist that are hundred percent selective for a single gas. Achieving such selectivity requires the use of methods to classify gases using analytical techniques. The use of Ga_2O_3 and CdO as gas sensors and study of the sensing properties such as the sensitivity , response time and recovery time using dopants are under way to meet their ever- increasing demands in new applications[72-75, 100].

2.11.1 Chemical Sensor

"A chemical sensor is a system that transforms chemical information, ranging from the concentration of a particular sample component to complete composition analysis, into an analytically useful signal," according to the International Union of Pure and Applied Chemistry (lUPAC). The above chemical information may originate from a chemical reaction of the analyses or from a physical property of the system investigated". Typically, chemical sensors usually consist from two main pieces, a transducer and a receptor. The receptor converts chemical input into an energy state that the transducer can calculate, where converts this energy into a useful, typically electrical, analytical signal[201].

Chemical sensors are classified in several different ways. One of the classifications uses the operating principle [202] . This theory can be used to differentiate between:

• Physical sensors.

• Chemical sensors.

• Biochemical sensors.

2.12. Gas Sensor Characteristics

2.12.1. The Sensitivity

This is a device that detects changes in the chemical and/or physical characteristics of the sensing material as a result of gas exposure. To enhance it, it will be necessary to work with the most appropriate sensor materials in each situation[203]. Typically, sensitivity(S) is defined as the relative variation of the sensitive thin film's resistance in percent per million (ppm) of the gas concentration applied. In our work sensitivity was determined from relations (2.41) and (2.42). Certain core parameters that define and specify the gas sensor in detail are mentioned in the equation below:

$$\frac{R_i}{R_g} = \frac{G_g}{G_a} \qquad \text{..... (2.40)}$$

Where:

R_i , R_g ,G_a and G_g are the film resistance in the air ,the film resistance in presence of a gas ,the film electrical conductance in the air and the film electrical conductance in presence of a gas, respectively.

Another approach to calculate the sensitivity (S) by using equations (2.41) and (2.42) for oxidizing and reducing gases and vapors, respectively [204-209] :

$$(S) = \frac{\Delta R}{R_i} = \left|\frac{R_i - R_g}{R_i}\right| \times 100\% \quad \text{..... (2.41)}$$

$$(S) = \frac{\Delta R}{R_g} = \left|\frac{R_g - R_i}{R_g}\right| \times 100\% \quad \text{..... (2.42)}$$

Also can be determined from current as in the relation written below [210, 211]:

$$S = \frac{I_g - I_a}{I_a} \times 100\% \quad \text{..... (2.43)}$$

Where: I_a and I_g are the sample current measured at ambient environment and under the test gas, respectively. The sensitivity is strong dependent on operating temperature ,film thickness, presence of additives and crystallite size[212].

2.12.2 Response Time

The response time (τ_{res}) can be defined as mentioned earlier in the literature, as the time interval over which sensor material resistance of the attains a fixed percentage (usually 90 %) of final value when the sensor is exposed to the full scale gas concentration. A short response time is highly desirable in application for example detection of flammable or combustible gases to prevent fire [207, 213].

2.12.3 Recovery Time

Which can be define as the time interval above which sensor resistance reduced to (10%) of the saturation rate when the target gas is switched off also can be define as the time required to recover to within (10%) of the original baseline when the flow of oxidizing or reducing gas is removed. Figure (2.7) displays how this is calculated from sensor data plotting the conductance as a function of time and the sensor sited in reference (or artificial) air a sensor should have a short recovery time in order to be ready for the next detection [206, 207, 214].

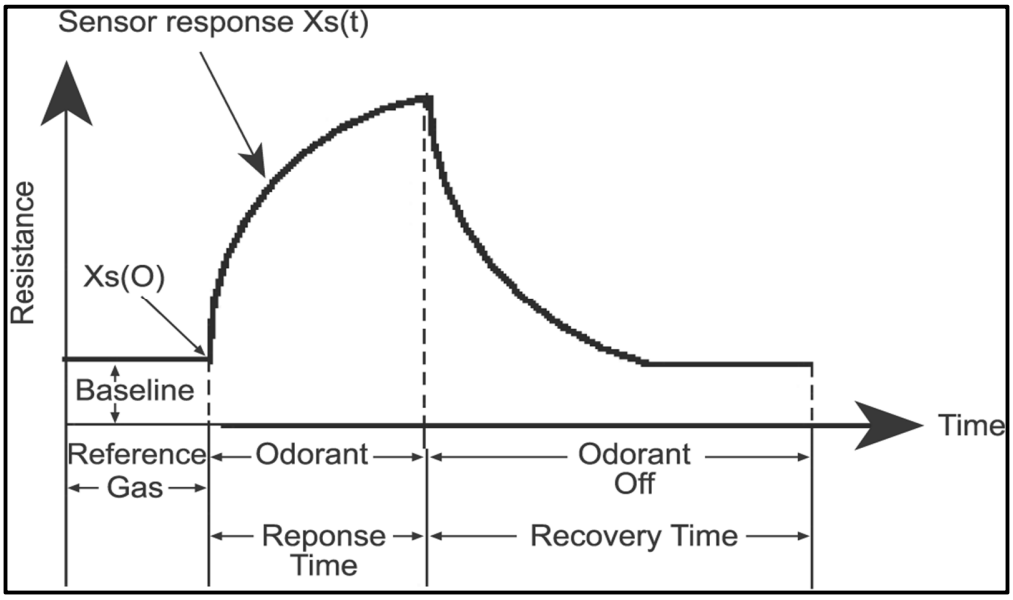

Figure (2.7): Atypical response curve of a ronductometric gas sensor [215].

Chapter Three

The Experimental Work

3.1 Introduction

This chapter includes the equipment description and the experimental details which have been used in investigation and fabrication of $Ga_2O_{3\ (1-X)}$ $CdO_{(X)}$ thin films using PLD method onto quartz substrates. The XRD, AFM, and FESEM techniques have been carried out to investigate the structural and morphological properties of the synthesized films. Also the electrical and the optical properties of the film have been studied. The sensing measurements presented by gas sensing are demonstrated as the final part in this work. Figure (3.1) depicts a schematic representation of the experimental study.

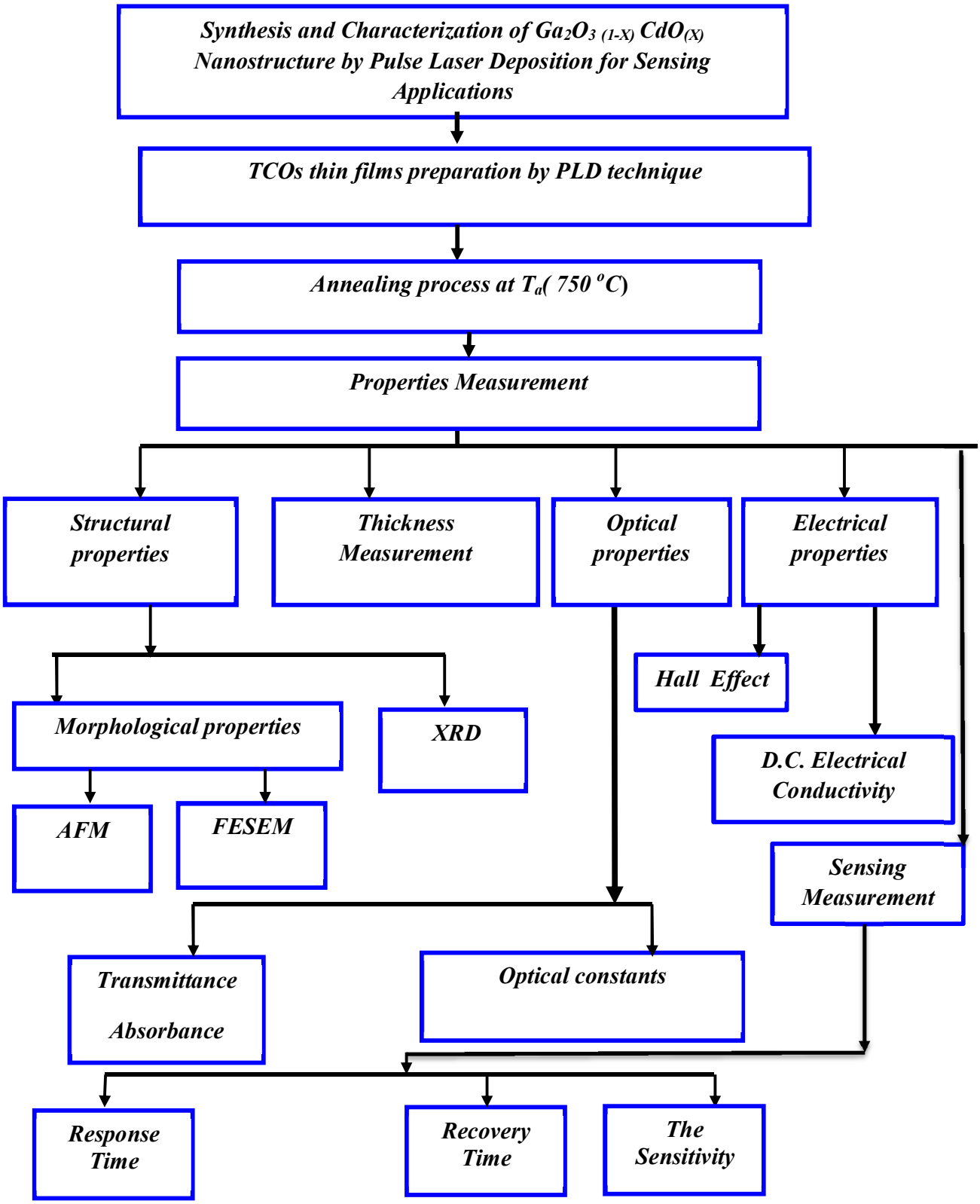

Figure (3.1): Schematic diagram of experimental work.

3.2 Targets Preparation

The $Ga_2O_{3\ (1-X)}CdO_{(X)}$ targets were used as powder ready materials supplied by (sigma chemical co.) with high purity (99.99%) , molar mass: 187.444 g/mol and 128.4112 g/mol for Ga_2O_3 and CdO, respectively, where used PLD method after hydraulic pressure of Ga_2O_3 and CdO were compressed into the shape of pellets (tablets) using a Chinese manufactured hydraulic piston with a strength of (300 kg/cm^2) as shown in figure (3.2). Before that the material was weighed and mixed as shown in the table (3.1).The pellets thickness of $Ga_2O_{3\ (1-X)}CdO_{(X)}$ targets were about (5) mm and (3) cm in diameter, and this provides a chance to use more sites than the piston pellets surface in processes of sedimentation to obtain more uniform films.

Table (3.1): Tablet weights and mixing ratios.

Sample name	Ga_2O_3 (g)	weight ratio	CdO(g)	weight ratio	Total (g)
0%	5	100%	0	0%	5
25% wt	3.75	75%	1.25	25%	5
50% wt	2.5	50%	2.5	50%	5
75% wt	1.25	25%	3.75	75%	5
100%	0	0%	5	100%	5

3.3 Films Deposition

The deposition process of thin films consists of the following steps:

3.3.1. Cleaning Substrates

To precipitate samples, quartz substrates have been used. The quartz substrates have been cutting into rectangular pieces (3.75 x 2.54) cm^2 with a thickness about (0.12) cm and (0.10) cm, respectively. The process of cleaning substrates are very important due to the influences of oil or dust effect on the properties of thin films. This process can be described as the following steps:

1) The substrates have been washed with distilled water and detergent to remove any contamination, then placed under tap water for 12 -15 min.
2) Using a clean beaker containing distilled water and placing the slides in it, the substrates can then be immersed in a beaker containing pure alcohol (C_2H_5OH) for 12-15 minutes to clear any oil.
3) The substrates was dried by exposing them to blown air and wiping them with fine cleaning paper. Finally, the slides are keeping in container and thus ready for the thin film deposition.

3.3.2 Pulsed Laser Deposition (PLD) Technique

The Q-switching Nd: YAG laser beam is focused via a window by a lens with a focal length of 30 cm as shown in figure (3.2). The beam of laser is passed into the chamber through a window made of quartz material. The chamber has more than one quartz windows, laser beam is admitted into one, whilst the others are employed in-situ plasma diagnostics and growth monitoring. The laser radiation is incident onto the surface of target with 45° angle. The substrate is positioned in target front (face to face) so that its surface is parallel to the targets. Between the substrate and the target, a

sufficient distance is maintained such that the incoming laser beam is not blocked by the substrate holding adjustment of the deposition components on a regular basis in order to get higher quality films via the process, such as heating the substrate, rotating the target, and positioning the substrate in respect to the target.

Figure (3.2):System of Pulsed Laser Deposition.

3.3.3 Nd: YAG Laser Source

Nd:YAG laser Q-switched , Second Harmonic Generation (SHG). (Diamond-288 pattern EPLS—Huafei Tongda Technology). For the deposition of $Ga_2O_{3\ (1-X)}CdO_{(X)}$ on various substrates, is utilized. The whole system is containing of light route system, power supply system, cooling system, computer controlling system, and the light route system is installed into the manual handle, controlling and cooling system are

installed into the machine box of power supply. The Nd: YAG laser system was utilized to precipitate thin films with easy-to-control major parameters, as shown in table (3.2).

Table (3.2): The Nd:YAG laser employed in the deposition process.

Wavelength	1064nm
Energy rate	500mJ
Pulse width	10 ns
Ambient temperature	30 ˚C
Frequency	6 Hz
Divergence	0.1mrad
Diameter of Beam	3 mm
Number of pulses	1000 pulse
Power supply	220 Volt
Cooling technique	inner circulation water cooling

3.3.4 Deposition Chamber

The deposition chamber is cylindrical in form. The chamber geometry may be created totally freely since the PLD technique does not require ultra-high vacuum. Pumping system, pressure monitoring, gas inlets, substrate, target, laser beam, and view components are often included in the chamber.

During the deposition process, the ablation target has been held in a vertical position by the target holder. It is necessary rotated during the deposition process, while the laser reaction spot is remained stationary. This arrangement provides an advantages, where the surface area of target may be used more effectively and successfully for a longer period without creating a hole.

3.3.5 Vacuum System

The deposition chamber has been fixed onto steel flange including a groove with O-ring for vacuum sealing and feed-through in the base for electrical connections (the substrate heater and control the stepper motor) and the chamber evacuated using rotary pump connecting directly to the chamber using steel flexible tubes to get a vacuum more than 10^{-2} mbar and by using Pirani gauge, monitoring the pressure inside the chamber. The rotary pump is a type (GALILEO TP model 949-9325S006) and it is the main part of the vacuum and diffusion pump from type (DIFFUSION PUMP DPF-4Z) which used to get vacuum of 10^{-6} mbar in chamber. For depositing all films and quartz substrates, has been used a Nd-YAG laser with deposition temperatures of (300) ^{o}C.

3.4 Deposition process

1. The vacuum chamber has been cleaning by acetone alcohol and a soft cloth after that leaving it about 24 h exposed to air.
2. Clean quartz and silicon substrates have been located on the substrate holder so that it is opposite the target placed on the rotating target holder so that the distance between the target and the substrate is (3) cm.
3. Focus the laser beam of Nd-YAG with energy (500mJ) and pulses number (1000) pulse on the targets using a lens with a convex focal length (30cm) on the surface of the rotating target at a fall angle of approximately 45^{o}.
4. The vacuum chamber is closed with all valves closed and the discharge process starts using opening the valve of rotary pump when the pressure reaches about(10^{-2})mbar then it closed and the valve of diffusion pump is opened until the vacuum chamber reaches (10^{-5})mbar.
5. To increase the material removed adhesion to the substrate, the substrate is heated by a halogen lamp until the temperature reaches 300˚C
6. Plasma state is produced by laser pulses and the particles reach to the substrate and deposit with the discharge chamber valve remaining open, all films were annealed in air at a temperature 750°C for 5 h.
7. Finally, the thin films of $Ga_2O_{3\ (1-X)}CdO_{(X)}$ material are obtained on quartz substrates and are subjected to structural, electrical, optical and gas sensor tests.

3.5 Measurement of Thin Films Thickness

The prepared films thickness was measured using the optical interference technique using a He-Ne laser with a wavelength (632.8) nm and incident angle 45° can be observed figure (3.3). The operation principle of above method is depend on the interference principle of light waves, which reflected from the prepared thin films surface and those that are reflected onto the substrate on which the films were deposited are prepared and can be using the following relation for calculated the thickness of the films [216]:

$$t = \frac{y}{x} \times \frac{\lambda}{2} \qquad \text{.....(3.1)}$$

Where: t, x, y and λ are the thickness of the film, width the light fringes, width the dark fringes and λ the wavelength of the laser light, respectively.

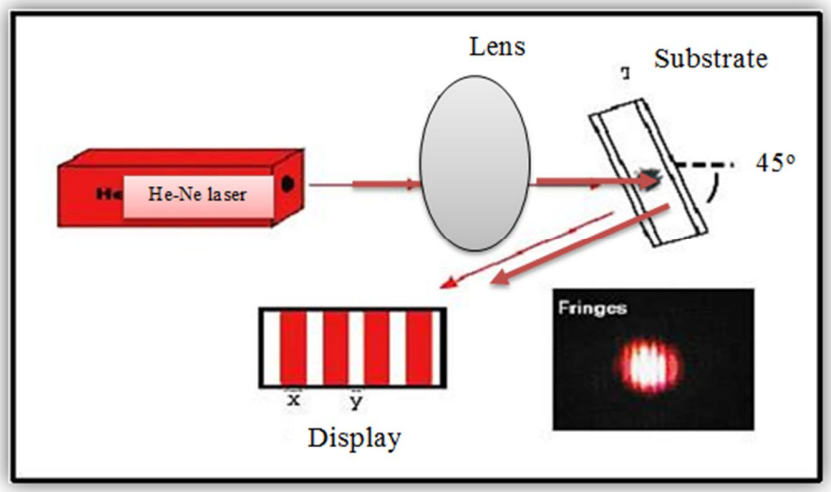

Figure(3.3):Thin film thickness measurement scheme using optical interference[216].

3.6 Structural Measurements and Topographic Surfaces

3.6.1 X-ray diffraction (XRD)

Technique of X-ray diffraction was used to examined the crystal structure of TCOs thin films ,The samples were examined using device from model (pw1730) PHILIPS company, which is located at Shahid Beheshti University , following specifications of the device included in the table(3.3):

Table (3.3): XRD device specifications.

Target	Cu
Step size	0.05deg
Time per step	1s
Wavelength	1.540598A°
Current	30 mA
Voltage	40 kV
Range (2θ)	from 10 to 80 deg.

3.6.2 Field Emission Scanning Electron Microscopic (FESEM)

Via high-resolution photographs and magnification, describe the essence and morphology of the prepared thin films' surface, as well as the internal structure of the thin films' substance. Photons with X-ray wavelengths are produced when primary electrons reaction with the sample. The atomic ratio in the sample can be measured using energy dispersive spectroscopy after this emission is detected by (ΣIGMA, JSM-7610F,Carl Zeiss, Germany) image operating at an accelerating voltage of 10 kV the surface morphology and element ratio of the prepared thin films was studied using FESEM which is located at Shahid Beheshti University.

3.6.3 Atomic Force Microscope (AFM)

For the purpose of knowing the thin films topography of the TCOs prepared using PLD technique, this was done by the Atomic Force Microscope (AFM) equipped by (BRUKER) type (ICON) which is located at Shahid Beheshti University.

3.7 Optical Measurements

Optical measurements including the transmittance and absorbance spectrum of deposited films were performed using (UV-Visible Spectrophotometer / 2700) two-beam supplied from the (CECIL) English company. The thin films are deposited on a quartz substrates that is well positioned in the substrate window, allowing light to radiate vertically to the thin film. A non-deposited quartz sample with a deposited quartz placed into the window is for the purpose of determining the absorbance of thin films only, it is often used as a reference to minimize the quartz influence. The optical energy gap (Eg) was determine as well as measuring the optical constants involve the absorption coefficient (α), which is located in our college .

3.8 Electrodes Deposition and Preparation of Masks

Three types of masks were made for electrical and sensing measurements. All masks are shown in the figure (3.4) are used aluminum sheets to get the required form of electrodes. These masks have the same dimensions as the substrate and have been attached and fully fastened to cover the substrate after cleaning. The golden electrodes were deposited on the surface of thin films using the spraying technique of the type

(CRESSINGTON-108). The device is located in the College of Science, University of Baghdad.

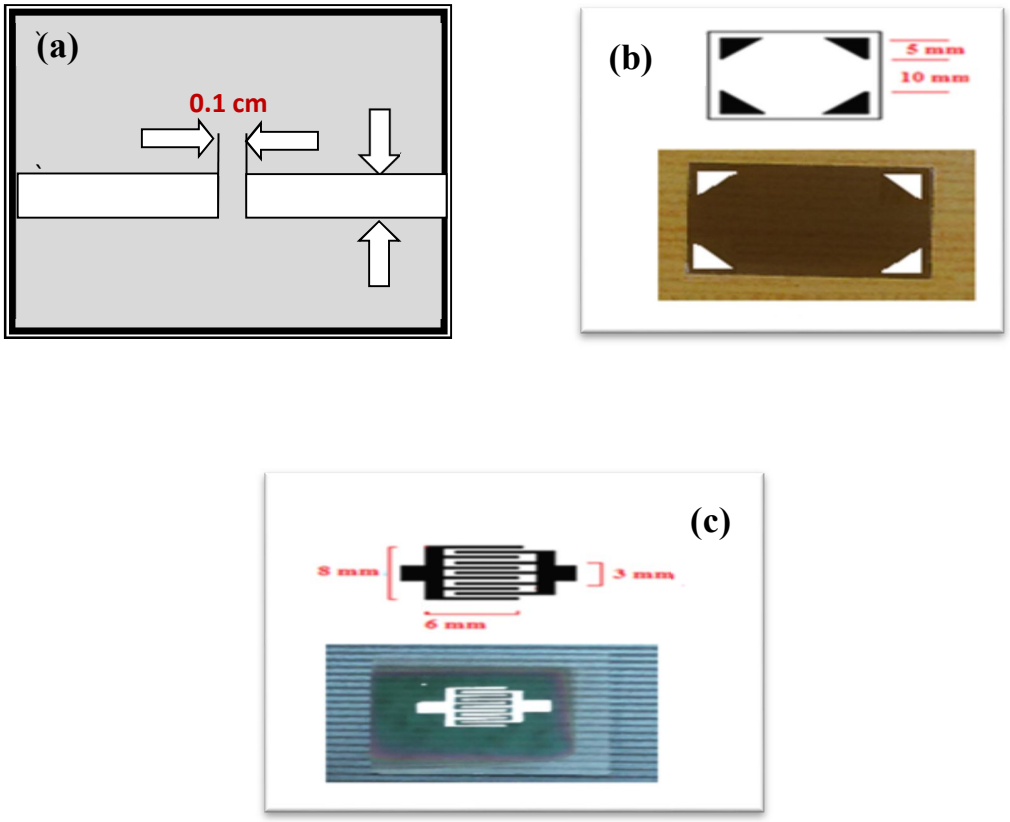

Figure (3.4): The mask patterns which used in (a) D.C conductivity measurement (b) Hall effect (c) sensing measurement.

3. 9 Electrical Properties

3.9.1 D.C Conductivity Measurements:

The direct electric conductivity (D.C) of the thin films deposited are measured through usage the device .It includes an electric oven type (Memmert Lab Oven UFB 400,400W) and Keithly version 2400, the films are positioned within the oven and from oven manage adjusted temperature to (453) ^{0}K, the films connecting with Keithly through wire and adjusted

onto resistant scale. The device is located in the College of Science, University of Baghdad.

3.9.2 Measurement of Hall Effect

Hall effect measurements of deposited films were carried out to calculated the charge carriers type and to calculated the Hall coefficient (R_H), concentration of carrier, resistivity and mobility, by using device(Measurement Hall Effect System) type of (HMS 3000) manufactured by (ECOPIA) Taiwanese origin with using intensity magnetic field (B = 0.55 T) and through the relationship between measured current (I) and Hall voltage (V_H), it is possible to identify both of type and density of charge carriers if the relationship is direct, the film is a positive type (p-type) while the relationship is inverse, the film is negative (n-type). The device is located in the College of Science, University of Baghdad.

3.10 Gas Sensor System

Sensor measurements carried out by measuring the variation in resistivity resulting from exposing the surface of the thin film to gas (NH_3 and NO_2), and the temperature is recorded by a thermocouple type-K (XB 9208B). The bias voltage was provided by the power provider (FARNELL E350). Resistance is recorded through (Fluke Digital Multimeter 8845A / 8846 A) and the sensor characteristics of thin films are measured using it. The device is located in the College of Science, University of Baghdad.

Chapter Four

Results and Discussion

4.1 Introduction

This chapter will present the results and analyses of the experimental measurements and testing of the deposited thin films, structural, optical, electrical, and gas sensor characteristics. XRD, AFM, SEM, and EDX are used to investigate the structural characteristics of $Ga_2O_{3\ (1-X)}CdO_{(X)}$. The optical characteristics are investigated, and additional parameters such as absorption coefficient, refractive index, extinction coefficient, and the real and imaginary parts of the dielectric constant are calculated as a function of wavelength. DC conductivity, Hall Effect, and electrical measurements of hetrojunctions, including current-voltage characteristics in two cases of darkness and illumination characteristics, are also included in the electrical properties. Finally, the gas sensing characteristics for all deposited thin films have been studied. It was found that the thickness of the thin films are (250 $\pm$5) nm.

4.2 Structural Properties

In this section, will be studied the structure and surface morphology properties for $Ga_2O_{3\ (1-X)}CdO_{(X)}$ thin film that deposited onto quartz substrates.

4.2.1 X-Ray Diffraction Analysis (XRD)

Figure(4.1) shows that, the XRD spectrum of pure Ga_2O_3 (0% CdO) , which shows peaks at 2θ equal to (30.0°), (33.6°) ,(35.1°) and (64.63°), which correspond to reflections from (400),(002), (111) and (512) based on standard (JCPDS Card No: 41-1103)[217] where the better orientation along (002) plane ,these reflections represent a polycrystalline structure with Monoclinic system .

The spectra of $Ga_2O_{3\ (1-X)}CdO_{(X)}$ films which exhibited sharp peaks in the case of pure CdO (100%) at 2θ equal to (33.0°), (38.2°) ,(55.2°), (65.9°) and (69.3°) , which correspond to reflections of Millar indices (111),(200), (220) ,(311)and (222), based on standard (JCPDS Card No: 05-0640)[218] while better orientation along (111) plane ,these reflections depict a polycrystalline cubic structure.

The patterns of XRD analysis of $CdGa_2O_4$ films of (25% wt , 50% wt and 75% wt) of CdO show notable peaks at 2θ equal to (29.3°),(34.6°),(36.2°),(42.0°),(45.9°),(52.1°),(55.5°) and (69.07°) , which correspond of reflections from (220),(311), (222) ,(400),(331),(422),(511) and (620), based on standard (JCPDS Card No:20-0863)[219] where the better orientation is (311) plane ,these reflections depict a polycrystalline structure with cubic system . The 25%wt, 50%wt and 75%wt films showed that $CdGa_2O_4$ compound according to standard (JCPDS Card No: 20-0863)[219] also can be seen that, the intensity of peaks at (36.2°) , (52.1°), (55.5°) and (69.07°) slightly increases as CdO concentration increasing due to the different of atomic radius 155 pm[220] and 130 pm[221] of Cd and Ga respectively.

The XRD confirmed data pattern has been listed in the table (4-1) which showed an excellent consistent with the interplanar distance standard values.

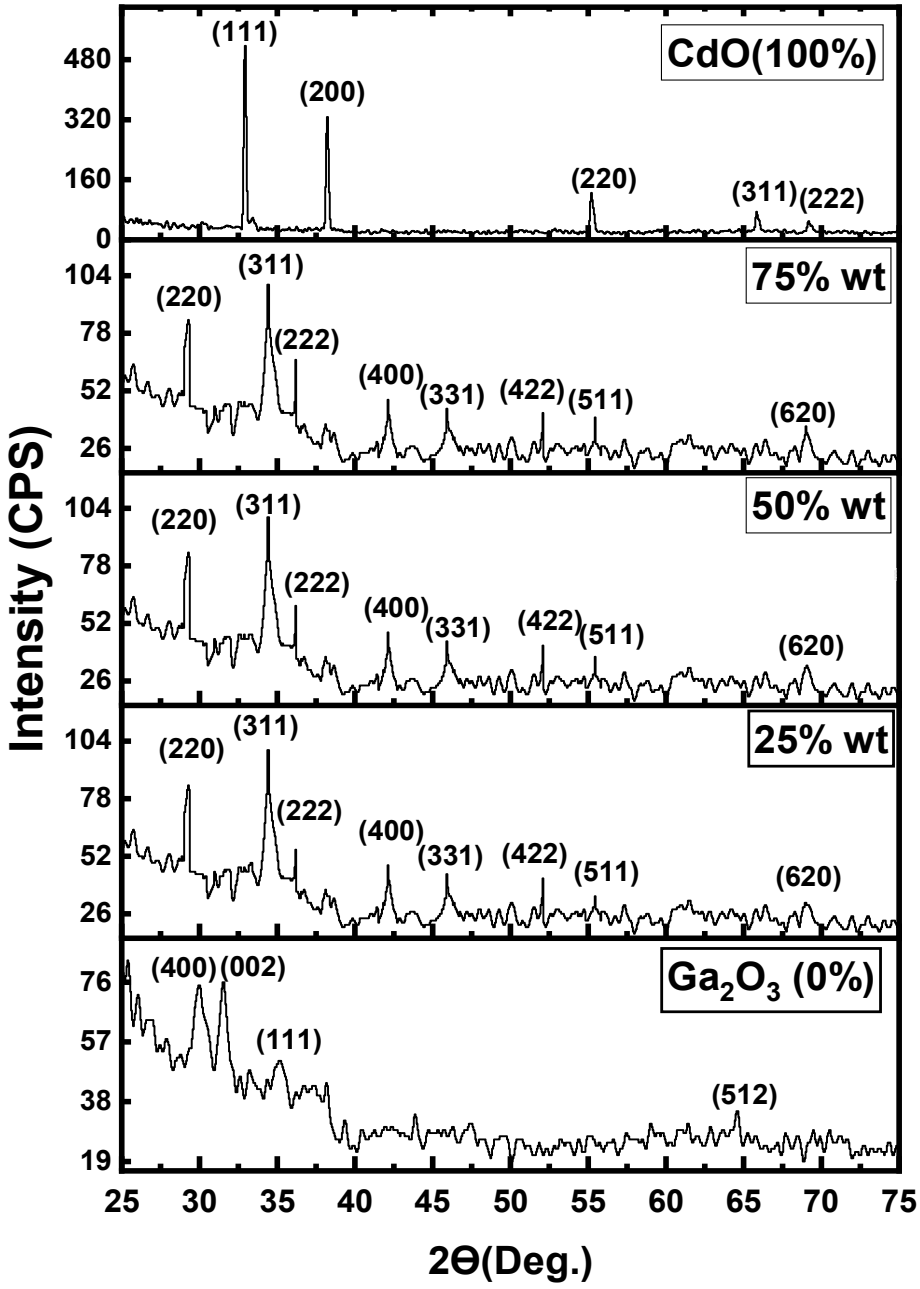

Figure (4.1): The X-ray diffraction (XRD) patterns of $Ga_2O_{3\ (1-X)}CdO_{(X)}$ films at different ratios.

Table (4.1): The confirmed data of XRD pattern of $Ga_2O_{3\ (1-X)}CdO_{(X)}$

Samples	Θ(deg)	Θ(rad)	Cos θ	FWHM (deg)	FWHM (rad)	C.S (nm)	dislocation density (δ) nm	Strain (ε) nm	hkl	Standard d(nm)	d (nm)
Ga_2O_3	15.04	0.262364	0.965779	0.25	0.004361	32.91981	0.000923	0.001053	400	2.82	2.8
	15.8	0.275622	0.962256	0.24	0.004187	34.41703	0.000844	0.001007	002	2.55	2.48
	17.565	0.306412	0.953422	0.26	0.004536	32.06393	0.000973	0.001081	111	2.93	2.87
25%wt	14.7	0.256433	0.967301	0.4	0.006978	20.54252	0.00237	0.001687	220	2.59	2.53
	17.295	0.301702	0.954832	0.39	0.006803	21.34438	0.002195	0.001624	311	3.04	3.08
	18.1	0.315744	0.950565	0.14	0.002442	59.72624	0.00028	0.00058	222	1.65	1.67
50%wt	14.7	0.256433	0.967301	0.4	0.006978	20.54252	0.00237	0.001687	220	2.59	2.53
	17.295	0.301702	0.954832	0.39	0.006803	21.34438	0.002195	0.001624	311	3.04	3.08
	18.1	0.315744	0.950565	0.16	0.002791	52.26046	0.000366	0.000663	222	1.65	1.67
75%wt	14.7	0.256433	0.967301	0.4	0.006978	20.54252	0.00237	0.001687	220	2.59	2.53
	17.295	0.301702	0.954832	0.39	0.006803	21.34438	0.002195	0.001624	311	3.04	3.08
	18.1	0.315744	0.950565	0.163	0.002843	51.29861	0.00038	0.000676	222	1.65	1.67
CdO	16.5	0.287833	0.958861	0.12	0.002093	69.07776	0.00021	0.000502	111	2.66	2.71
	19.1	0.333189	0.945004	0.12	0.002093	70.09068	0.000204	0.000495	200	3.06	2.95
	27.6	0.481467	0.886317	0.18	0.00314	49.82116	0.000403	0.000696	220	1.88	1.66

As shown in table (4.1) , the structure of all the films within nanoscale and the calculated average value of crystallite size film equals to (33.13, 33.87, 31.38, 31.06, 62.99) nm for 0%, 25%wt, 50%wt, 75%wt and 100% , respectively. And the values of average crystallite size of the $Ga_2O_{3\ (1-X)}CdO_{(X)}$ have been decreased due to the addition of CdO to the Ga_2O_3 to make the compound cadmium gallium oxide. Hence the average values of the dislocations (δ) and the strain (ε) are listed in the table (4.2). The values of the dislocations (δ) and the strain (ε) have been increases as the concentrated ratios (0 %, 25%wt, 50%wt, and 75%wt) of CdO increasing, because the films have high crystalline quality and low imperfections, and the better is related to CdO, but at 100wt% the values are low, and the crystalline size are higher than other values.

Table (4.2): The important calculated structural parameters of $Ga_2O_{3\ (1-X)}CdO_{(X)}$

samples	avg.(D)	avg.(δ)× 10^{-3}	avg. strain× 10^{-3}
0%	33.13	0. 913	1.047
25% wt	33.87	1.615	1.297
50% wt	31.38	1.644	1.325
75% wt	31.06	1.648	1.329
100%	62.99	0. 272	0. 564

4.2.2 Atomic Force Microscope (AFM)

The average roughness (R_a), the root mean square (RMS) values, and average grain size of thin films prepared using PLD technique were decreases as the ratio weights increasing because of conforming crystalline between two oxides, and so get associated and these decreasing Ra, RMS and grain sizes of the specimen as tabulated in the table (4.3), which show that $Ga_2O_{3\ (1-X)}CdO_{(X)}$ thin films annealed at temperature 750 ^{0}C for 5h in the air . Our results showed that the roughness of the prepared films decreases with the increasing in the concentration of CdO. The production of agglomerated grains one on top of the other is shown by the white patches in these figures. As a result, nearby grains cluster together to create enormous clusters. As a result, It is refereed that grains in white areas are bigger than those in other areas. It can also be noted that, increasing the concentration of cadmium oxide improves the structural properties and the crystalline structure of the films, and this leads to the improvement of the rest (stabilization) of the properties, such as the sensitivity properties, and this is in excellent agreement with the results of both XRD and FESEM. Figures (4.2), (4.3), (4.4), (4.5) and (4.6) show the three-dimensional and two-dimensional images of the films deposited by laser method, which were annealed under the same conditions, which caused regulation in molecular positions where it can be seen that the films become more homogeneous when the concentration of CdO increases in addition to position ordered.

Table (4.3): AFM parameters for $Ga_2O_{3\ (1-X)}CdO_{(X)}$ thin films.

Sample	RMS (nm)	R_a(nm)	Average Diameter (nm)
0%wt	3.77	3.49	98.5
25%wt	3.19	3.06	94.7
50%wt	2.58	2.81	92.6
75%wt	2.08	2.01	91.2
100%wt	3.05	3.09	95.6

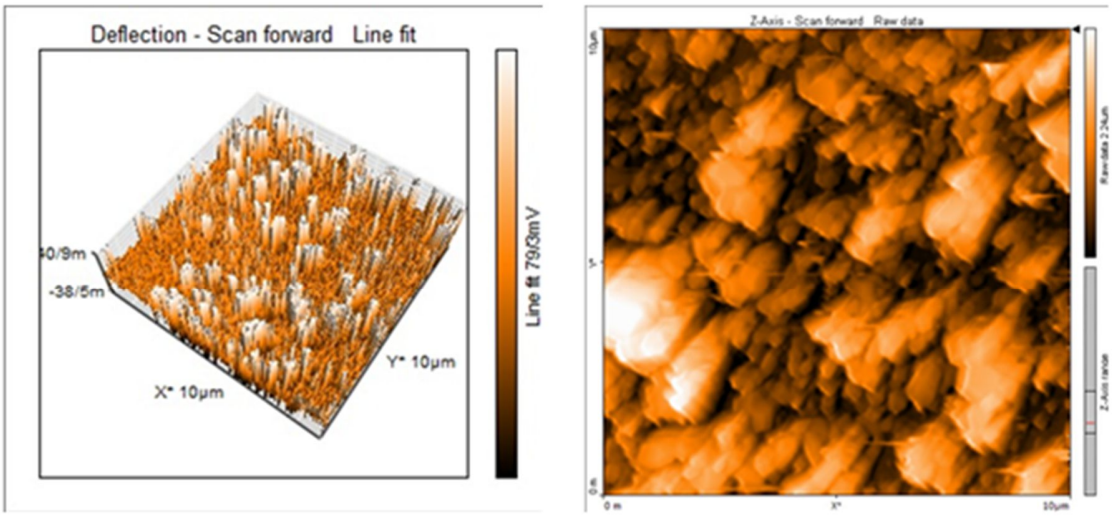

a b

Figure (4.2a,b): Topographic surface of 0%wt (Ga_2O_3)films in (a) 3-D (b) 2-D

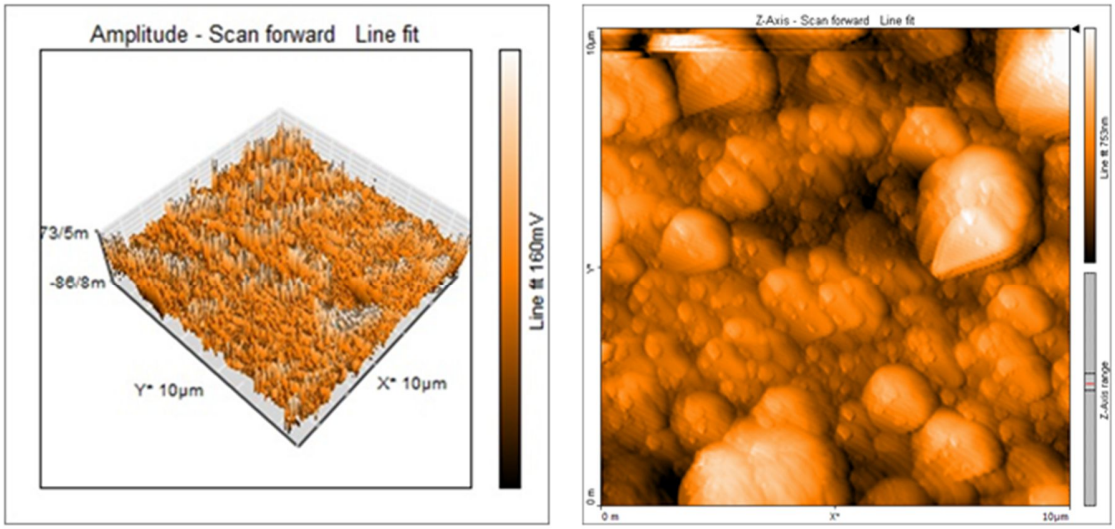

Figure (4.3a,b): Topographic surface of 25%wt of CdO films in (a) 3-D (b) 2-D

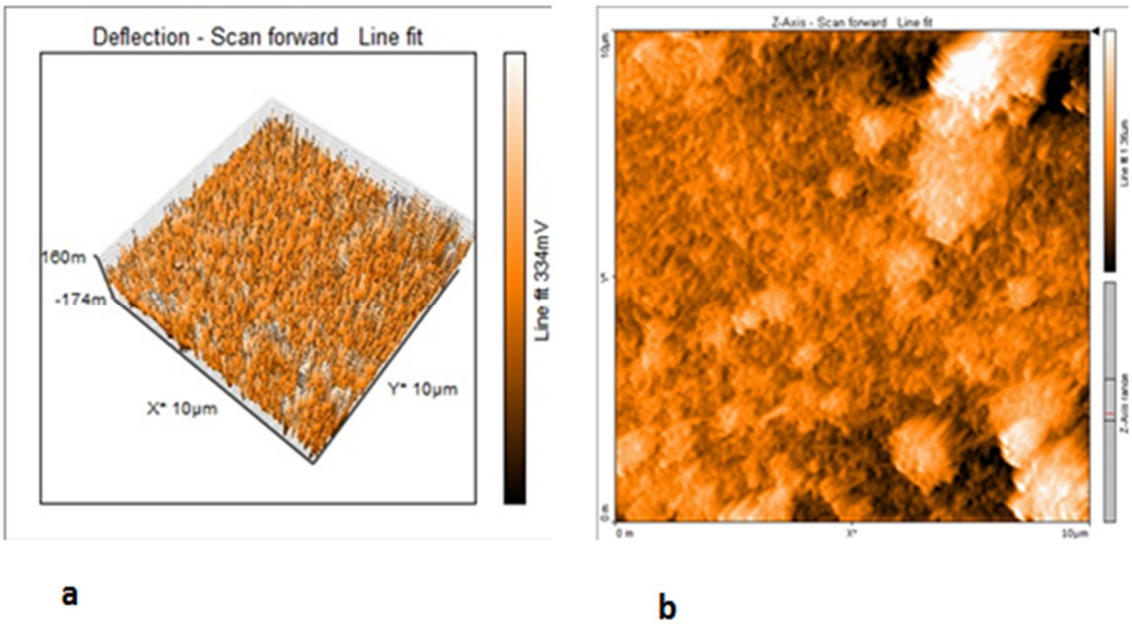

Figure (4.4a,b): Topographic surface of 50%wt of CdO films in (a) 3-D (b) 2-D

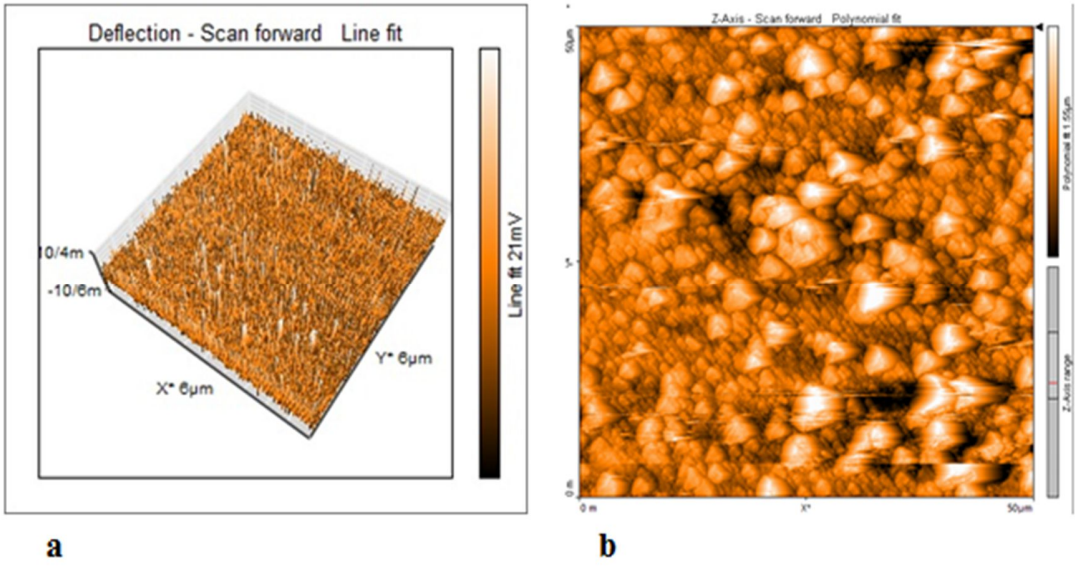

Figure (4.5a,b): Topographic surface of 75%wt of CdO films in (a) 3-D (b) 2-D

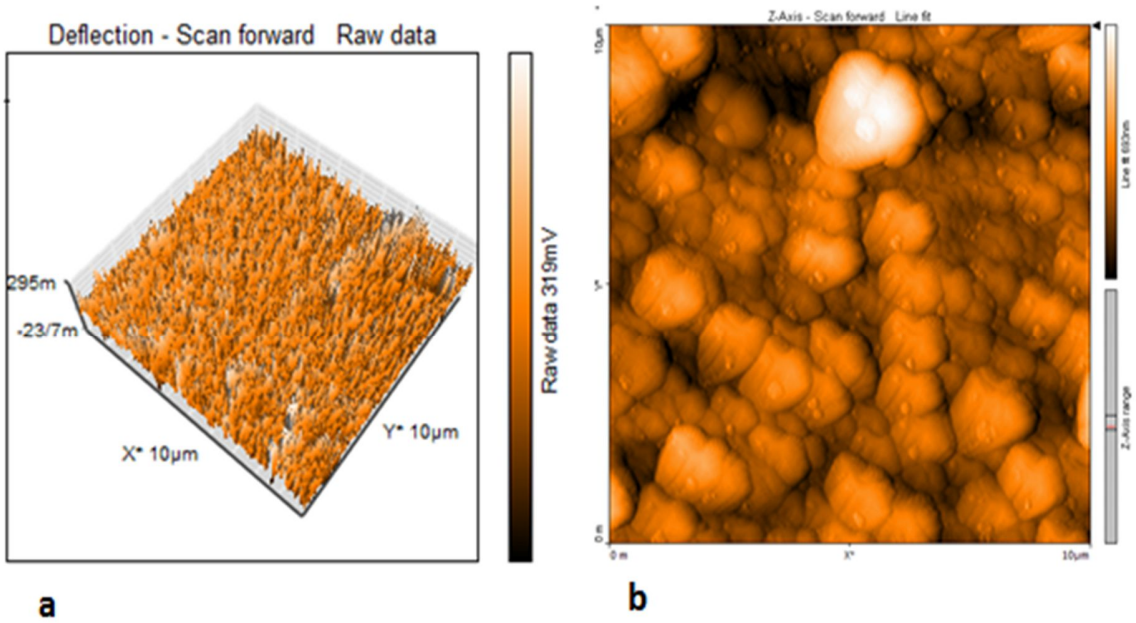

Figure (4.6a,b): Topographic surface of 100%wt(CdO) films in (a) 3-D (b) 2-D

4.2.3 Field emission Scan Electronic Microscope (FESEM)

The FESEM was used to examine the morphology of surface and estimate films that had not uniform morphology of surface through the analytical findings of (FESEM) for films deposited on quartz substrates prepared using the PLD technique.

The electrical and optical properties of TCO films are understood to be influenced by their surface properties, which are essential factors for applications in optoelectronic systems[222].

FESEM images of $Ga_2O_{3\ (1-X)}CdO_{(X)}$ which were deposited under the same conditions and the same annealing temperature for all films. From the images, various sizes of grains have been see in $Ga_2O_{3\ (1-X)}CdO_{(X)}$. The figures show clusters and agglomerates due to 5 hour high temperature annealing (750°C) for all films under studying. It is observed that the shape of the grains are semi spherical for all films. While the films of pure Ga_2O_3(0%) ,25% wt and 50%wt of CdO are a semi spherical shape with a hole that showed in figures (4.7), (4.8) and (4.9), With the increasing in the concentration of cadmium oxide, it can be observed that the holes in the grains disappear and its clusters to make the grains more dense as shown in figures (4.10) and (4.11) for 75% wt of CdO and CdO (100%) respectively .The average particles size of the films are approximately, 98.4nm,96.8nm,94.2nm,92.1nm and 93.9nm for Ga_2O_3 (0%),25% wt,50% wt ,75% wt of CdO and CdO (100%), respectively so that the average particles size decreases with increasing CdO concentration.

The increases grain boundary density and decreases grain size due to the same reason mentioned above, which is an increasing in CdO

concentration. It has been observed that there is a little homogeneity of film grains that take the semi spherical shape with a decrease in grain size because of an increasing in the concentration of CdO and formed the compound of $CdGa_2O_4$ in the case of 25% wt, 50% wt and 75% wt of CdO. FESEM result agreement to XRD results.

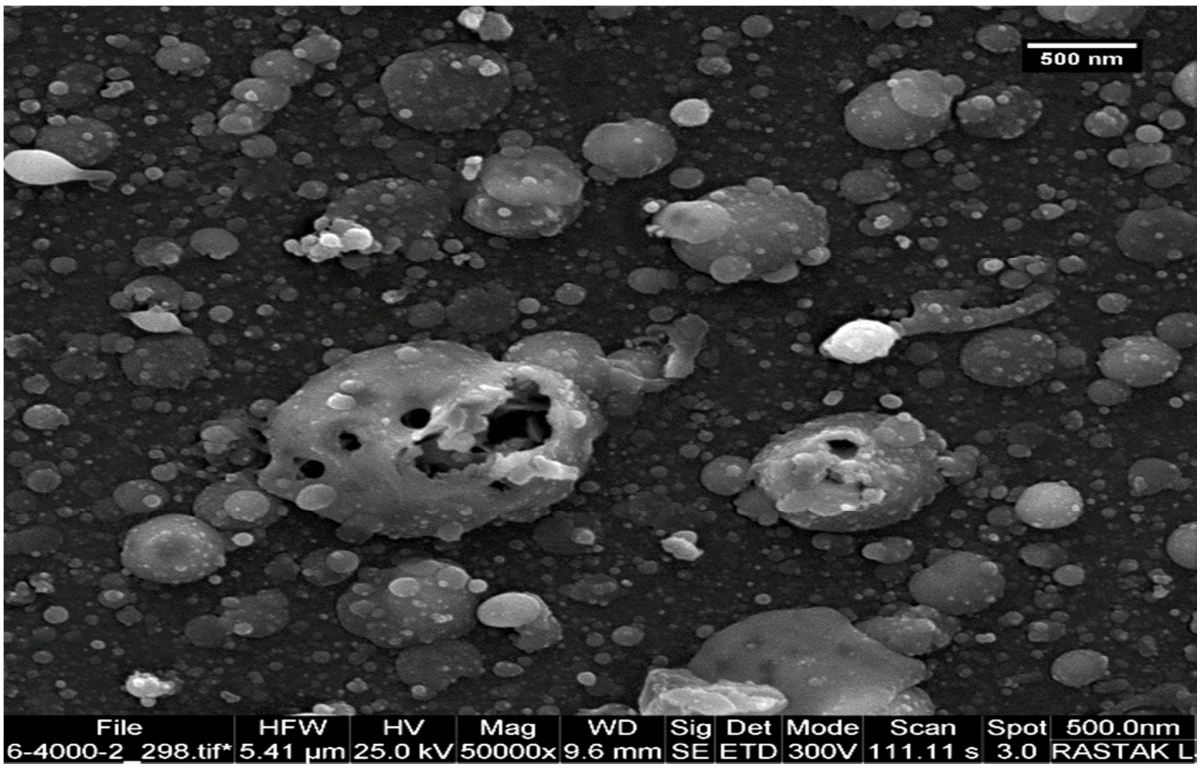

Figure(4.7): The FESEM image of pure Ga_2O_3 (0%) thin film.

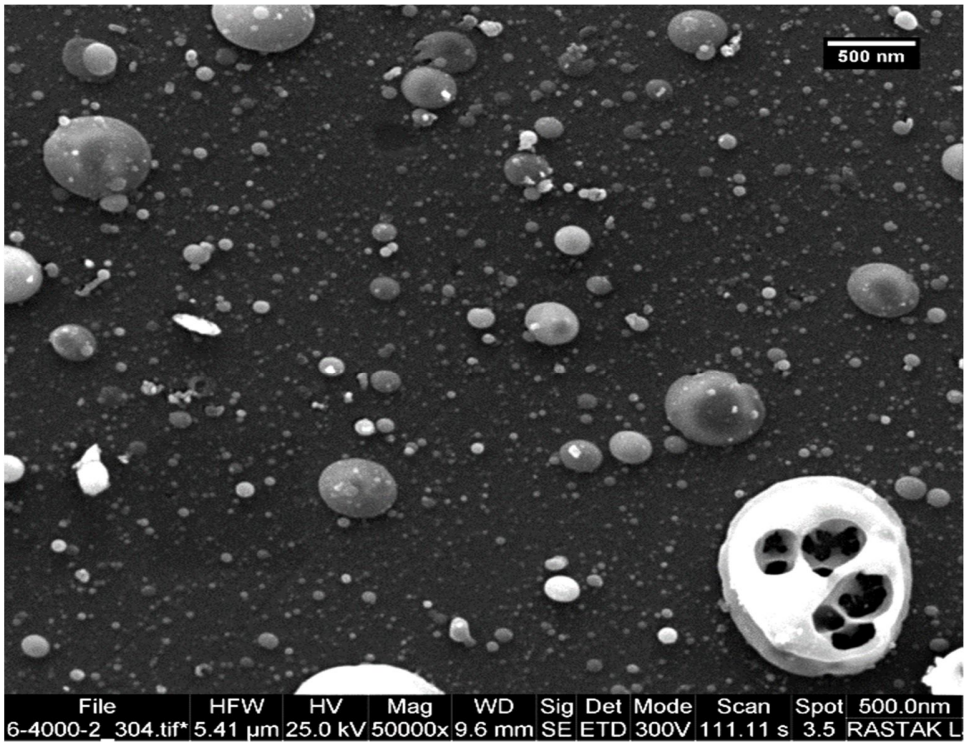

Figure(4.8): The FESEM image of (25% wt) of CdO thin film.

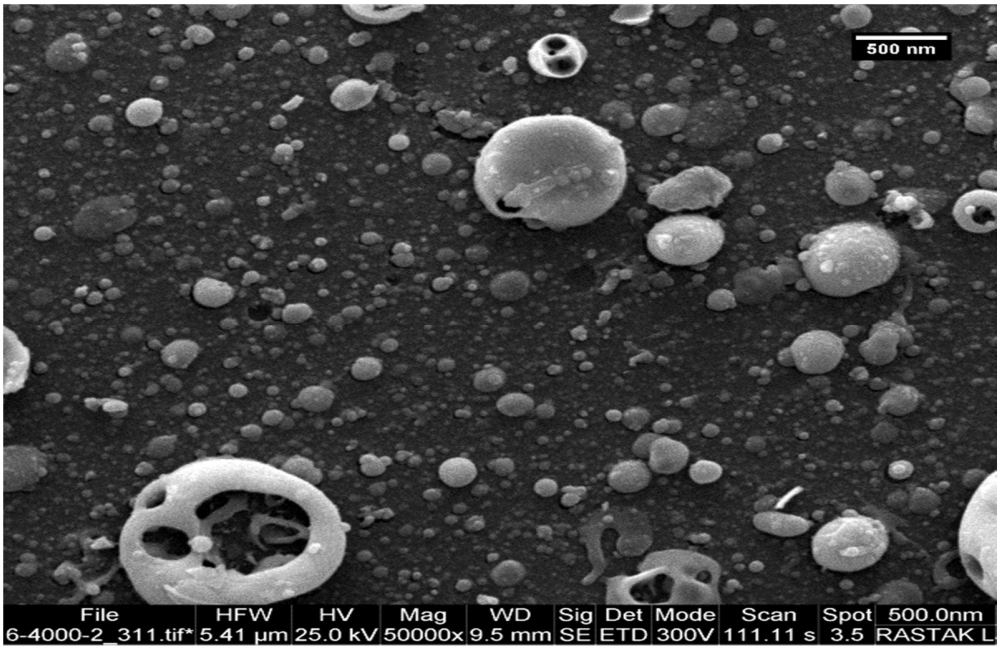

Figure(4.9): The FESEM image of (50% wt) of CdO thin film.

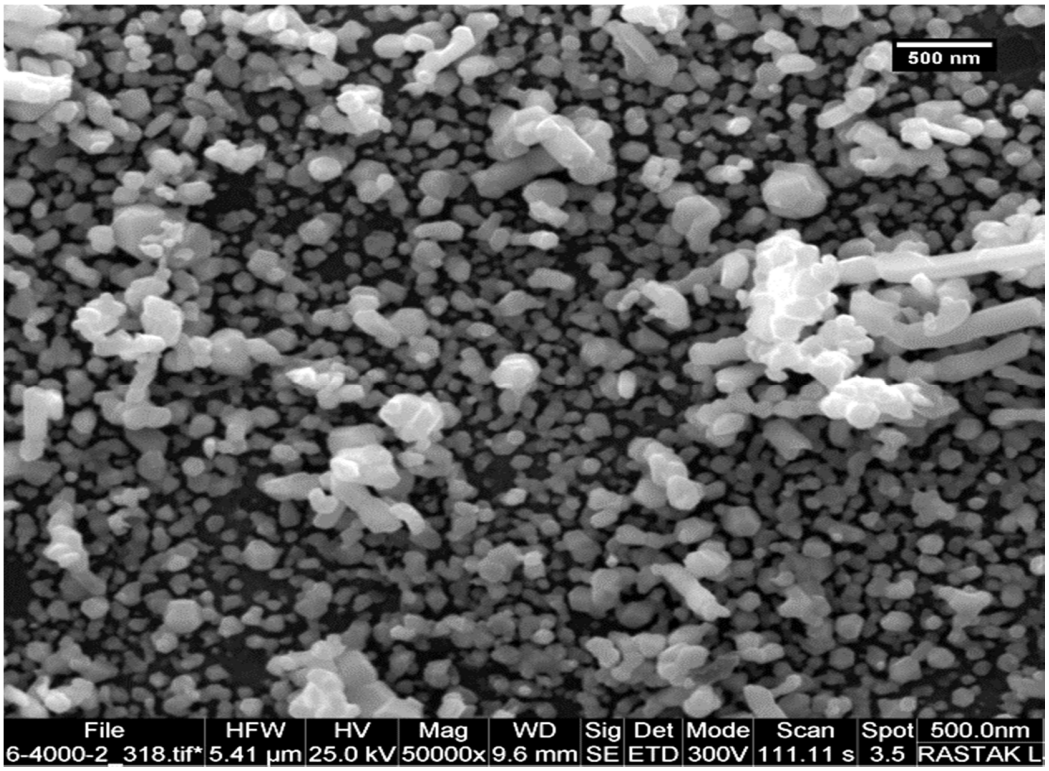

Figure(4.10): The FESEM image of (75% wt) of CdO thin film.

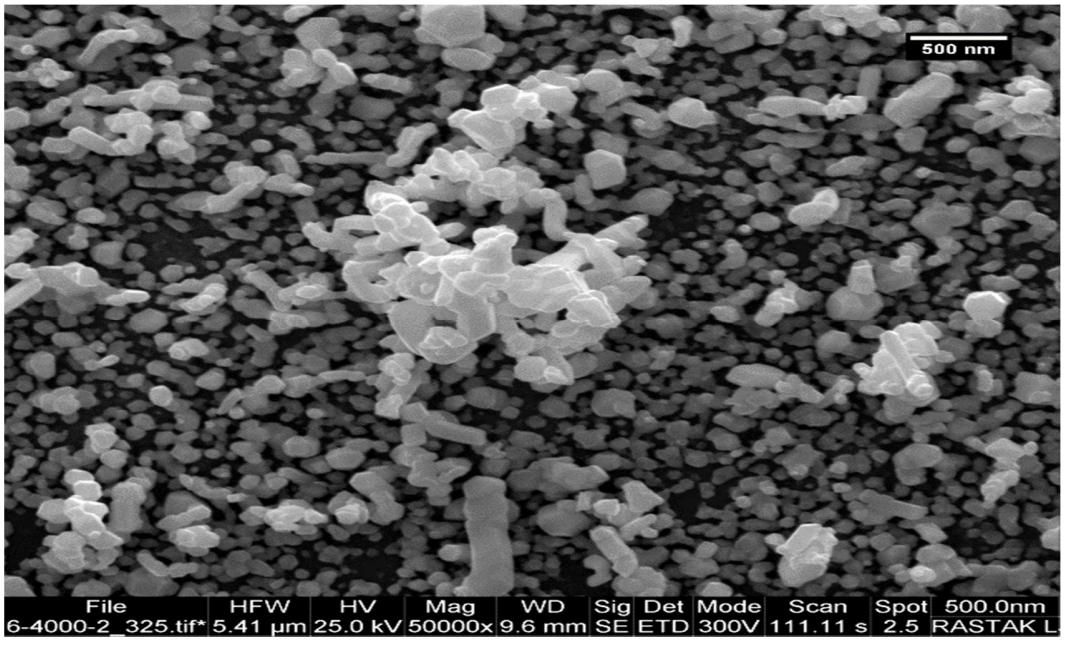

Figure(4.11): The FESEM image of pure CdO (100%) thin film.

4.2.4 Elemental Analysis

Figures (4.12), (4.13), (4.14), (4.15), and (4.16) show the (EDXS) spectra of Ga_2O_3 $_{(1-X)}CdO_{(X)}$ thin films at weight ratios (0%wt, 25%wt,75%wt and 100%wt) of CdO, respectively. Ga and O lines are easily seen in the EDX spectrum for 0% sample. Ga, Cd and O chemical elements can be observed in the EDX spectrum for 25%, 50% and 75% samples, which corresponds to the formation of $CdGa_2O_4$ compound also, an increasing in cadmium concentration can be observed. Finally Cd and O chemical elements can be observed in the EDX spectrum for 100% sample. The films components with high purity as listed in the table (4.4).

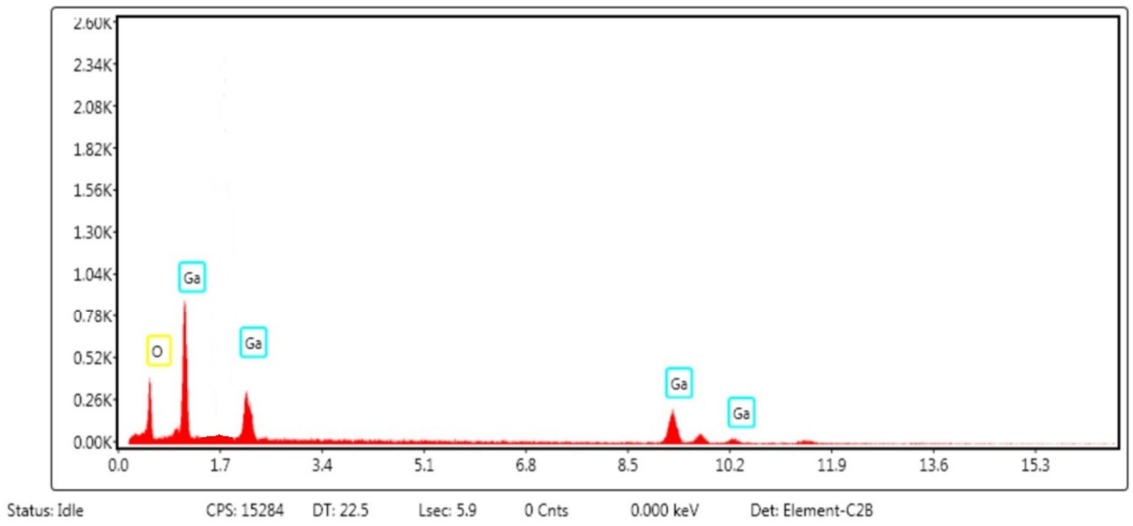

Figure(4.12):EDX spectra for 0% (Ga_2O_3) prepared films.

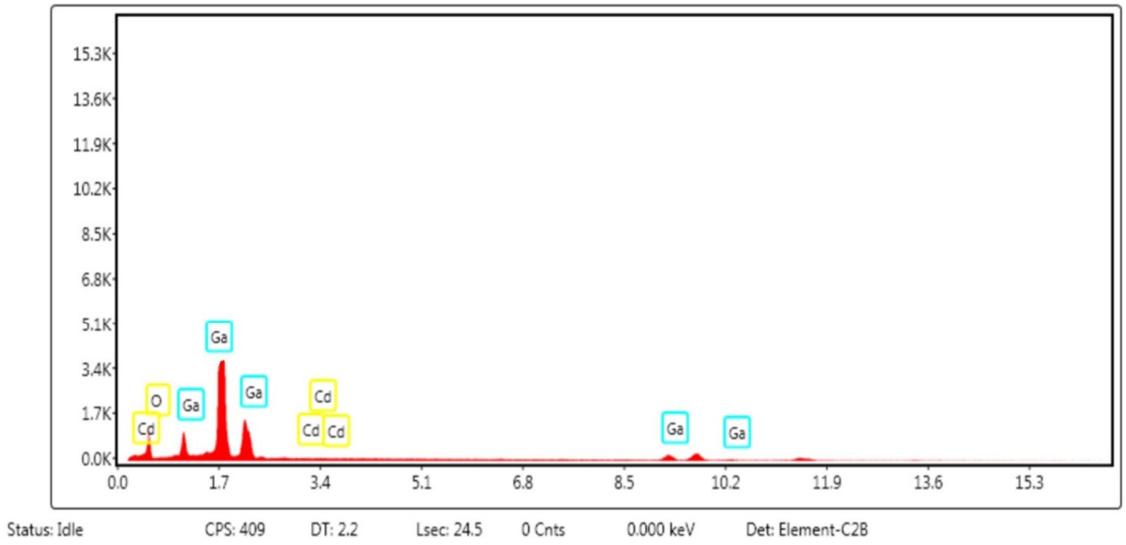

Figure(4.13):EDX spectra for 25% of CdO prepared films.

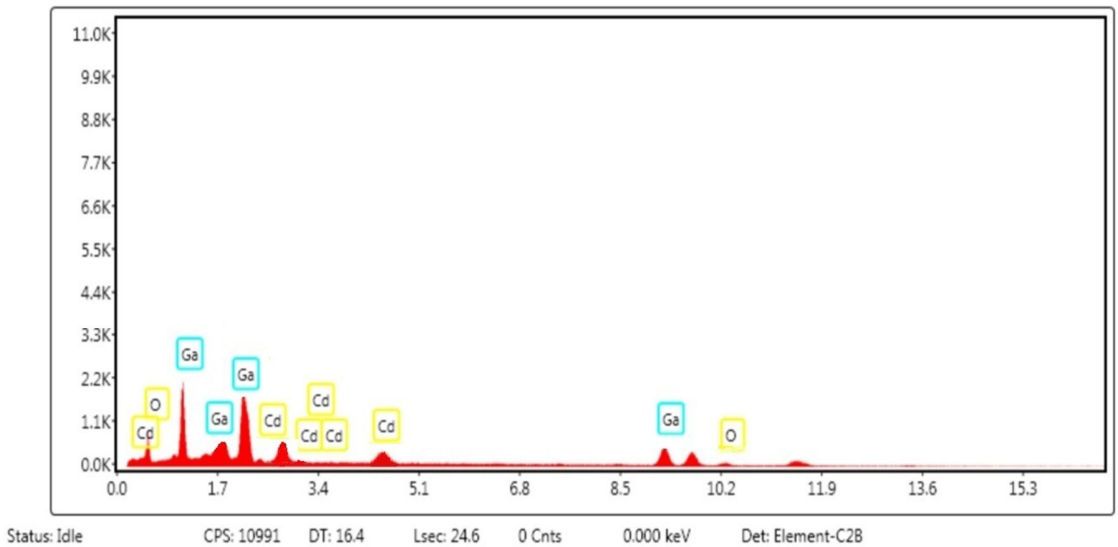

Figure(4.14):EDX spectra for 50% of CdO prepared films.

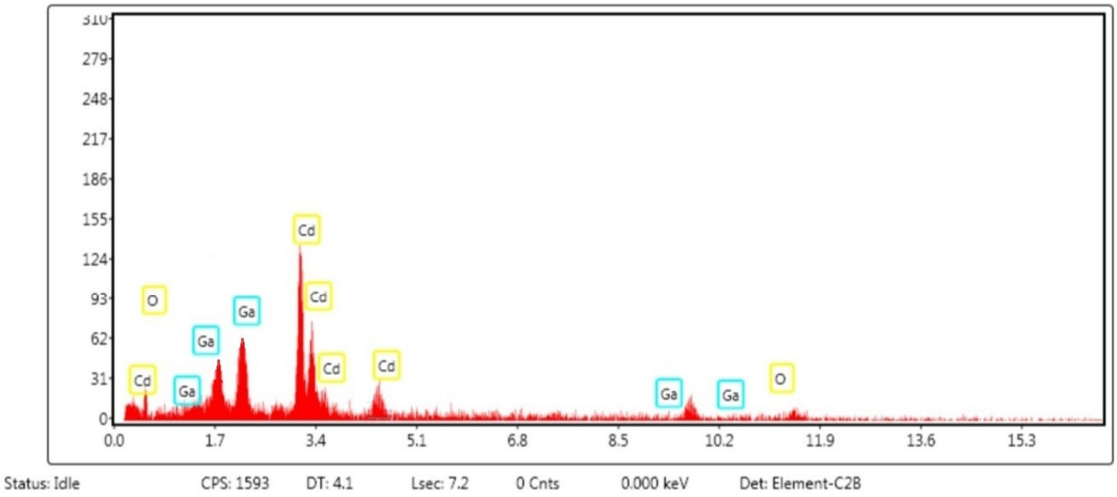

Figure(4.15):EDX spectra for 75% of CdO prepared films.

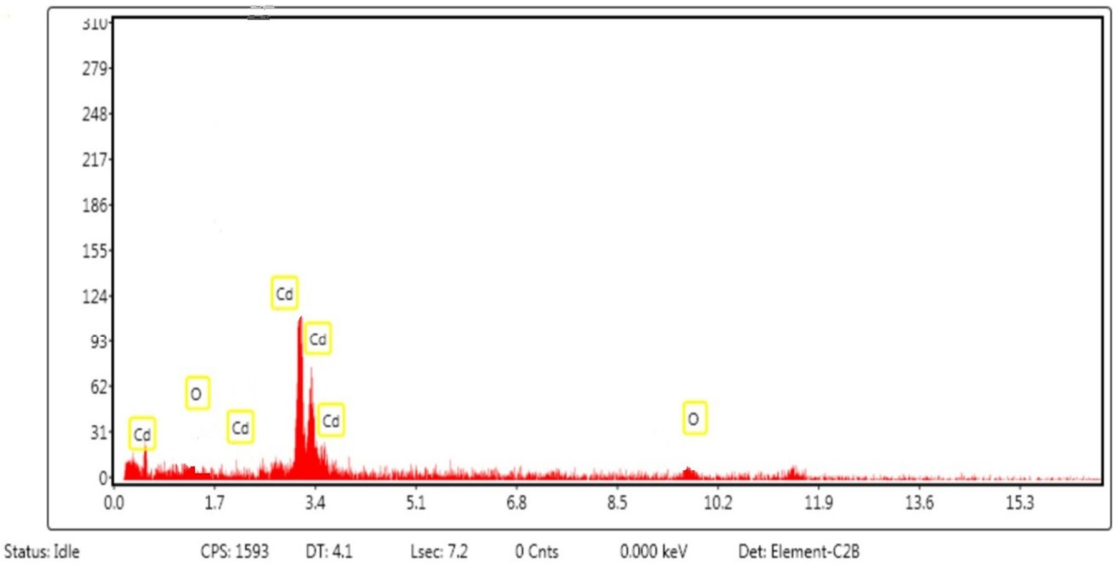

Figure(4.16):EDX spectra for 100%(CdO) prepared films.

Table (4.4): The elements ratios of EDX analysis of $Ga_2O_{3\ (1-X)}CdO_{(X)}$ films

Sample	Compound percentage (at%)			Total
	Ga	Cd	O	
0%	66	0	34	100
25%	48.78	20.58	30.64	100
50%	38.61	37.05	24.34	100
75%	23.12	56.49	20.39	100
100%	0	73.49	26.51	100

4.3 Optical Properties

4.3.1 Absorbance Spectrum

As shown in the figure (4.17), the absorbance variation as a function of wavelength for all samples under investigation in the range (200–900nm). The absorbance of all films has high values near the fundamental absorption edge (282nm) for Ga_2O_3 and shifted to higher wavelengths (red shift) with increase of CdO concentration as shown in the same figure, and then decreases as the wavelength increases. In general, all samples have low absorbance in the visible and near infrared regions. This can be explained as follows: at long wavelengths, incident photons do not have enough energy to interact with atoms onto the surface of the film, so they are transmitted. When the wavelength of an incident photon decreases, the interaction between it and the material occurs, and the absorbance rises[223] . The absorbance for the $Ga_2O_{3\ (1-X)}CdO_{(X)}$ thin films where the maximum absorption value 95%, 86%, 78%, 65% and 32% for 0%, 25% wt, 50% wt, 75% wt of CdO and 100% respectively at 219nm, 215nm, 209nm, 203nm and 206nm respectively . It can be seen that the absorbance decreases with increasing CdO concentration because the energy gap decreasing.

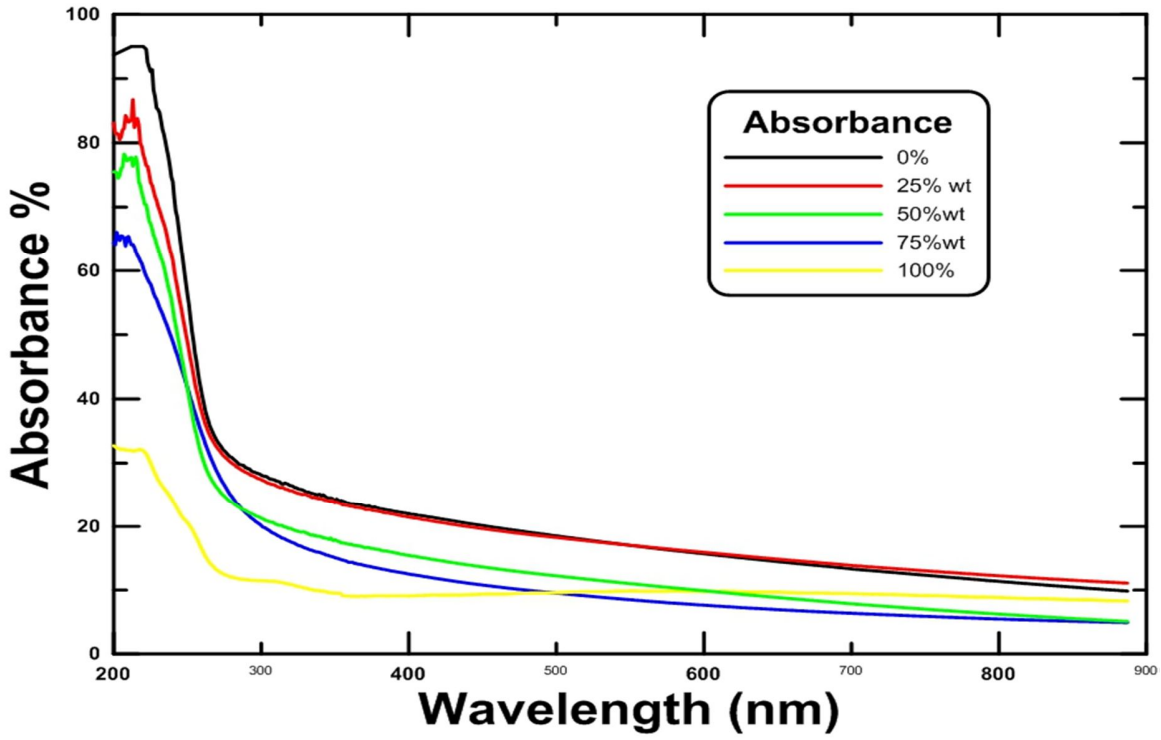

Figure (4.17): Optical absorbance spectra of $Ga_2O_{3\ (1-X)}CdO_{(X)}$ thin films deposited using PLD.

4.3.2 Transmittance Spectrum

Figure (4.18) shows the optical transmission of $Ga_2O_{3\ (1-X)}CdO_{(X)}$ thin films as a function of wavelength in the range (200 –800 nm). In the transmission spectrum, there are a few fluctuations, which it is occur because of the interferences in the films which caused by the reflection at various interfaces involving the film-substrate interface and interface of film with air , and comparable phenomena occur generally in transparent films[136, 224, 225]. The max transmittance value of these thin films lies within 42%, 55%, 65% 70% and 80% for 0%, 25% wt, 50% wt, 75% wt of CdO and 100% at 305nm, 320nm, 331nm, 349nm and 355nm, respectively. The transmittance shows improvement with increase in CdO concentration.

The reason of the increased transmittance duo to the energy gap of CdO is much less than that of Ga_2O_3, so the transmittance is improved. The optical transmission values decrease as the CdO concentration rises; this behavior may be due to an increase in free electrons as the CdO concentration rises.

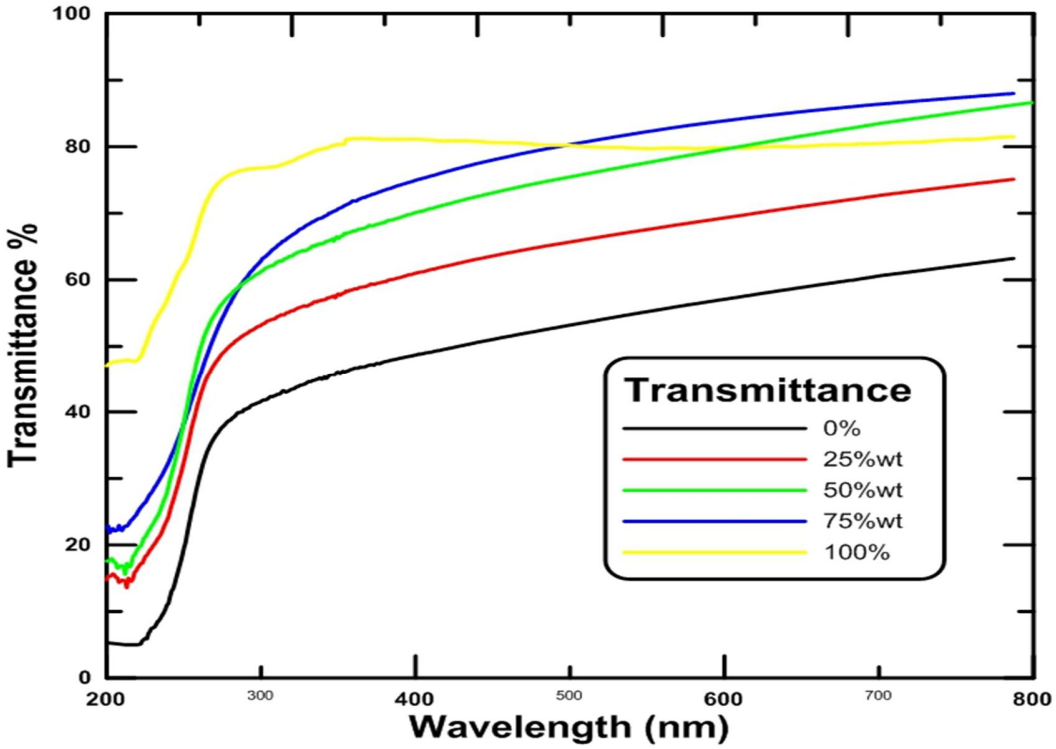

Figure (4.18): Optical transmission spectra of $Ga_2O_{3\ (1-X)}CdO_{(X)}$ thin films .

4.3.3 Absorption Coefficient

The eq. (2.16) has been used to measure the absorption coefficient (α). This coefficient is determined by the energy of incident photon (hυ), the semiconductor energy gap, and the electronic transitions type. The variation of absorption coefficients versus wavelength in the range of (200-900) nm for $Ga_2O_{3\ (1-X)}CdO_{(X)}$ films are shown in figure(4.19). Absorption coefficients values of these thin films lies within the highest peaks were (115×10^3, 99×10^3, 92×10^3, $75 \times 10^3$and 3×10^3) cm^{-1} for 0%, 25%wt, 50%wt, 75%wt of CdO and 100% , respectively. The absorption

coefficients value of $Ga_2O_{3\ (1-X)}CdO_{(X)}$ decreases with increasing the amount of CdO. This is because the absorption value coefficient indicates the ability of the film material to absorb the energy of the incident radiation, and by referring to the figure (4.17), can be seen that, the absorbance of cadmium oxide is the lowest, so it caused a decrease in the absorption coefficient.

.

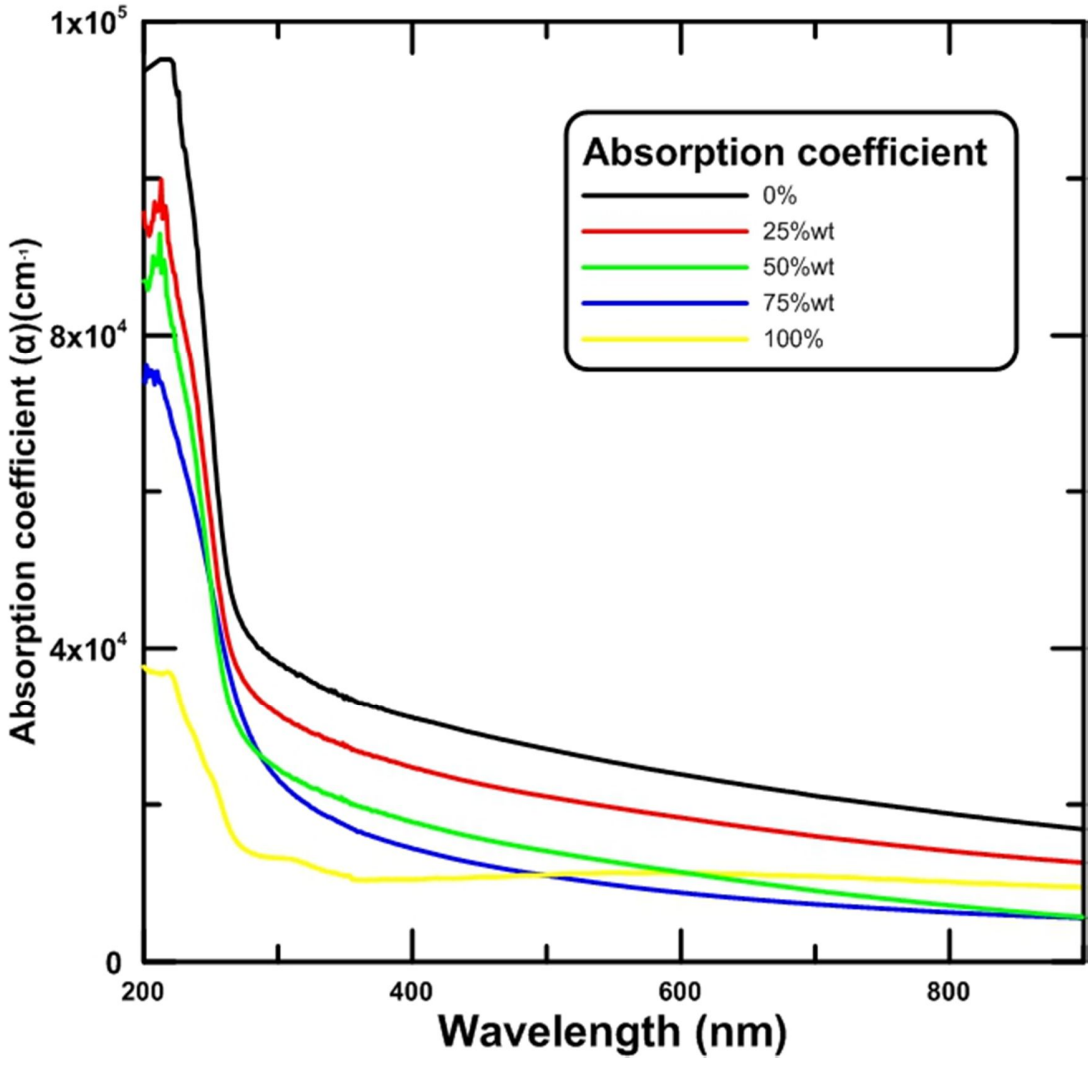

Figure(4.19): Variation of absorption coefficients with wavelength for $Ga_2O_{3\ (1-X)}CdO_{(X)}$ thin films.

4.3.4 Optical Energy Gap

The calculated energy gap are drawn between $(\alpha h\upsilon)^2$and $(h\upsilon)$photon energy as shown in figure (4.20) .The values of band gap can be determined by tauc plots as shown in figure were evaluated using extrapolating the linear section of the plot to energy axis. As the amount of CdO increases the E_g dropped monotonously because the CdO molecules contribute by charge carriers or the conductivity after addition of CdO increasing. The obtained values of energy gap were tabulated in table (4.5).

Table (4.5): Energy gap values as compared to some previous references.

Samples	E_g (eV) our work	Other work
0%	4.65	4.85 [226] 4.9 [142]
25% wt	4.48	
50% wt	4.37	
75% wt	4.18	
100%	2.42	2.52 [227] 2.459[228]

The values of our work for pure samples is almost in agreement with references[226] and [142] for Ga_2O_3 and it also corresponds to [227] and [228] for CdO.

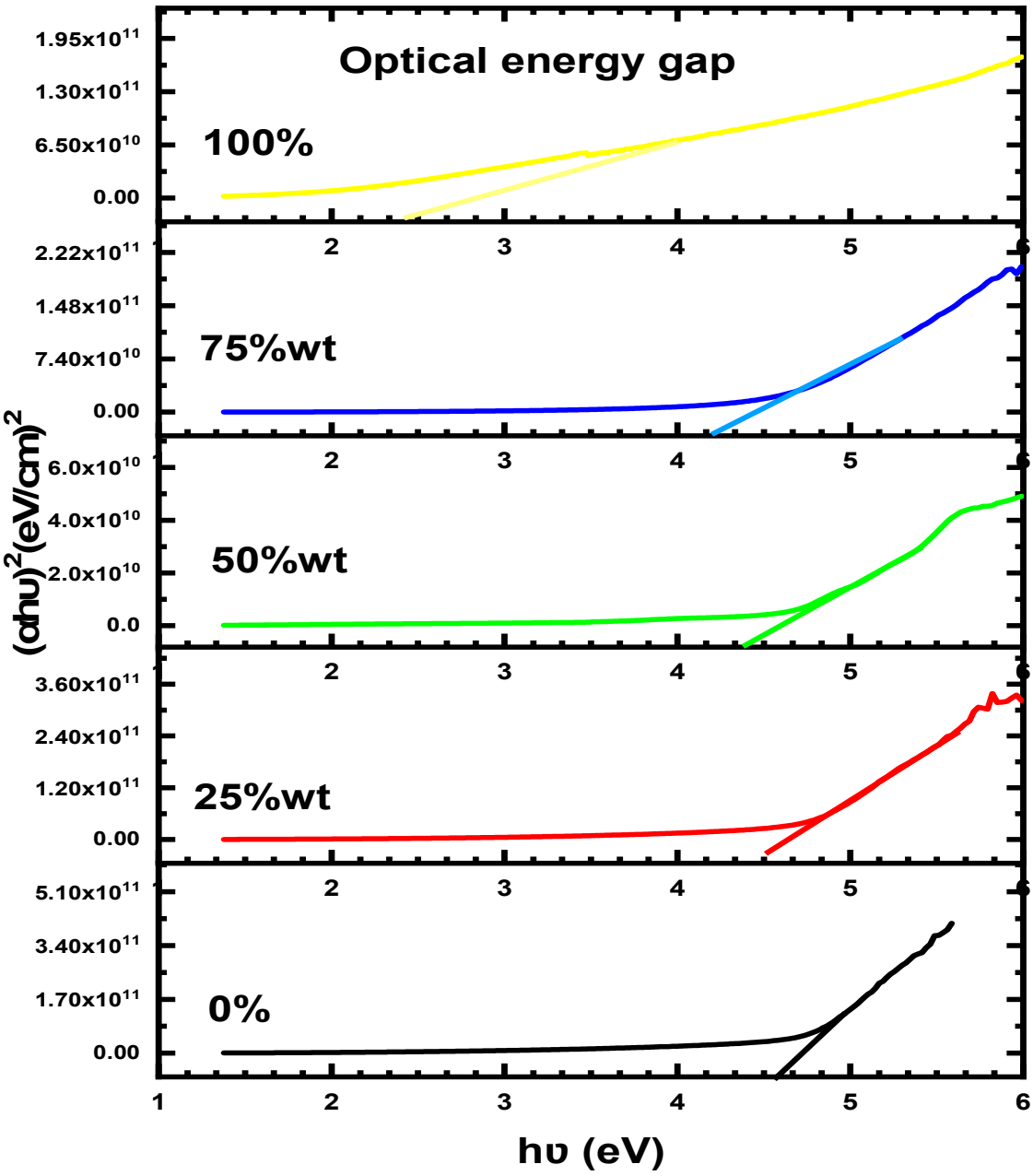

Figure (4.20): $(\alpha h\nu)^2$ vs. hν plot of $Ga_2O_{3\ (1-X)}CdO_{(X)}$ films deposited with a different ratio of CdO.

4.4 The Electrical Properties of $Ga_2O_{3\ (1-X)}CdO_{(X)}$ Thin Films

The electrical properties of $Ga_2O_{3\ (1-X)}CdO_{(X)}$ films deposited onto quartz substrates, which include Hall effect and D.C conductivity , It was discussed after doing its calculations.

4.4.1 The D.C Conductivity

According to table (4.6), the samples Ga_2O_3 (0%)wt and 25%wt of CdO are p-type, which is due to the fact that the electric behavior in film 0%wt (pure Ga_2O_3) is dominant in these samples, because the proportion of gallium is higher than cadmium .It can be seen that the electrical resistance increases with temperature as the charge mobility increases, and this behavior is similar to materials with a positive temperature coefficient, whose resistance increases with increasing temperature as shown in figure (4.21).

When the temperature of a semiconducting material rises, the charge-carrier concentration rises as well as a result, there are more charge carriers accessible for recombination, enhancing the semiconductor's conductivity. As the conductivity of the semiconductor material increases, the resistivity of the material decreases, resulting in a negative temperature coefficient.

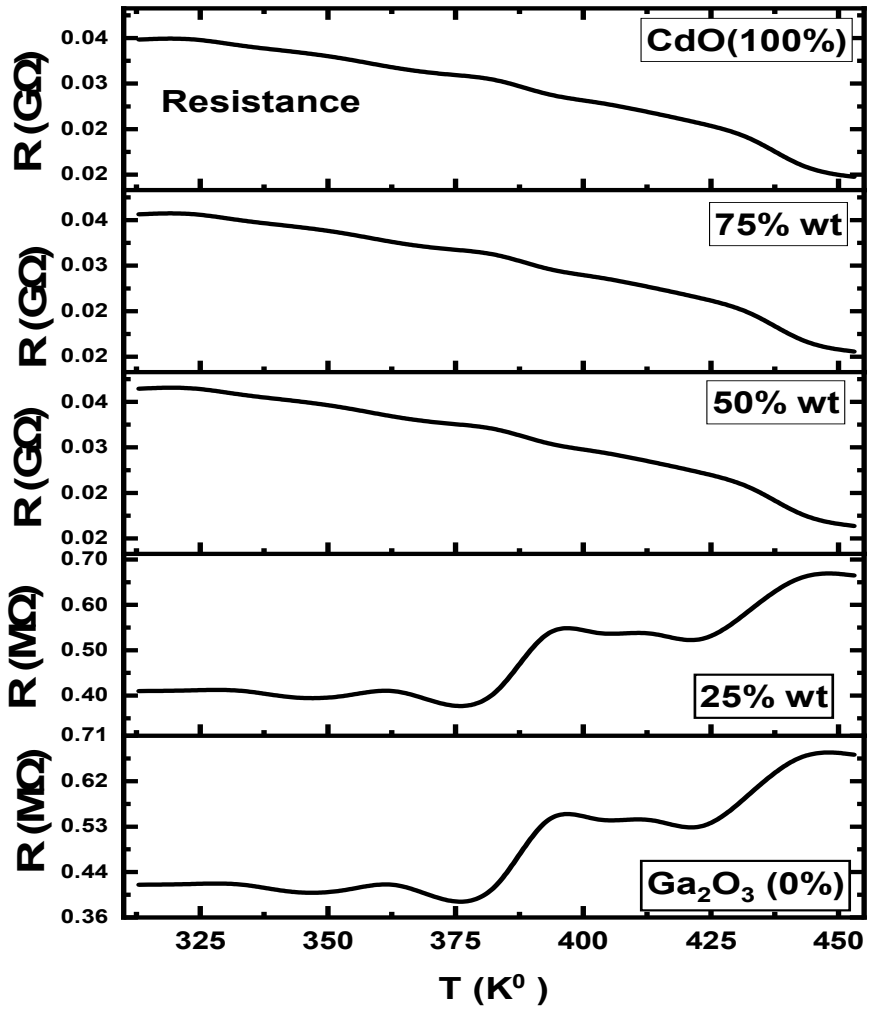

Figure (4.21):Variation of resistance as a function of temperature.

For the 50%wt, 75%wt of CdO and 100%%wt (pure CdO) films, it is noticeable that they are n-type, and it can be noted that the proportion of cadmium is equal to or greater than the proportion of gallium in the films, so the electrical behavior of CdO is the dominant behavior in these films, where with the increase in temperature, the electrical resistance decreasing, and it is worth noting that this behavior is similar to the behavior of semiconductors. This reason is due to a decreases in the charge mobility with an increasing in temperature, and thus the resistance of the electric current passing through it

decreases, causing a decrease in the value of the electrical resistance. It can be noted that this behavior is like that of materials with a negative temperature coefficient of resistance.

Figure (4.22) shows the resistivity relationship as a function of temperature, and it is clear that its behavior is the same as the behavior of electrical resistance, as it increases with increasing temperature for p-type films and decreases with temperature for n-type films.

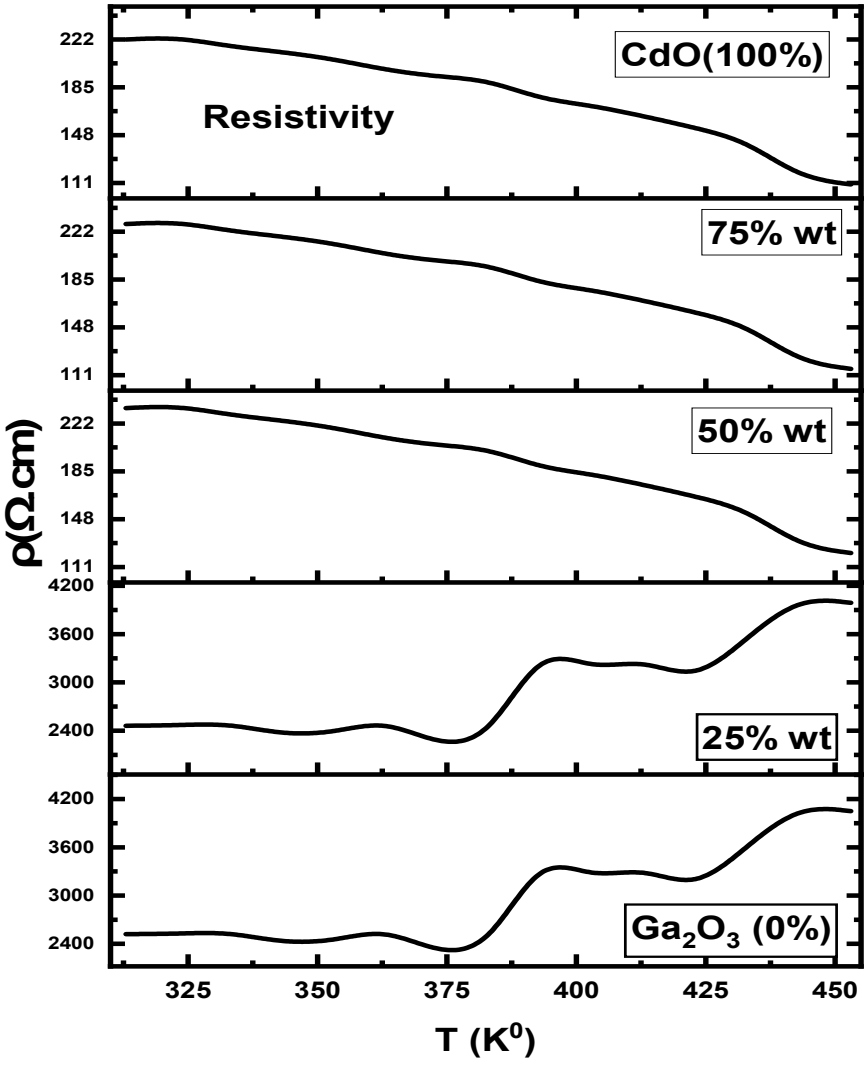

Figure(4.22):Variation of resistivity as a function of temperature.

The conductivity relationship with temperature can be observed in figure (4.23), where the behavior inverse to the behavior of the electrical resistance, where the conductivity decreases with the increase in temperature for p-type films, while it increases with increasing temperature for n-type films for the same reasons above.

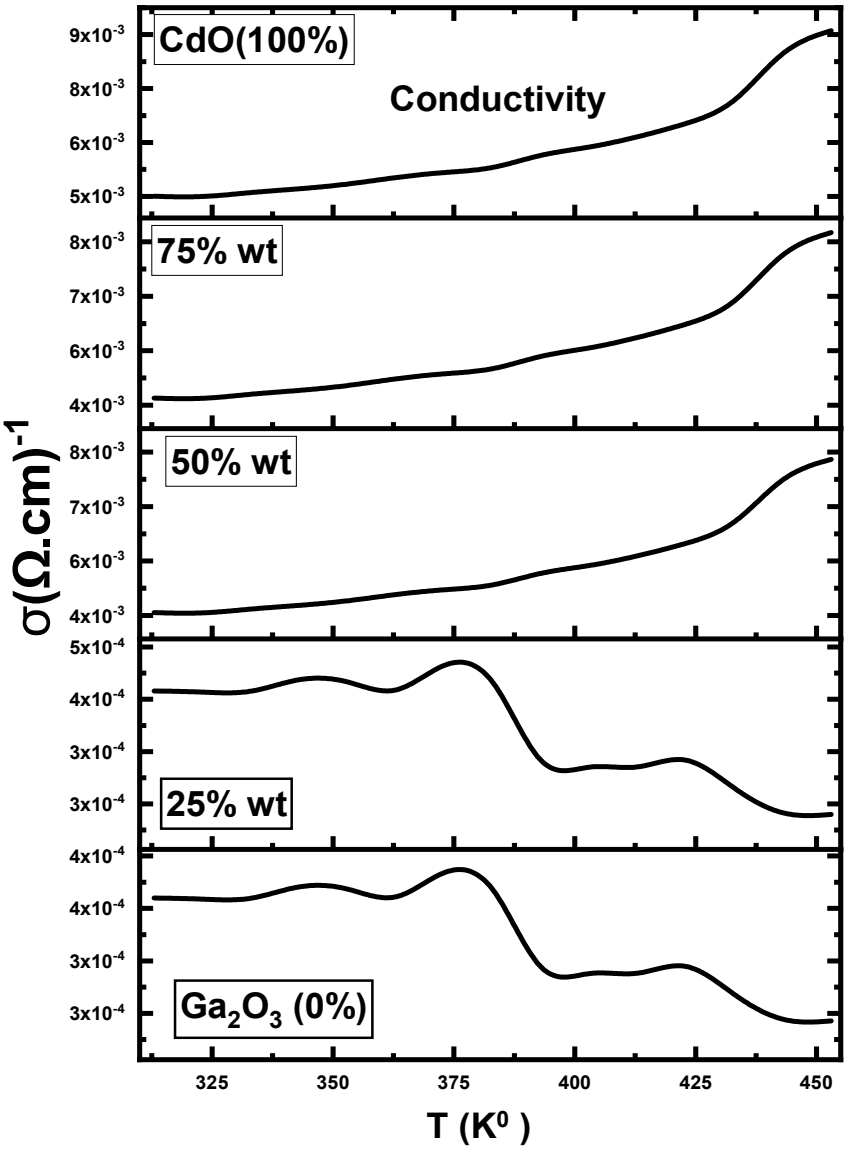

Figure (4.23): Variation of conductivity as a function of temperature.

4.4.2 Hall Effect Measurements

The electrical properties require knowledge of the Hall coefficient (R_H). Also the electrical characteristics of $(Ga_2O_3)_x(CdO)_{x-1}$ composite films were determined using a Hall voltage measurement at RT in a constant magnetic field of (0.55 Tesla). The results showed that the 0% wt (pure Ga_2O_3) and 25%wt of CdO samples are p-type and this agree with references [229, 230].

The effect of the electrical behavior of Ga_2O_3 on the electrical properties of the 25% wt of CdO sample is dominant, because the proportion of Ga_2O_3 is high in relation to CdO in the film. While noting that the films become n-type when the proportions are equal or the proportion of CdO is greater than Ga_2O_3 in films, where the electrical behavior of CdO becomes dominant in samples 50%wt and 75%wt of CdO. For thin films of type p, it can be seen that the concentration of carriers of 25% wt of CdO is the highest, while 50% wt for films of type n is the highest. The highest value of mobility is $1.91\times 10^{6}(cm^2V^{-1}s^{-1})$ while the lowest is 271×10^{-1} $(cm^2V^{-1}s^{-1})$ for 0%wt (pure Ga_2O_3) and 50%wt of CdO, respectively. For other values, can be seen table (4.6).

Table (4.6): Hall parameters for $Ga_2O_{3\ (1-X)}CdO_{(X)}$ films at room temperature.

Sample Name	Resistivity ρ(Ω.cm)	Concentration of Carriers n_H cm^{-3}	Hall Coefficient RH (cm^3C^{-1})	Conductivity $\sigma(\Omega.cm)^{-1}$	Mobilit μ_H ($cm^2V^{-1}s^{-1}$)	Type of Carriers
0%wt	5.37×10^{-2}	6.09×10^{13}	1.02×10^{5}	1.86×10^{1}	1.91×10^{6}	p
25%wt	5.49×10^{-2}	1.28×10^{14}	4.89×10^{4}	1.82×10^{1}	8.90×10^{5}	p
50%wt	8.37×10^{4}	-2.75×10^{16}	-2.27×10^{2}	119×10^{-3}	271×10^{-1}	n
75%wt	6.28×10^{-2}	-5.16×10^{15}	-1.21×10^{3}	1.59×10^{1}	1.93×10^{4}	n
100%wt	6.36×10^{-2}	-5.89×10^{14}	-1.06×10^{4}	1.57×10^{1}	1.67×10^{5}	n

4.5 Sensing Measurements

4.5.1 The operation temperature of prepared sensor

The influence of the operation temperature and compound mixing ratio are studied with the aim of improving operating temperature, response time and recovery time to the lowest possible values on sensitivity of films. The operating temperature of a sensor can be define as the temperature at which its resistance remains constant. The existence of a certain volume of gas of interest has only a slight effect on the resistance shifting [231, 232].

Figures (4.24) and (4.25) are displayed the sensitivity in the range (25°C to 300 °C) as a function of operation temperature. For $Ga_2O_{3\ (1-X)}CdO_{(X)}$ (0%, 25% wt, 50% wt, 75% wt, and 100% wt) of CdO with laser energy (500mJ) which are deposited on quartz substrates at (300^oC) and annealing at 750^0C for 5hr in the air, then the samples exposed to 3 % NO_2

and 10% NH_3 in the air ambient injected into the measuring chamber . When the temperature at 200°C, the samples have a greater sensitivity for NO_2 gas and have a greater sensitivity with operation temperature at room temperature(RT) for NH_3 gas.

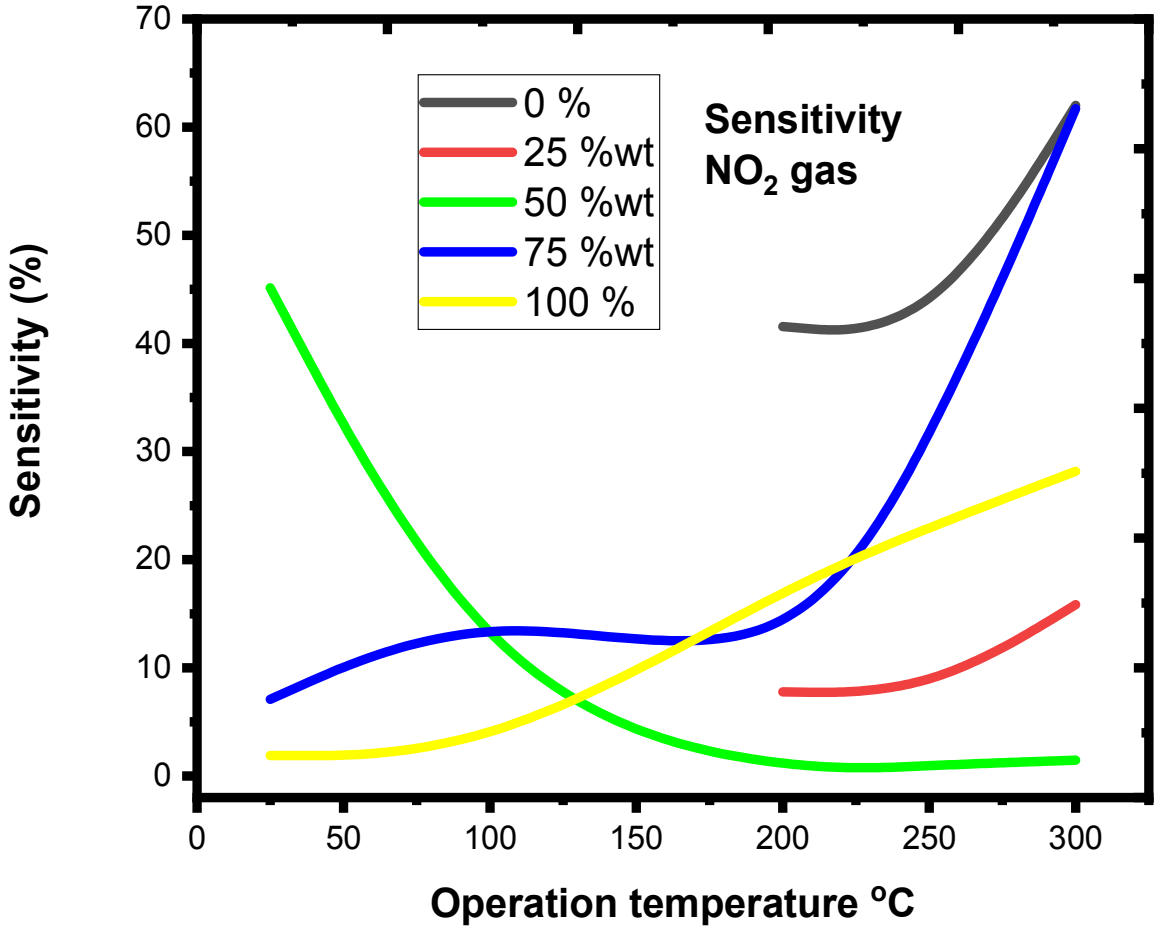

Figure(4.24): Sensitivity vs. operating temperature of the $Ga_2O_{3\ (1-X)}CdO_{(X)}$ films using NO_2 as gas sensing technique .

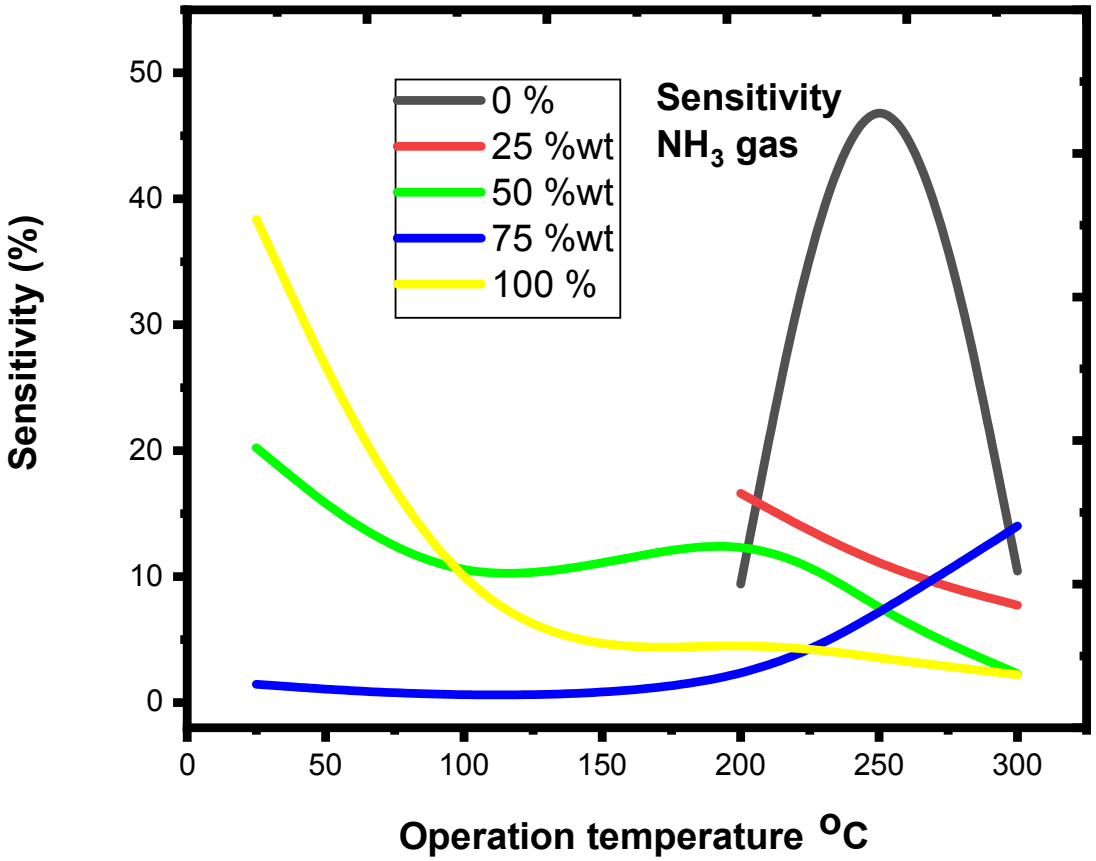

Figure (4.25): Sensitivity vs. operating temperature of the $Ga_2O_{3\ (1-X)}CdO_{(X)}$ films using NH_3 as gas sensing technique.

The maximum sensitivity of tested gas sensor to 60 ppm of NO_2 about 61.7% at around 300°C for 75%wt of CdO composite , while the 50%wt of CdO composite have 0.8% lowest sensitivity to NO_2 on the other hand, it is the best at RT. It should also be noted that the optimum sensing temperature required for the maximum sensitivity at around 300°C for the $Ga_2O_{3\ (1-X)}CdO_{(X)}$ gas sensor. When NH_3 is used as the probing gas, the maximum sensitivity of samples gas sensor to 200 ppm of NH_3 can reach 48.2% for pure Ga_2O_3, and the optimum sensing temperature of composite sensor is at

around (200 - 300) °C. All the above results have shown that the sensitivities to the oxidizing and reducing gases have been greatly enhanced. The reason can be attributed to the raised amount of surface oxygen species have been adsorbed. Also it can be noted that, the samples have equal and large amount of CdO with respect to Ga_2O_3 have enhance sensitivity at room temperature for to the oxidizing NO_2 and reducing NH_3 gases as it obvious in figures. This result can be explained by reference to cadmium oxide has a smaller energy gap (2.52 eV) [227] than Ga_2O_3 (4.85 eV) [226]. As well as the decrease in the crystal size as mentioned in the results of the X-ray and also FESEM. When crystal size decreases that means an increase in the crystal boundaries, and this results in an increase in the exchange of charge between them, which leads to an increase in the sensitivity.

4.5.2 Response Time and Recovery Time

Figures (4.26) and (4.27) show the relationship between the response time of $Ga_2O_{3\ (1-X)}CdO_{(X)}$ with operating temperature. Because of the increased oxygen adsorption on the surface, conduction electrons are extracted from the near-surface area, resulting in an electron-depleted surface layer. Also because of the number of active adsorption sites are increased, sensors have a faster reaction time.

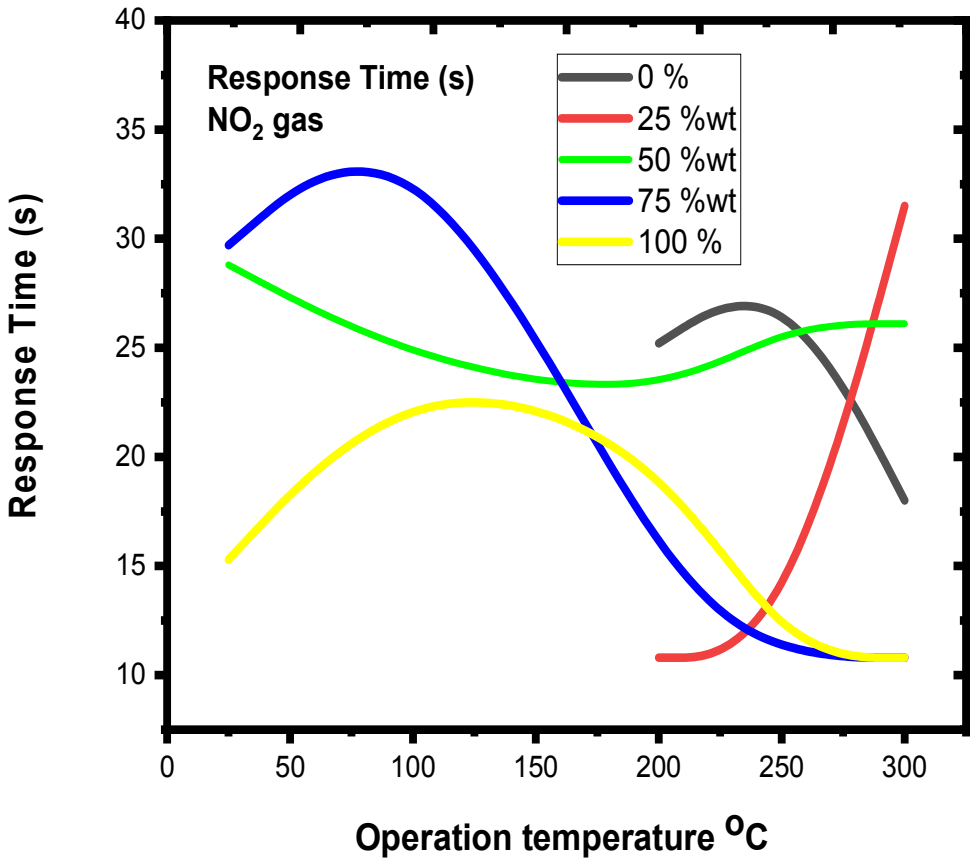

Figure(4.26): Response time vs. operation temperature of the $Ga_2O_{3\ (1-X)}CdO_{(X)}$ gas sensor using NO_2 gas.

The response time with rising operating temperature for NO_2 and NH_3 test gases are shown in the figures, the response time decreases with increasing operating temperature. The fast response speed for NO_2 gas (10.8 s) for 75% wt of CdO sample at 250^oC and (9s) for pure Ga_2O_3 at 250^oC for NH_3 gas.

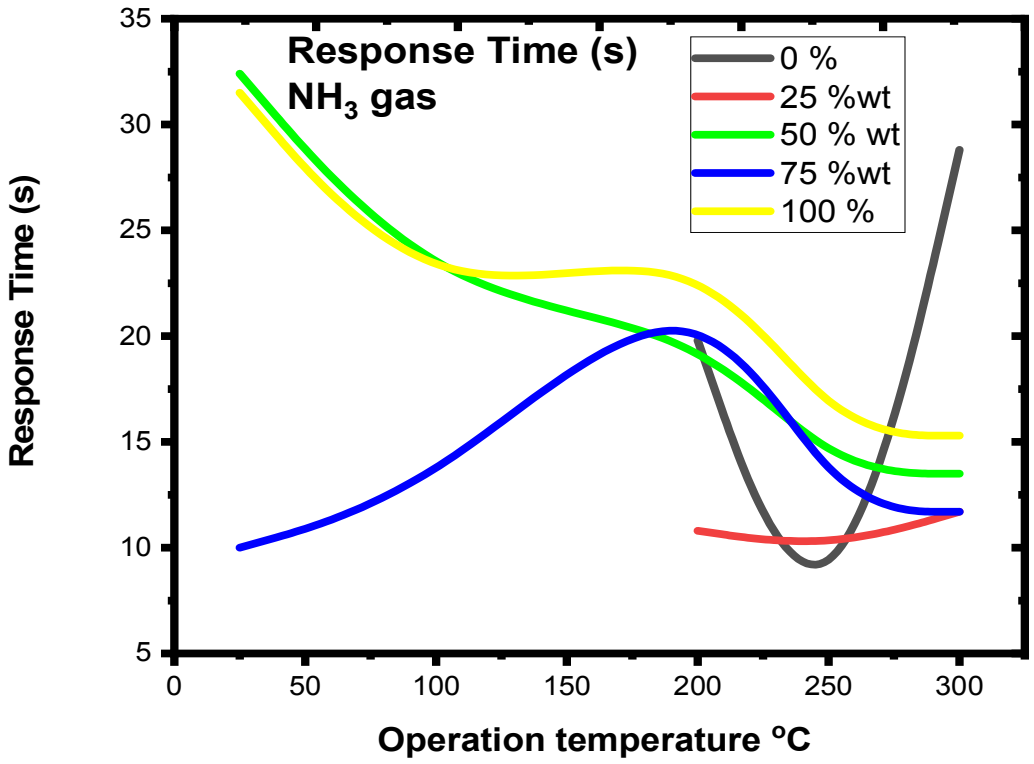

Figure(4.27): Response time vs. operation temperature of the $Ga_2O_{3\ (1-X)}CdO_{(X)}$ gas sensor using NH_3 gas.

Figures (4.28) and (4.29) show the recovery time with rising operating temperature for NO_2 and NH_3 test gases, the recovery time decreases with increasing operating temperature. The fast recover speed for NO_2 gas (45 s) for 50% wt of CdO sample at 300°C and (39.6s) for NH_3 gas for 50% wt of CdO sample at 300°C.

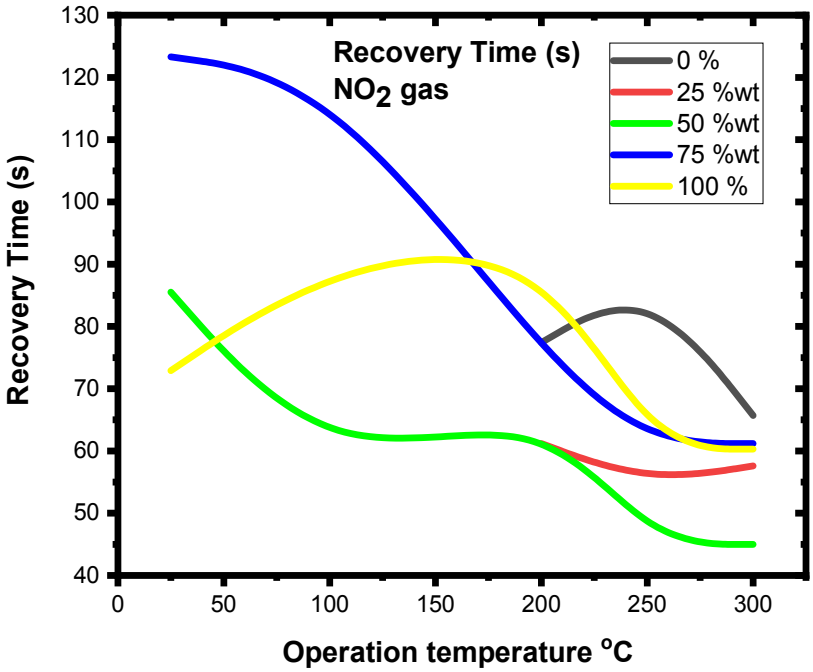

Figure(4.28): Recovery time vs. operation temperature of the $Ga_2O_{3\ (1-X)}CdO_{(X)}$ gas sensor using NO_2 gas.

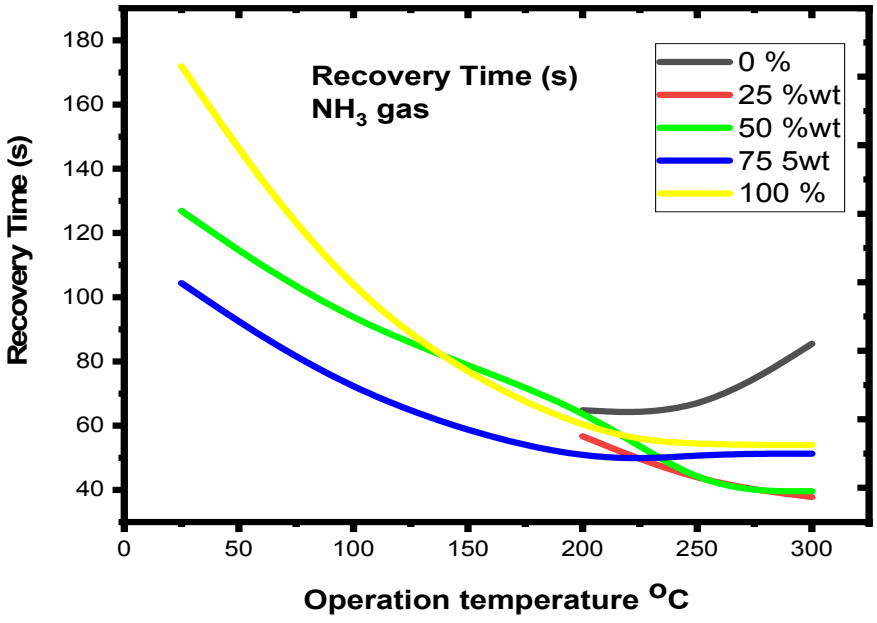

Figure (4.29): Recovery time vs. operation temperature of the $Ga_2O_{3\ (1-X)}CdO_{(X)}$ gas sensor using NH_3 gas.

The rapid response and recovery sensor for NO_2 and NH_3 gases may be attributed to faster gas oxidation and reduction[233], where the work mechanism and activation energy of surface reactions both decrease with decreasing grain size and an increase in vacancies produced upon composite lattice[234]. Conduction electrons are removed from the region of near-surface by enhanced oxygen adsorption on the surface, resulting in an electron-depleted surface layer. Because of the raised number of active adsorption sites, sensors were able to respond quickly. As seen in the figures, raising the operation temperature reduces the recovery time and response time in general. A fast response time, as well as a fast recovery time, are usually required in real situations.

4.5.3 Resistance Variation with Time of $Ga_2O_{3\ (1-X)}CdO_{(X)}$

Figures (4.30 to 4.34) shows the variation in resistance with time of pure and $Ga_2O_{3\ (1-X)}CdO_{(X)}$ when exposed to 3 %NO_2 and 10% NH_3 in the air ambient injected into the measuring chamber, with bias voltage (V) held at (3V) at each sample's optimum operating temperature. The resistances are directly calculated with time, and the resistance of sensor reaches a stable state before the gases are opened, allowing the gas to mix with the air into the chamber.

The causes of variations of resistance with time of diffusion of gases that occupy the vacancies in the films trough the interval of time and this is depend on the concentration of CdO in the composites and the types of gas. The sensors efficiency also depend upon the number times affected to the gases(NO_2 ,NH_3).Also the variations of affected temperature will repeat the arrangements the molecules as result to changes the types of gases. It observed that the resistances decrease as the temperature increase because

the re-arrangements of CdO in Ga_2O_3 in light the concentrations of CdO in composites with reaction the rising of temperature.

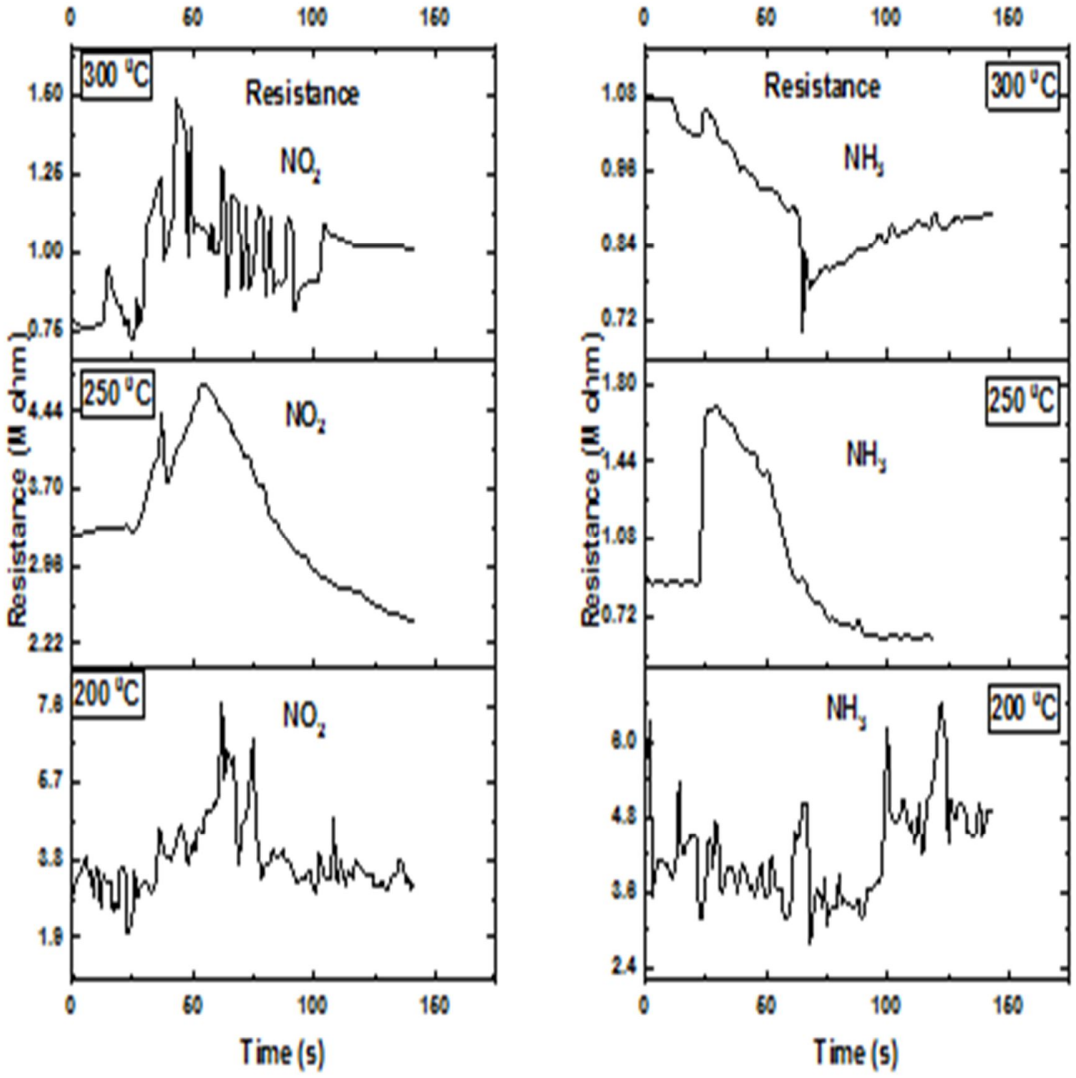

Figure(4.30): The variation resistance with time for different operation temperature of NO_2 and NH_3 gases for the pure Ga_2O_3 (0%) gas sensor.

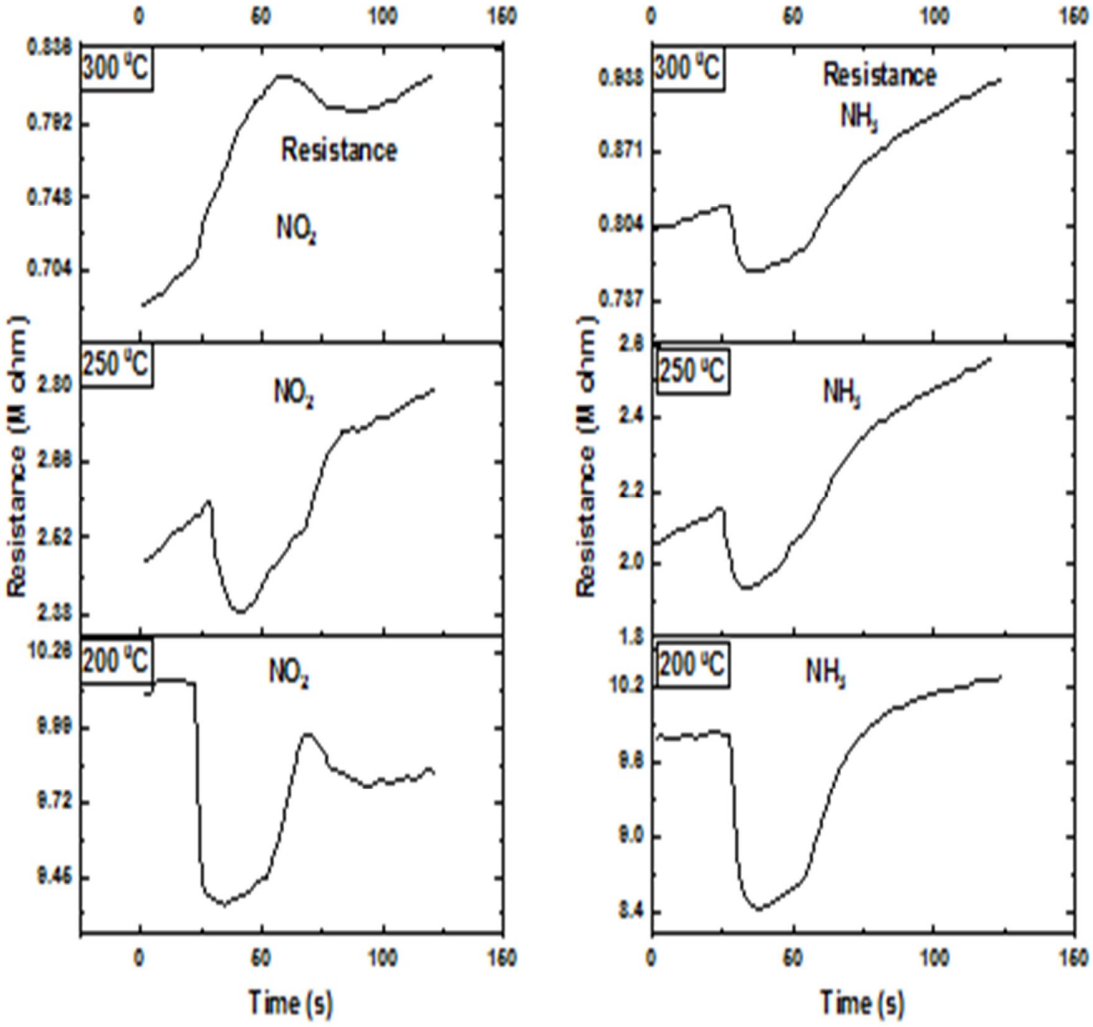

Figure(4.31): The variation resistance with time for different operation temperature of NO_2 and NH_3 gases for the 25%wt of CdO gas sensor.

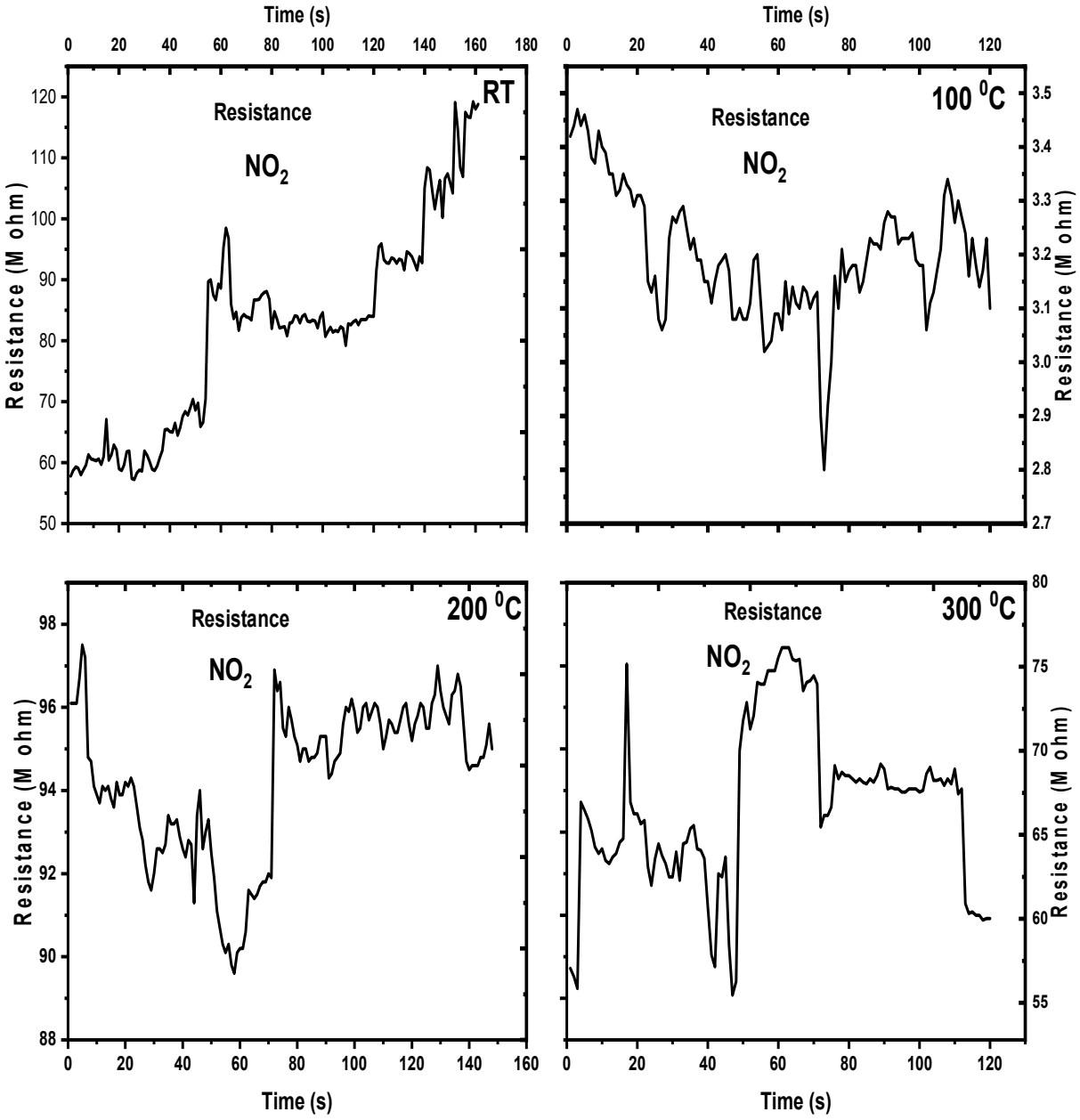

Figure(4.32a): The variation resistance with time for different operation temperature of NO_2 gas for the 50%wt of CdO gas sensor.

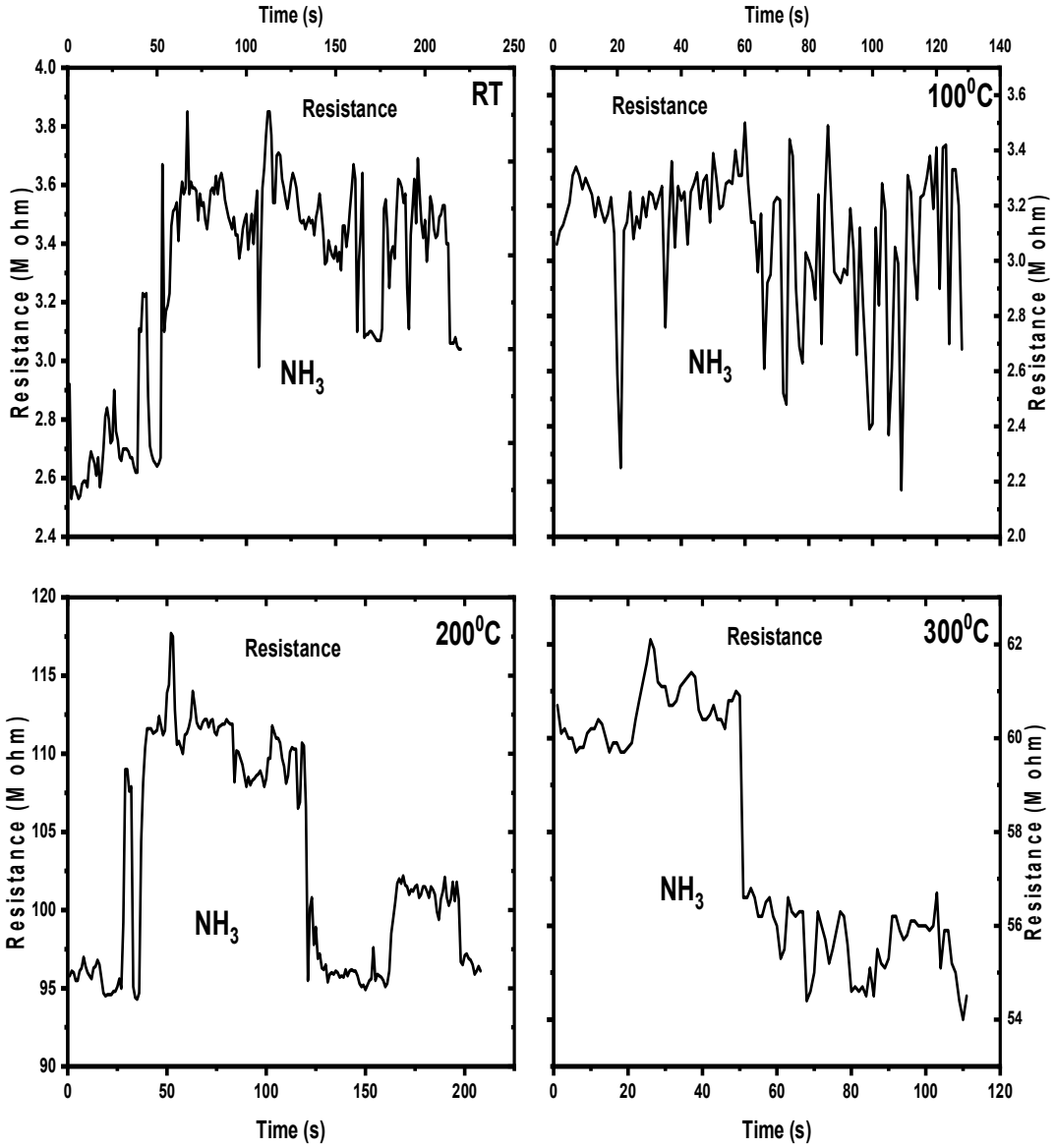

Figure(4.32b): The variation resistance with time for different operation temperature of NH_3 gas for the 50%wt of CdO gas sensor.

Figures (4.30), (4.31) and (4.32) shows the resistance behavior with time for two test gases NH_3 and NO_2. When samples were exposed to NO_2 and NH_3 gases on the surface, their resistance decreased. The

$Ga_2O_{3\ (1-X)}CdO_{(X)}$ has dual behave n-type semiconductor for NH_3 test gas and p-type for NO_2 test gas, which is similar to the behavior of samples coming from that, these variation occurs because it was generated positive surplus carriers(p-type) for NO_2 gas.

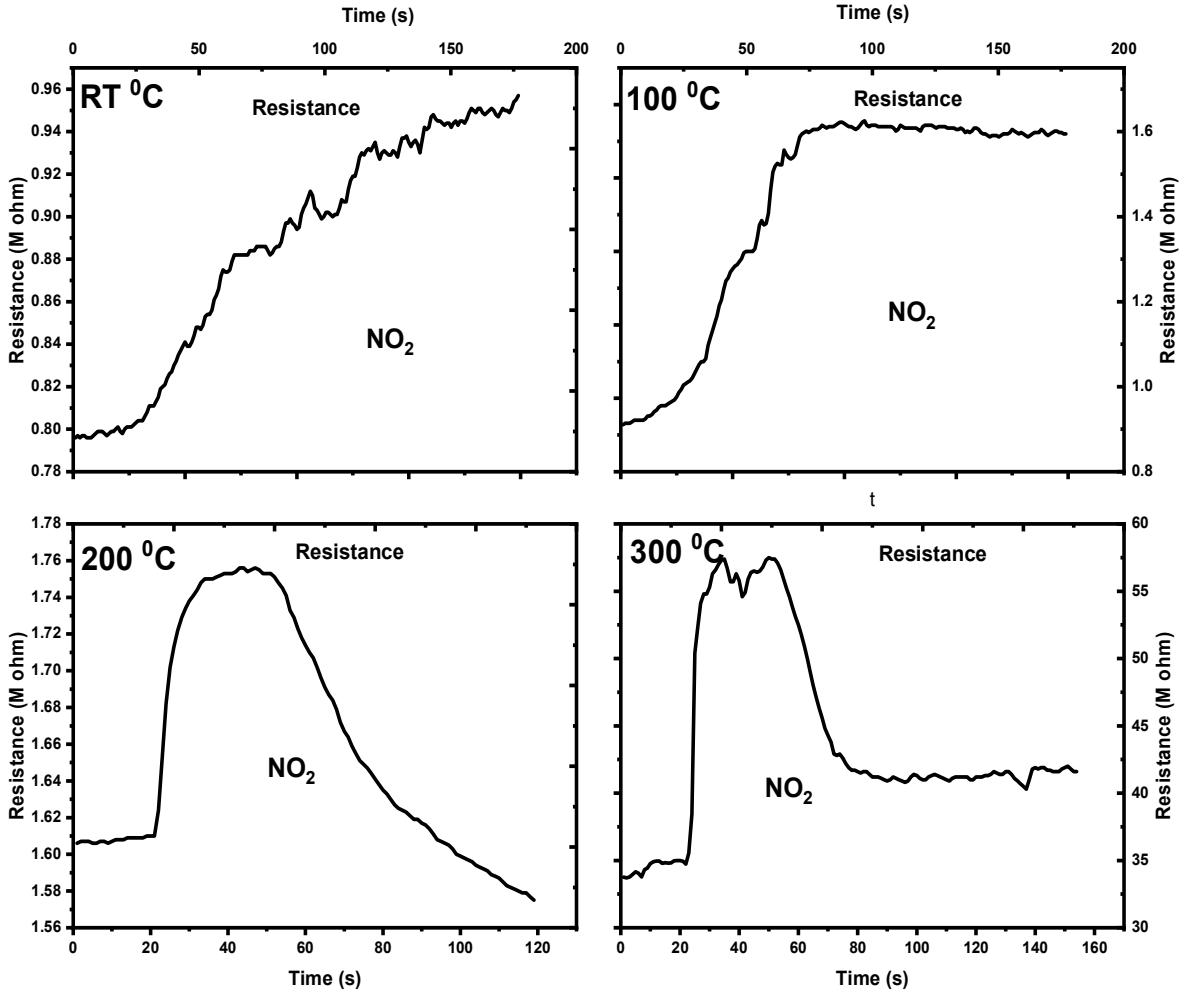

Figure(4.33a): The variation resistance with time for different operation temperature of NO_2 gas for the 75%wt of CdO gas sensor.

.

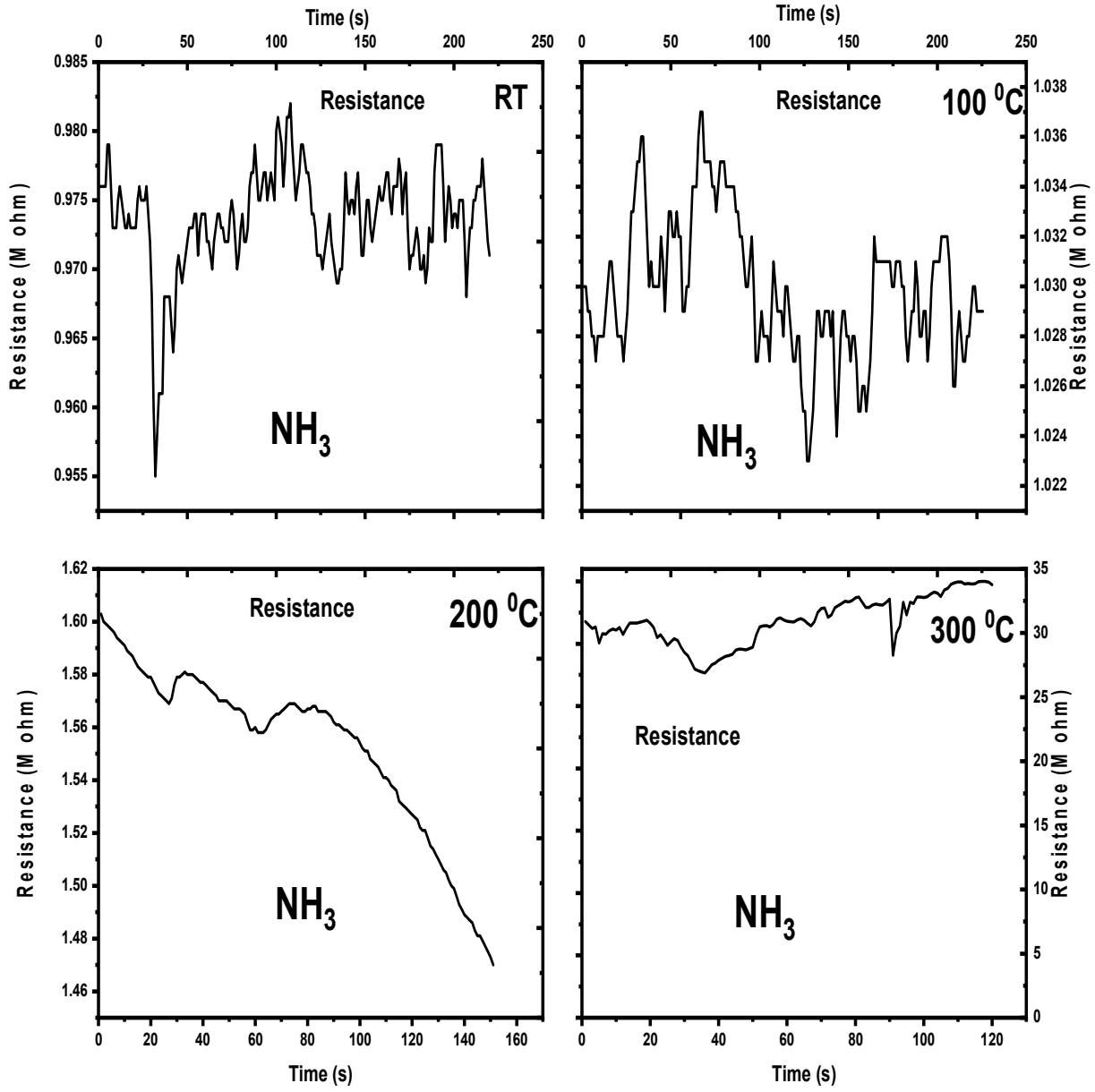

Figure(4.33b): The variation resistance with time for different operation temperature of NH_3 gas for the 75%wt of CdO gas sensor.

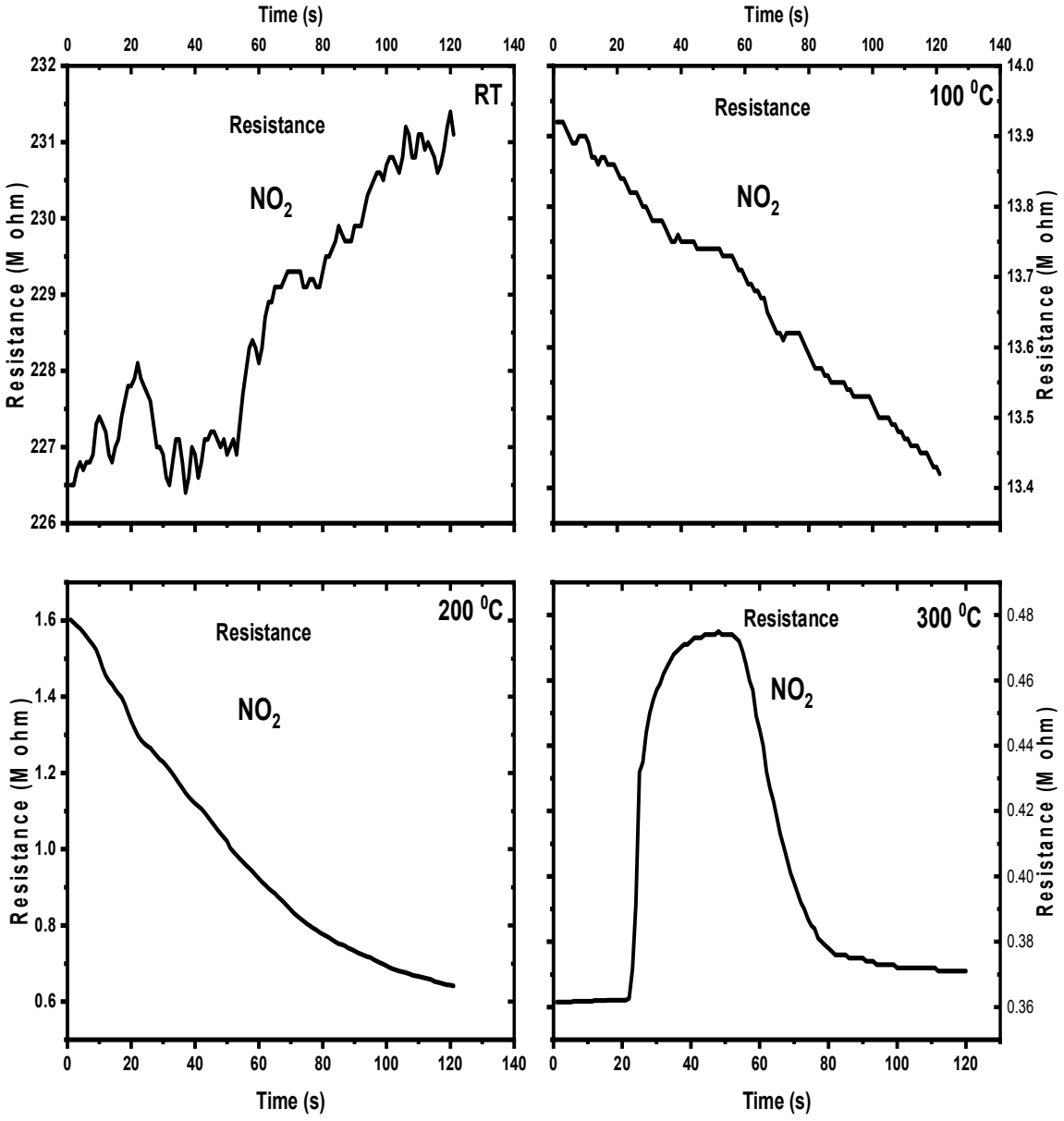

Figure(4.34a): The variation resistance with time for different operation temperature of NO_2 gas for the pure CdO (100%) gas sensor.

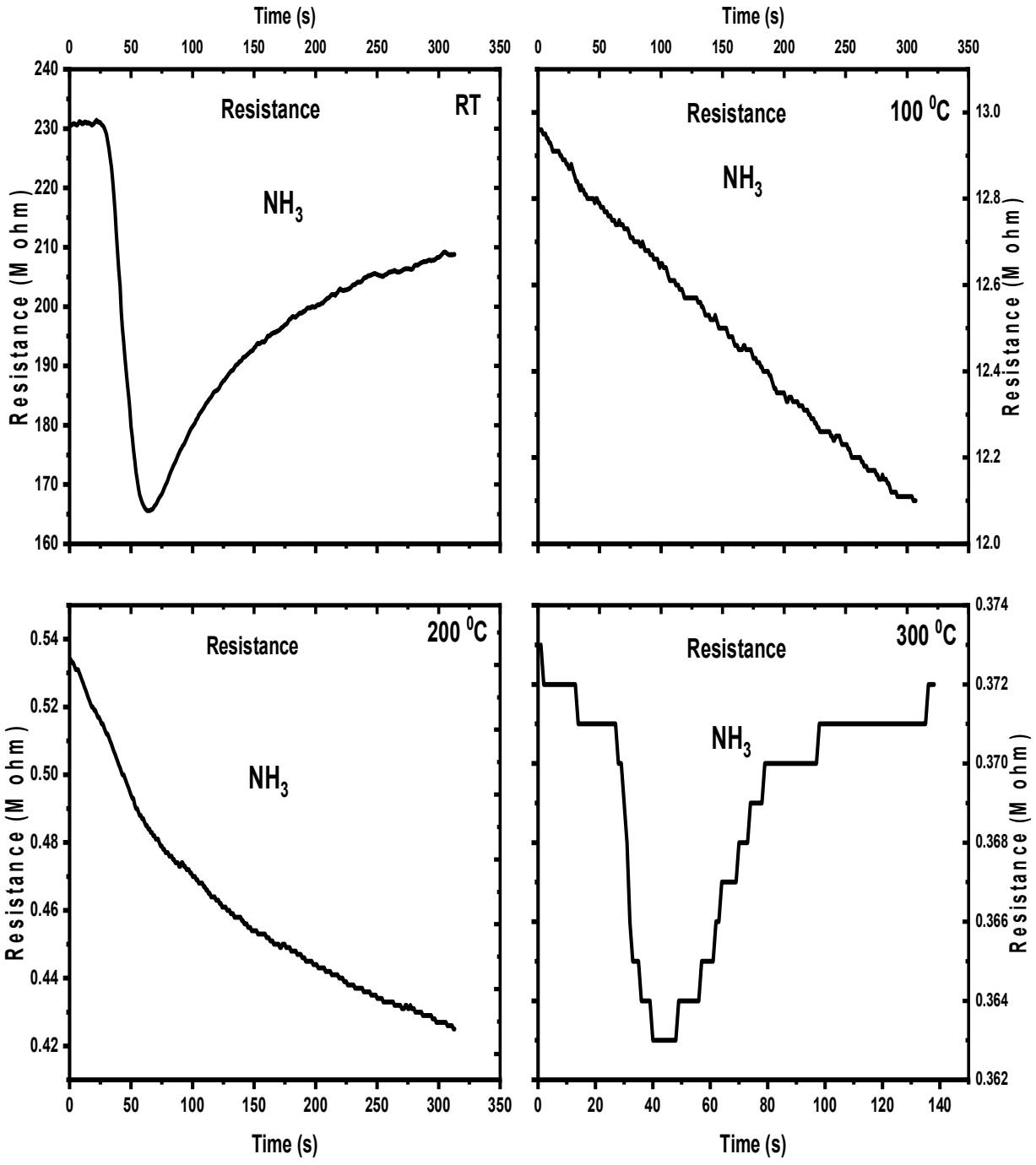

Figure(4.34b): The variation resistance with time for different operation temperature of NH_3 gas for the pure CdO(100%) gas sensor.

The resistance decreases abruptly until reaches a stable state, at which point the gas is turned off. The resistance of the electrical system then reverted to its original state. The existence of the reaction between the surface atoms and the gas molecules of the sensing film determines a sensor's ability to detect the presence of gas.

Figures (4.33) and (4.34) shows that when samples were exposed to NO_2 gas on the surface, their resistance increased while it decreased when exposed to NH_3 gas. The different behaviors of the samples show that pure CdO and the 75%wt of CdO composite have higher selectivity beavers for NO_2 oxidizing gas and NH_3 reducing gas, particularly at 300^{o}C.

4.6 Conclusions

In this section, the most important conclusions that have been reached in this research will be presented for the most important measurements and observations, which include the following:

1. Pulsed laser deposition has proven to be effective in the production of thin films at high pressures $\geq (10^{-4}$mbar).
2. The X-ray diffraction of $Ga_2O_{3\ (1-X)}CdO_{(X)}$ films prepared by a pulsed laser deposition method revealed that the films are polycrystalline, and when cadmium oxide is added to gallium oxide at a percentage of 25%wt of CdO or more, the compound $CdGa_2O_4$ is formed. The crystalline sizes are decreasing with increase with CdO percent addition.
3. Through the atomic force microscope (AFM) images, it was observed that the grain size decreases with increasing CdO concentration, and the film 75%wt of CdO can be considered as the smallest size of grain

size . There is also a decrease in the surface roughness rate and square root rate by increasing the CdO concentration with other fixed laser parameters.

4. By using Field Emission Scan Electronic Microscope (FESEM), the images show semi spherical shape of nanoparticles with a hole for pure 0%, 25% wt and 50%wt of CdO films while semi-spherical without a hole for other films, and a decrease in particle size when CdO is added.
5. The absorbance decreases with increasing of CdO concentration.
6. The optical energy gap decreases with increasing CdO concentration, and the lowest energy gap after the formation of compound $CdGa_2O_4$ is 4.18 eV for the films 75%wt.
7. The resistance and the resistivity increase with the increase of the temperature for the films 0%wt and 25%wt of CdO and vice versa for the other films.
8. The 0% film is p-type, and its electrical behavior remains dominant for the 25%wt film, while the 100% n- type film, and its electrical behavior is dominant on the (50%wt and 75%wt) of CdO films.
9. The samples have a greater sensitivity for NO_2 gas and have a greater sensitivity with operation temperature at room temperature (RT) for NH_3 gas.
10. For gas sensors samples with equal proportions or more CdO work at room temperature.
11. The response time and recovery time decreases with increasing operating temperature.

12. The fast response speed for NO_2 gas for 75% wt of CdO sample at 250^{o}C and (pure Ga_2O_3) for NH_3 gas.
13. The fast recover speed of NO_2 gas for 50% wt of CdO sample at 300^{o}C and 50% wt of CdO sample for NH_3 gas at 300^{o}C.

4.7 Future work and Suggestions

In the future, the following work may be proposed:

1. Synthesis and characterization TCOs semiconductor for biological sensing by PLD.
2. The use of TCOs for the manufacture of semiconductor laser media or random laser.
3. TCOs : synthesis and characterization using Pulsed Laser-Ablation in Liquids(PLAL).

References

1. R. Klinger, *Thin film deposition technologies, and structure/property relationships applied to solid state ionic conductors*. Solid State Ionics, 1992. **52**(1-3): p. 249.
2. D. L. Smith and D. W. Hoffman, *Thin-film deposition: principles and practice.* Physics Today, 1996. **49**: p. 60.
3. A. Wagendristel and Y. Wang, *An introduction to physics and technology of thin films*, World scientific, 1994.
4. J. Poortmans and V. Arkhipov, *Thin film solar cells: fabrication, characterization and applications*. Vol. 5. 2006: John Wiley & Sons.
5. K. Chopra, *Thin Film Phenomena MC Graw Hill Co.* New York, USA, 1969.
6. R. Siegel, E. Hu, and M. Roco. *WTEC panel report on R & D status and trends in nanoparticles, nanostructured materials, and nanodevices*. in *Workshop*. 1997.
7. A. Kumar, Y. Chung, J. Moore, and J. Smugeresky, *Surface engineering: Science and technology I. Warrendale, PA: The Minerals.* Metals & Materials Society, 1999.
8. A. Kumar, Y.-w. Chung, and R. W. Chia, *Hard Coatings Based on Borides, Carbides and Nitrides: Synthesis, Characterization and Application,*Minerals, Metals, & Materials Society, 1998.
9. T. Wagner, *Thin film science*, in *European White Book On Fundamental Research In Materials Science*. 2001.
10. L. Eckortova, *Physics of Thin Films Plenum Press*. New York and London, 1977.
11. J. R. Stetter and W. R. Penrose, *Understanding chemical sensors and chemical sensor arrays (electronic noses): Past, present, and future.* Sensors update, 2002. **10**(1): p. 189.
12. C. Wagner, *The mechanism of the decomposition of nitrous oxide on zinc oxide as catalyst.* The Journal of Chemical Physics, 1950. **18**(1): p. 69.
13. K. L. Chopra, S. Major, and D. K. Pandya, *Transparent conductors A status review.* Thin Solid Films, 1983. **102**(1): p. 1.
14. T. Seiyama, A. Kato, K. Fujiishi, and M. Nagatani, *A new detector for gaseous components using semiconductive thin films.* Analytical Chemistry, 1962. **34**(11): p. 1502.
15. G. Advani and A. Jordan, *Thin films of SnO_2 as solid state gas sensors.* Journal of Electronic Materials, 1980. **9**(1): p. 29.

16. P. Tischer, H. Pink, and L. Treitinger, *Operation and stability of SnO_2 gas sensors.* Japanese journal of applied physics, 1980. **19**(S1): p. 513.
17. H. Pink, L. Treitinger, and L. Vité, *Preparation of fast detecting SnO2 gas sensors.* Japanese journal of applied physics, 1980. **19**(3): p. 513.
18. I. Lee, S. J. Choi, K.-M. Park, S. S. Lee, S. Choi, I. D. Kim, and C. Park, *The stability, sensitivity and response transients of ZnO, SnO_2 and WO_3 sensors under acetone, toluene and H2S environments.* Sensors and Actuators B: Chemical, 2014. **197**: p. 300.
19. L. Deng, X. Ding, D. Zeng, S. Tian, H. Li, and C. Xie, *Visible-light activate mesoporous WO_3 sensors with enhanced formaldehyde-sensing property at room temperature.* Sensors and Actuators B: Chemical, 2012. **163**(1): p. 260.
20. T. Chen, Q. Liu, Z. Zhou, and Y. Wang, *The fabrication and gas-sensing characteristics of the formaldehyde gas sensors with high sensitivity.* Sensors and Actuators B: Chemical, 2008. **131**(1): p. 301.
21. L. Zhang, J. Zhao, H. Lu, L. Gong, L. Li, J. Zheng, H. Li, and Z. Zhu, *High sensitive and selective formaldehyde sensors based on nanoparticle-assembled ZnO micro-octahedrons synthesized by homogeneous precipitation method.* Sensors and Actuators B: Chemical, 2011. **160**(1): p. 364.
22. R. Cattrall, *Chemical Sensors,* Oxford University Press, New York, 1997.
23. S. M. Sze and K. K. Ng, *Physics of semiconductor devices* ,John wiley & sons, 2006.
24. M. V. Nikolic, V. Milovanovic, Z. Z. Vasiljevic, and Z. Stamenkovic, *Semiconductor gas sensors: Materials, technology, design, and application.* Sensors, 2020. **20**(22): p. 6694.
25. J. Jeevanandam, A. Barhoum, Y. S. Chan, A. Dufresne, and M. K. Danquah, *Review on nanoparticles and nanostructured materials: history, sources, toxicity and regulations.* Beilstein journal of nanotechnology, 2018. **9**(1): p. 1050.
26. S. Anu Mary Ealia and M. P. Saravanakumar, *A review on the classification, characterisation, synthesis of nanoparticles and their application.* IOP Conference Series: Materials Science and Engineering, 2017. **263**: p. 032019.
27. Y. Shen, L. Lu, Q. Lu, Z. Jin, and K. Lu, *Tensile properties of copper with nano-scale twins.* Scripta Materialia, 2005. **52**(10): p. 989.
28. S. Zhang, W. Li, C. Li, and J. Chen, *Synthesis, characterization, and electrochemical properties of $Ag_2V_4O_{11}$ and $AgVO_3$ 1-D*

nano/microstructures. The Journal of Physical Chemistry B, 2006. **110**(49): p. 24855.
29. A. Stadler, *Transparent conducting oxides—an up-to-date overview.* Materials, 2012. **5**(4): p. 661.
30. T. J. Coutts, T. O. Mason, J. Perkins, and D. S. Ginley, *Transparent conducting oxides: status and opportunities in basic research.* Proc. Electrochem. Soc, 1999. **99**(1999): p. 274.
31. J. Dudonis, A. Jotautis, and R. Naujokaitis, *A Study of Cd SnO Thin Film Deposited at Low Temperature using Reactive Magnetron Sputtering*. Elektronika IR Elektrotechnika. **47**(5).
32. L. R. P. Kassab, M. E. Fukumoto, V. D. D. Cacho, N. U. Wetter, and N. I. Morimoto, *Spectroscopic properties of $Yb3^{+}$ doped $PbO–Bi_2O_3–Ga_2O_3$ glasses for IR laser applications.* Optical Materials, 2005. **27**(10): p. 1576.
33. K. Chopra, S. Major, and D. Pandya, *Transparent conductors—a status review.* Thin Solid Films, 1983. **102**(1): p. 1.
34. R. B. King, *Encyclopedia of inorganic chemistry*, John Wiley & Sons, 1994.
35. B. Ingram, G. Gonzalez, D. Kammler, M. Bertoni, and T. O. Mason, *Chemical and structural factors governing transparent conductivity in oxides.* Journal of Electroceramics, 2004. **13**(1-3): p. 167.
36. R. Roy, V. Hill, and E. Osborn, *Polymorphism of Ga_2O_3 and the system $Ga_2O_3—H_2O$.* Journal of the American Chemical Society, 1952. **74**(3): p. 719.
37. S. Stepanov, V. Nikolaev, V. Bougrov, and A. Romanov, *Gallium OXIDE: Properties and application a review.* Reviews on Advanced Materials Science, 2016. **44**: p. 63.
38. H. Von Wenckstern, *Group-III sesquioxides: growth, physical properties and devices.* Advanced Electronic Materials, 2017. **3**(9): p. 1600350.
39. S. Yoshioka, H. Hayashi, A. Kuwabara, F. Oba, K. Matsunaga, and I. Tanaka, *Structures and energetics of Ga_2O_3 polymorphs*. Journal of Physics: Condensed Matter, 2007. **19**(34): p. 346211.
40. H. He, R. Orlando, M. A. Blanco, R. Pandey, E. Amzallag, I. Baraille, and M. Rérat, *First-principles study of the structural, electronic, and optical properties of Ga_2O_3 in its monoclinic and hexagonal phases.* Physical Review B, 2006. **74**(19): p. 195123.

41. H. He, M. Blanco, and R. Pandey, *Electronic and ther-modynamic properties of 13Ga_20_a.* Applied physics letters, 2006. **88**(261904): p. 1.

42. P. Kroll, R. Dronskowski, and M. Martin, *Formation of spinel-type gallium oxynitrides: a density-functional study of binary and ternary phases in the system Ga–O–N.* Journal of Materials Chemistry, 2005. **15**(32): p. 3296.
43. H. Y. Playford, A. C. Hannon, E. R. Barney, and R. I. Walton, *Structures of uncharacterised polymorphs of gallium oxide from total neutron diffraction.* Chemistry–A European Journal, 2013. **19**(8): p. 2803.
44. M. Saurat and A. Revcolevschi, *Preparation by floating zone method, of refractory oxide monocrystals, in particular of gallium oxide, and study of some of their properties.* Revue Internationale Des Hautes Temperatures Et Des Refractaires, 1971. **8**(3-4): p. 291.
45. J. Kohn, G. Katz, and J. Broder, *Characterization of β-Ga_2O_3 and its Alumina Isomorph, θ-Al_2O_3.* American Mineralogist: Journal of Earth and Planetary Materials, 1957. **42**(5-6): p. 398.
46. S. Pearton, J. Yang, P. H. Cary IV, F. Ren, J. Kim, M. J. Tadjer, and M. A. Mastro, *A review of Ga_2O_3 materials, processing, and devices.* Applied Physics Reviews, 2018. **5**(1): p. 011301.
47. S. D. Lee, K. Akaiwa, and S. Fujita, *Thermal stability of single crystalline alpha gallium oxide films on sapphire substrates.* physica status solidi (c), 2013. **10**(11): p. 1592.
48. E. G. Villora, K. Shimamura, T. Ujiie, and K. Aoki, *Electrical conductivity and lattice expansion of β-Ga_2O_3 below room temperature.* Applied Physics Letters, 2008. **92**(20): p. 202118.
49. Z. Galazka, K. Irmscher, R. Uecker, R. Bertram, M. Pietsch, A. Kwasniewski, M. Naumann, T. Schulz, R. Schewski, and D. Klimm, *On the bulk β-Ga_2O_3 single crystals grown by the Czochralski method.* Journal of Crystal Growth, 2014. **404**: p. 184.
50. J. Åhman, G. Svensson, and J. Albertsson, *A reinvestigation of β-gallium oxide.* Acta Crystallographica Section C: Crystal Structure Communications, 1996. **52**(6): p. 1336.
51. Y. Kokubun, K. Miura, F. Endo, and S. Nakagomi, *Sol-gel prepared β-Ga_2O_3 thin films for ultraviolet photodetectors.* Applied Physics Letters, 2007. **90**(3): p. 031912.

52. J. Hao and M. Cocivera, *Optical and luminescent properties of undoped and rare-earth-doped Ga_2O_3 thin films deposited by spray pyrolysis.* Journal of Physics D: Applied Physics, 2002. **35**(5): p. 433.
53. P. Wellenius, A. Suresh, J. Foreman, H. Everitt, and J. Muth, *A visible transparent electroluminescent europium doped gallium oxide device.* Materials Science and Engineering: B, 2008. **146**(1-3): p. 252.
54. M. Hai-Lin, F. Duo-Wang, and N. Xiao-Shan, *Preparation and NO_2-gas sensing property of individual β-Ga_2O_3 nanobelt.* Chinese Physics B, 2010. **19**(7): p. 076102.
55. F. Zhu, Z. Yang, W. Zhou, and Y. Zhang, *Annealing effects on the structural and optical properties of β-Ga_2O_3 nanobelts synthesized by microwave plasma chemical vapor deposition.* Physica E: Low-dimensional Systems and Nanostructures, 2006. **33**(1): p. 151.
56. Z. Liu, T. Yamazaki, Y. Shen, T. Kikuta, N. Nakatani, and Y. Li, *O_2 and CO sensing of Ga_2O_3 multiple nanowire gas sensors.* Sensors and Actuators B: Chemical, 2008. **129**(2): p. 666.
57. L. Jianjun, Y. Jinliang, S. Liang, and L. Ting, *Electrical and optical properties of deep ultraviolet transparent conductive Ga_2O_3/ITO films by magnetron sputtering.* Journal of Semiconductors, 2010. **31**(10): p. 103001.
58. S. Geller, *Crystal structure of β-Ga_2O_3.* The Journal of Chemical Physics, 1960. **33**(3): p. 676.
59. M. Lorenz, J. Woods, and R. Gambino, *Some electrical properties of the semiconductor β-Ga_2O_3.* Journal of Physics and Chemistry of Solids, 1967. **28**(3): p. 403.
60. M. Ogita, N. Saika, Y. Nakanishi, and Y. Hatanaka, *Ga_2O_3 thin films for high-temperature gas sensors.* Applied Surface Science, 1999. **142**(1-4): p. 188.
61. T. Oshima, T. Okuno, and S. Fujita, *Ga_2O_3 thin film growth on c-plane sapphire substrates by molecular beam epitaxy for deep-ultraviolet photodetectors.* Japanese journal of applied physics, 2007. **46**(11R): p. 7217.
62. R. Suzuki, S. Nakagomi, Y. Kokubun, N. Arai, and S. Ohira, *Enhancement of responsivity in solar-blind β-Ga_2O_3 photodiodes with a Au Schottky contact fabricated on single crystal substrates by annealing.* Applied Physics Letters, 2009. **94**(22): p. 222102.
63. M. Passlack, N. Hunt, E. Schubert, G. Zydzik, M. Hong, J. Mannaerts, R. Opila, and R. Fischer, *Dielectric properties of electron-beam deposited Ga_2O_3 films.* Applied Physics Letters, 1994. **64**(20): p. 2715.

64. M. Higashiwaki, K. Sasaki, A. Kuramata, T. Masui, and S. Yamakoshi, *Gallium oxide (Ga_2O_3) metal-semiconductor field-effect transistors on single-crystal β-Ga_2O_3 (010) substrates*. Applied Physics Letters, 2012. **100**(1): p. 013504.
65. K. Sasaki, M. Higashiwaki, A. Kuramata, T. Masui, and S. Yamakoshi, *Ga2O3 Schottky Barrier Diodes Fabricated by Using Single-Crystal beta -Ga_2O_3-(010) Substrates*. IEEE electron device letters, 2013. **34**(4): p. 493.
66. M. Higashiwaki, K. Sasaki, T. Kamimura, M. Hoi Wong, D. Krishnamurthy, A. Kuramata, T. Masui, and S. Yamakoshi, *Depletion-mode Ga_2O_3 metal-oxide-semiconductor field-effect transistors on β-Ga_2O_3 (010) substrates and temperature dependence of their device characteristics*. Applied Physics Letters, 2013. **103**(12): p. 123511.
67. M. Ogita, K. Higo, Y. Nakanishi, and Y. Hatanaka, *Ga_2O_3 thin film for oxygen sensor at high temperature*. Applied Surface Science, 2001. **175**: p. 721.
68. W. Cui, X. Zhao, Y. An, D. Guo, X. Qing, Z. Wu, P. Li, L. Li, C. Cui, and W. Tang, *Direct charge carrier injection into Ga_2O_3 thin films using an In2O3 cathode buffer layer: their optical, electrical and surface state properties*. Journal of Physics D: Applied Physics, 2017. **50**(13): p. 135109.
69. C. Baban, Y. Toyoda, and M. Ogita, *Oxygen sensing at high temperatures using Ga_2O_3 films*. Thin Solid Films, 2005. **484**(1-2): p. 369.
70. C.-I. Baban, Y. Toyoda, and M. Ogita, *High temperature oxygen sensor using a Pt–Ga_2O_3–Pt sandwich structure*. Japanese journal of applied physics, 2004. **43**(10R): p. 7213.
71. M. Fleischer and H. Meixner, *Characterization of gas-sensitive, polycrystalline Ga_2O_3 thin-films*. J. Mater. Sci. Lett., 1992. **11**: p. 1728.
72. M. Fleischer and H. Meixner, *Sensing reducing gases at high temperatures using long-term stable Ga_2O_3 thin films*. Sensors and Actuators B: Chemical, 1992. **6**(1-3): p. 257.
73. J. Frank, M. Fleischer, and H. Meixner, *Electrical doping of gas-sensitive, semiconducting Ga_2O_3 thin films*. Sensors and Actuators B: Chemical, 1996. **34**(1-3): p. 373.
74. M. Fleischer, L. Höllbauer, and H. Meixner, *Effect of the sensor structure on the stability of Ga_2O_3 sensors for reducing gases*. Sensors and Actuators B: Chemical, 1994. **18**(1-3): p. 119.

75. F. Réti, M. Fleischer, H. Meixner, and J. Giber, *Effect of coadsorption of reducing gases on the conductivity of β-Ga_2O_3 thin films in the presence of O2.* Sensors and Actuators B: Chemical, 1994. **19**(1-3): p. 573.
76. M. Fleischer and H. Meixner, *Selectivity in high-temperature operated semiconductor gas-sensors.* Sensors and Actuators B: Chemical, 1998. **52**(1-2): p. 179.
77. M. Fleischer and H. Meixner, *Gallium oxide thin films: a new material for high-temperature oxygen sensors.* Sensors and Actuators B: Chemical, 1991. **4**(3-4): p. 437.
78. M. Fleischer and H. Meixner, *Improvements in Ga_2O_3 sensors for reducing gases.* Sensors and Actuators B: Chemical, 1993. **13**(1-3): p. 259.
79. W. M. Haynes, *CRC handbook of chemistry and physics,* CRC press, 2014.
80. E. G. Víllora, S. Arjoca, K. Shimamura, D. Inomata, and K. Aoki. -*Ga_2O_3 and single-crystal phosphors for high-brightness white LEDs and LDs, and Ga_2O_3 potential for next generation of power devices*. in *Oxide-based Materials and Devices* ,International Society for Optics and Photonics, 2014.
81. I. Bhaumik, R. Bhatt, S. Ganesamoorthy, A. Saxena, A. Karnal, P. Gupta, A. Sinha, and S. Deb, *Temperature-dependent index of refraction of monoclinic Ga_2O_3 single crystal.* Applied optics, 2011. **50**(31): p. 6006.
82. Z. Guo, A. Verma, X. Wu, F. Sun, A. Hickman, T. Masui, A. Kuramata, M. Higashiwaki, D. Jena, and T. Luo, *Anisotropic thermal conductivity in single crystal β-gallium oxide.* Applied Physics Letters, 2015. **106**(11): p. 111909.
83. H. Stumpf and A. Russel, *1. W. Newsome and CM Tucker.* Ind. Eng. Chem, 1950. **42**(7).
84. F. Streintz, *Ueber die elektrische Leitfähigkeit von gepressten Pulvern.* Annalen der Physik, 1902. **314**(12): p. 854.
85. K. Badeker, *Concerning the electricity conductibility and the thermoelectric energy of several heavy metal bonds.* Annalen der Physik, 1907. **22**: p. 749.
86. M. Ortega, G. Santana, and A. Morales-Acevedo, *Optoelectronic properties of CdO/Si photodetectors.* Solid-State Electronics, 2000. **44**(10): p. 1765.
87. R. Ferro and J. Rodrıguez, *Influence of F-doping on the transmittance and electron affinity of CdO thin films suitable for solar cells*

technology. Solar Energy Materials and Solar Cells, 2000. **64**(4): p. 363.

88. M. H. Suhail, I. M. Ibrahim, and G. M. Rao, *Characterization and gas sensitivity of cadmium oxide thin films prepared by thermal evaporation technique.* Journal of Electron Devices, 2012. **13**: p. 965.
89. Z. Zhao, D. Morel, and C. Ferekides, *Electrical and optical properties of tin-doped CdO films deposited by atmospheric metalorganic chemical vapor deposition.* Thin Solid Films, 2002. **413**(1-2): p. 203.
90. L. Su, N. Grote, and F. Schmitt, *Diffused planar InP bipolar transistor with a cadmium oxide film emitter.* Electronics Letters, 1984. **20**(18): p. 716.
91. O. Vigil, F. Cruz, A. Morales-Acevedo, G. Contreras-Puente, L. Vaillant, and G. Santana, *Structural and optical properties of annealed CdO thin films prepared by spray pyrolysis.* Materials Chemistry and Physics, 2001. **68**(1-3): p. 249.
92. R. Mishra, A. Sharma, and S. Prakash, *Gas sensitivity and characterization of cadmium oxide (CdO) semi conducting thin film deposited by spray pyrolysis technique.* Digest Journal of Nanomaterials and Biostructures, 2009. **4**(3): p. 511.
93. K. Gurumurugan, D. Mangalaraj, and S. K. Narayandass, *Correlations between the optical and electrical properties of CdO thin films deposited by spray pyrolysis.* Thin Solid Films, 1994. **251**(1): p. 7.
94. G. Santana, A. M. Acevedo, O. Vigil, F. Cruz, G. C. Puente, and L. Vaillant, *Structural and optical properties of (ZnO) x (CdO) 1-x thin films obtained by spray pyrolysis.* Superficies y vacío, 1999(9): p. 300.
95. T. Subramanyam, S. Uthanna, and B. S. Naidu, *Preparation and characterization of CdO films deposited by DC magnetron reactive sputtering.* Materials Letters, 1998. **35**(3-4): p. 214.
96. N. Ueda, H. Maeda, H. Hosono, and H. Kawazoe, *Band-gap widening of CdO thin films.* Journal of applied Physics, 1998. **84**(11): p. 6174.
97. A. Tadjarodi and M. Imani, *Synthesis and characterization of CdO nanocrystalline structure by mechanochemical method.* Materials Letters, 2011. **65**(6): p. 1025.
98. H. Hobert and B. Seltmann, *Infrared study of $SiO_2/TiO_2/CdO$ layers on glass prepared by the sol-gel method.* Journal of non-crystalline solids, 1996. **195**(1-2): p. 54.

99. A. A. Yousif and M. H. Hasan, *Gas sensitivity and morphologically characterized of nanostructure CdO doped In_2O_3 films deposited by pulsed laser deposition*. J. Biosens. Bioelectron, 2015. **6**(4): p. 4.
100. R. Chandiramouli and B. Jeyaprakash, *Review of CdO thin films.* Solid State Sciences, 2013. **16**: p. 102.
101. U. D. o. Health and H. Services, *Toxicological Profile for Cadmium. Draft for Public Comment.* Agency for Toxic Substances and Disease Registry, Atlanta, 1997.
102. P. Patnaik, *Handbook of inorganic chemicals*. Vol. 529,McGraw-Hill New York, 2003.
103. I. Inchem, *Chemical Safety Information from Intergovernmental Organizations.* Canadian Centre for, 2011.
104. M. Fleischer and H. Meixner, *Oxygen sensing with long-term stable Ga2O3 thin films.* Sensors and Actuators B: Chemical, 1991. **5**(1): p. 115.
105. M. Fleischer and H. Meixner, *Improvements in Ga_2O_3 sensors for reducing gases.* Sensors and Actuators B: Chemical, 1993. **13**(1): p. 259.
106. M. Fleischer, L. Höllbauer, and H. Meixner, *Effect of the sensor structure on the stability of Ga_2O_3 sensors for reducing gases.* Sensors and Actuators B: Chemical, 1994. **18**(1): p. 119.
107. M. Fleischer and H. Meixner, *A selective CH_4 sensor using semiconducting Ga_2O_3 thin films based on temperature switching of multigas reactions.* Sensors and Actuators B: Chemical, 1995. **25**(1): p. 544.
108. M. Fleischer, M. Seth, C. D. Kohl, and H. Meixner, *A selective H2 sensor implemented using Ga_2O_3 thin-films which are covered with a gas-filtering SiO_2 layer.* Sensors and Actuators B: Chemical, 1996. **36**(1): p. 297.
109. J. Frank, M. Fleischer, and H. Meixner, *Electrical doping of gas-sensitive, semiconducting Ga_2O_3 thin films.* Sensors and Actuators B: Chemical, 1996. **34**(1): p. 373.
110. F. Réti, M. Fleischer, I. V. Perczel, H. Meixner, and J. Giber, *Detection of reducing gases in air by β-Ga_2O_3 thin films using self-heated and externally (oven-) heated operation modes.* Sensors and Actuators B: Chemical, 1996. **34**(1): p. 378.
111. T. Schwebel, M. Fleischer, H. Meixner, and C. D. Kohl, *CO-Sensor for domestic use based on high temperature stable Ga_2O_3 thin films.* Sensors and Actuators B: Chemical, 1998. **49**(1): p. 46.

112. J. Frank, M. Fleischer, H. Meixner, and A. Feltz, *Enhancement of sensitivity and conductivity of semiconducting Ga_2O_3 gas sensors by doping with SnO2.* Sensors and Actuators B: Chemical, 1998. **49**(1): p. 110.
113. G. K. Flingelli, M. M. Fleischer, and H. Meixner, *Selective detection of methane in domestic environments using a catalyst sensor system based on Ga_2O_3.* Sensors and Actuators B: Chemical, 1998. **48**(1): p. 258.
114. M. Ogita, N. Saika, Y. Nakanishi, and Y. Hatanaka, *Ga_2O_3 thin films for high-temperature gas sensors.* Applied Surface Science, 1999. **142**(1): p. 188.
115. T. Schwebel, M. Fleischer, and H. Meixner, *A selective, temperature compensated O2 sensor based on Ga_2O_3 thin films.* Sensors and Actuators B: Chemical, 2000. **65**(1): p. 176.
116. K. Gurumurugan, D. Mangalaraj, S. K. Narayandass, K. Sekar, and C. P. G. Vallabhan, *Characterization of transparent conducting CdO films deposited by spray pyrolysis.* Semiconductor Science and Technology, 1994. **9**(10): p. 1827.
117. X. Liu, Z. Xu, Y. Liu, and Y. Shen, *A novel high performance ethanol gas sensor based on CdO/Fe_2O_3 semiconducting materials.* Sensors and Actuators B: Chemical, 1998. **52**(3): p. 270.
118. K. Gurumurugan, D. Mangalaraj, and S. Narayandass, *Magnetron sputtered transparent conducting CdO thin films.* Journal of Electronic Materials, 1996. **25**(5): p. 765.
119. T. Minami, Y. Takeda, T. Kakumu, S. Takata, and I. Fukuda, *Preparation of highly transparent and conducting Ga_2O_3–In_2O_3 films by direct current magnetron sputtering.* Journal of Vacuum Science & Technology A, 1997. **15**(3): p. 958.
120. T. Minami, *Transparent and conductive multicomponent oxide films prepared by magnetron sputtering.* Journal of Vacuum Science & Technology A, 1999. **17**(4): p. 1765.
121. M. Ogita, K. Higo, Y. Nakanishi, and Y. Hatanaka, *Ga_2O_3 thin film for oxygen sensor at high temperature.* Applied Surface Science, 2001. **175-176**: p. 721.
122. U. Hoefer, J. Frank, and M. Fleischer, *High temperature Ga_2O_3-gas sensors and SnO_2-gas sensors: a comparison.* Sensors and Actuators B: Chemical, 2001. **78**(1): p. 6.
123. T. Weh, J. Frank, M. Fleischer, and H. Meixner, *On the mechanism of hydrogen sensing with SiO_2 modificated high temperature Ga_2O_3 sensors.* Sensors and Actuators B: Chemical, 2001. **78**(1): p. 202.

124. Y. Li, A. Trinchi, W. Wlodarski, K. Galatsis, and K. Kalantar-zadeh, *Investigation of the oxygen gas sensing performance of Ga_2O_3 thin films with different dopants.* Sensors and Actuators B: Chemical, 2003. **93**(1): p. 431.
125. C. Xiangfeng and Z. Chenmou, *Preparation and gas-sensing properties of $CdGa_2O_4$ semiconductors.* Materials Chemistry and Physics, 2004. **88**(1): p. 110.
126. G. Eranna, B. C. Joshi, D. P. Runthala, and R. P. Gupta, *Oxide Materials for Development of Integrated Gas Sensors—A Comprehensive Review.* Critical Reviews in Solid State and Materials Sciences, 2004. **29**(3-4): p. 111.
127. C. Baban, Y. Toyoda, and M. Ogita, *Oxygen sensing at high temperatures using Ga_2O_3 films.* Thin Solid Films, 2005. **484**(1): p. 369.
128. R. J. Deokate, S. V. Salunkhe, G. L. Agawane, B. S. Pawar, S. M. Pawar, K. Y. Rajpure, A. V. Moholkar, and J. H. Kim, *Structural, optical and electrical properties of chemically sprayed nanosized gallium doped CdO thin films.* Journal of Alloys and Compounds, 2010. **496**(1): p. 357.
129. M. Isai, S. Kayano, and N. Yamaguchi, *Preparation and evaluation of Ga_2O_3 oxygen sensors.* Transactions of the Materials Research Society of Japan, 2011. **36**(2): p. 253.
130. H. Kim, C. Jin, S. An, and C. Lee, *Fabrication and CO gas-sensing properties of Pt-functionalized Ga_2O_3 nanowires.* Ceramics International, 2012. **38**(5): p. 3563.
131. S. Kumar and R. Singh, *Nanofunctional gallium oxide (Ga_2O_3) nanowires/nanostructures and their applications in nanodevices.* physica status solidi (RRL) – Rapid Research Letters, 2013. **7**(10): p. 781.
132. R. Chandiramouli and B. G. Jeyaprakash, *Review of CdO thin films.* Solid State Sciences, 2013. **16**: p. 102.
133. S. Nakagomi, T. Sai, and Y. Kokubun, *Hydrogen gas sensor with self temperature compensation based on β-Ga_2O_3 thin film.* Sensors and Actuators B: Chemical, 2013. **187**: p. 413.
134. R. Pandeeswari and B. G. Jeyaprakash, *High sensing response of β-Ga_2O_3 thin film towards ammonia vapours: Influencing factors at room temperature.* Sensors and Actuators B: Chemical, 2014. **195**: p. 206.
135. A. Goyal, B. S. Yadav, O. P. Thakur, and A. K. Kapoor. *Structural and Optical Characterization of β-Ga_2O_3 Thin Films Grown by*

Pulsed Laser Deposition. in *Physics of Semiconductor Devices*. 2014. Cham: Springer International Publishing.

136. E. Li, H. Zhuo, H. He, N. Wang, and T. Liu, *Structural, optical, and electrical properties of low-concentration Ga-doped CdO thin films by pulsed laser deposition.* Journal of Materials Science, 2016. **51**(15): p. 7179.
137. A. Ramizy and I. M. Ibrahim, *Preparation and Study of Cadmium Oxide Doped Gallium Oxide Thin Films and application of Gas Sensor.* Journal of Kufa-physics, 2017. **9**(2): p. 10.
138. I. E. Demin and A. G. Kozlov, *Effect of composition on properties of In_2O_3–Ga_2O_3 thin films.* Journal of Physics: Conference Series, 2017. **858**: p. 012009.
139. I. E. Demin and A. G. Kozlov, *Selectivity of the gas sensor based on the 50%In_2O_3–50%Ga_2O_3 thin film in dynamic mode of operation.* Journal of Physics: Conference Series, 2018. **944**: p. 012027.
140. P. Gupta, M. Kumar, and R. Nagarajan, *Interplay between defects and cation nonstoichiometry in lithium-substituted $CdGa_2O_4$ leading to multifunctional behavior.* The Journal of Physical Chemistry C, 2018. **122**(38): p. 22094.
141. M. Kumar, S. Kumar, V. Kumar, and R. Singh, *5 - Growth, properties, and applications of β-Ga_2O_3 nanostructures*, in *Gallium Oxide*, S. Pearton, F. Ren, and M. Mastro, Editors. 2019, Elsevier. p. 91.
142. D. Guo, Q. Guo, Z. Chen, Z. Wu, P. Li, and W. Tang, *Review of Ga2O3-based optoelectronic devices.* Materials Today Physics, 2019. **11**: p. 100157.
143. H. Yang, Y. Liu, X. Luo, Y. Li, D.-S. Wuu, K. He, and Z. C. Feng, *Effects of growth temperature and thickness on structure and optical properties of Ga_2O_3 films grown by pulsed laser deposition.* Superlattices and Microstructures, 2019. **131**: p. 21.
144. H. Shen, K. Baskaran, Y. Yin, K. Tian, L. Duan, X. Zhao, and A. Tiwari, *Effect of thickness on the performance of solar blind photodetectors fabricated using PLD grown β-Ga_2O_3 thin films.* Journal of Alloys and Compounds, 2020. **822**: p. 153419.
145. V. Zade, N. Makeswaran, B. L. Boyce, F. Paraguay-Delgado, and C. Ramana, *Structural and mechanical properties of nanocrystalline Ga_2O_3 films made by pulsed laser deposition onto transparent quartz substrates.* Nano Express, 2021. **2**(2): p. 020006.
146. H. Wen, Y. Jiang, C. Jiao, X. Chu, S. Liang, and L. He, *High gas sensing selectivity and sensitivity of $CdGa_2O_4$ nanospheres to ppb-*

level formaldehyde. Inorganic Chemistry Communications, 2021: p. 108752.
147. M. S. Brown and C. B. Arnold, *Fundamentals of laser-material interaction and application to multiscale surface modification*, in *Laser precision microfabrication*. 2010, Springer. p. 91.
148. H. Smith and A. Turner, *Pulse Laser Deposition-Versatile Thin Film Technique*. Appl. Optic, 1965. **4**: p. 147.
149. M. N. Ashfold, F. Claeyssens, G. M. Fuge, and S. J. Henley, *Pulsed laser ablation and deposition of thin films.* Chemical Society Reviews, 2004. **33**(1): p. 23.
150. C. A. Hampel and G. G. Hawley, *Encyclopedia of chemistry.* 1973.
151. E. T. S. Al-Waisy, *Pulsed laser deposition of some TCO films for optoelectronic Application.* Ph. DthesisUniversity of Technology Department of Applied Science, 2006.
152. D. Chrisey and G. Hubler, *Pulsed Laser Deposition of Thin Films, John Wiley & Sons.* New York, 1994.
153. A. Giardini, V. Marotta, A. Morone, S. Orlando, and G. Parisi, *Thin films deposition in RF generated plasma by reactive pulsed laser ablation.* Applied Surface Science, 2002. **197**: p. 338.
154. O. Svelto and D. C. Hanna, *Principles of lasers*. Vol. 1.,Springer, 2010.
155. D. B. Chrisey and G. K. Hubler, *Pulsed laser deposition of thin films.* 1994.
156. X. Vilanova, *Development of a Thin Film Gas Sensor for Oxygen Detection at Trace Levels*., Ph. D. Thesis, Helsinki University of Technology, 2006.
157. A. Ashrafi and C. Jagadish, *Review of zincblende ZnO: Stability of metastable ZnO phases.* Journal of applied Physics, 2007. **102**(7): p. 4.
158. R. Ajimsha and M. Jayaraj, *Growth and Characterization of ZnO based Heterojunction diodes and ZnO Nanostructuresby Pulsed Laser Ablation*., Department of Physics, 2008.
159. X. Han, G. Wang, J. Jie, X. Zhu, and J. Hou, *Properties of Zn1−xCoxO thin films grown on silicon substrates prepared by pulsed laser deposition*. Thin Solid Films, 2005. **491**(1-2): p. 249.
160. D. Geohegan, D. Chrisey, and G. Hubler, *Pulsed laser deposition of thin films.* Chrisey and GK Hubler (eds), Wiely, New York, 1994.
161. M. Vendan, *Ultrafast laser deposition and microfabrication of thin films for MEMS structures.* 2006.

162. H. Hartnagel, *Semiconducting transparent thin films*,CRC Press, 1995.
163. F. Adurodija, H. Izumi, T. Ishihara, H. Yoshioka, M. Motoyama, and K. Murai, *Influence of substrate temperature on the properties of indium oxide thin films.* Journal of Vacuum Science & Technology A: Vacuum, Surfaces, and Films, 2000. **18**(3): p. 814.
164. A. Suzuki, T. Matsushita, T. Aoki, Y. Yoneyama, and M. Okuda, *Pulsed laser deposition of transparent conducting indium tin oxide films in magnetic field perpendicular to plume.* Japanese journal of applied physics, 2001. **40**(4B): p. L401.
165. R. Eason, *Pulsed laser deposition of thin films: applications-led growth of functional materials,*John Wiley & Sons, 2007.
166. G. E. Jauncey, *The Scattering of X-Rays and Bragg's Law.* Proceedings of the National Academy of Sciences of the United States of America, 1924. **10**(2): p. 57.
167. W. Friedrich, P. Knipping, M. v. Laue, and I.-E. bei Röntgenstrahlen, *Sitzungsberichte der Mathematisch-Physikalischen Classe der Königlich-Bayerischen Akademie der Wissenschaften zu München*., München,1912.
168. D. E. Sands, *Introduction to crystallography,* Courier Corporation, 1993.
169. C. Kittel, P. McEuen, and P. McEuen, *Introduction to solid state physics*. Vol. 8. ,Wiley New York, 1996.
170. A. H. O. Alkhayatt and S. K. Hussian, *Fluorine dopant concentration effect on the structural and optical properties of spray deposited nanocrystalline ZnO thin films.* Surfaces and Interfaces, 2017. **8**: p. 176.
171. P. Mallick and C. Sahoo, *Effect of CuO addition on the structural and optical properties of NiO nanoparticles.* Nanosci. Nanotechol, 2013. **3**: p. 52.
172. P. Chate, D. Sathe, and P. Hankare, *Electrical and crystallographic properties of nanocrystalline CdSe 0.5 S 0.5 composite thin films deposited by dip method.* Journal of Materials Science: Materials in Electronics, 2011. **22**(2): p. 111.
173. J. Pankove, *Optical processes in semiconductors Prentice-Hall*. New Jersey, 1971. **92**.
174. E. Meyer, *Atomic force microscopy.* Progress in surface science, 1992. **41**(1): p. 3.

175. F. Zhang, H. Li, and Q. Guo, *Structural and Electrical Properties of Ga_2O_3 Films Deposited under Different Atmospheres by Pulsed Laser Deposition.* Journal of Electronic Materials, 2018. **47**(11): p. 6635.
176. H. Cik Rohaida Che, C. T. Foo, and O. Nor Azillah Fatimah. *Field Emission Scanning Electron Microscope (FESEM) Facility in BTI*. in *NTC 2015: Nuclear Technical Convention* ,Malaysia,2015.
177. W. Zhou, R. Apkarian, Z. L. Wang, and D. Joy, *Fundamentals of scanning electron microscopy (SEM)*, in *Scanning microscopy for nanotechnology*, Springer, 2006.
178. A. Ul-Hamid, *A beginners' guide to scanning electron microscopy*. Vol. 1. ,Springer, 2018.
179. S. K. Patra, *A novel chemical approach to fabricate ZnO Nanostructure.* Master of Technology (Thesis), 2008.
180. J. Sans, A. Segura, J. Sánchez-Royo, V. Barber, M. Hernández-Fenollosa, and B. Marí, *Correlation between optical and transport properties of Ga-doped ZnO thin films prepared by pulsed laser deposition*. Superlattices and Microstructures, 2006. **39**(1-4): p. 282.
181. I. Hamberg, C. G. Granqvist, K.-F. Berggren, B. E. Sernelius, and L. Engström, *Band-gap widening in heavily Sn-doped In_2O_3.* Physical Review B, 1984. **30**(6): p. 3240.
182. S. Ryabtsev, N. Hadia, and E. Domashevskaya, *Study of ZnO, SnO_2 and ZnO/SnO_2 nanostructures synthesized by the gas-transport.* Kondensirovannye sredy i mezhfaznye granitsy= Condensed Matter and Interphases, 2010. **12**(1): p. 17.
183. J. Pankove, *Optical processes on semiconductors Dover publication.* Inc. New york, 1971.
184. R. J. Elliott and A. F. Gibson, *An introduction to solid state physics and its applications,* Barnes & Noble, 1974.
185. D. C. Look, J. W. Hemsky, and J. Sizelove, *Residual native shallow donor in ZnO.* Physical review letters, 1999. **82**(12): p. 2552.
186. S. Pati, A. Maity, P. Banerji, and S. Majumder, *Qualitative and quantitative differentiation of gases using ZnO thin film gas sensors and pattern recognition analysis.* Analyst, 2014. **139**(7): p. 1796.
187. L. Kazmerski, *Polycrystalline and amorphous thin films and devices,* Elsevier, 2012.
188. D. Caiteanu, E. György, S. Grigorescu, I. Mihailescu, G. Prodan, and V. Ciupina, *Growth of oxide thin films for optical gas sensor applications.* Applied Surface Science, 2006. **252**(13): p. 4582.
189. A. A. Islam and A. Mondal, *Recent Developments in Condensed Matter Physics and Nuclear Science: Proceedings of the International*

Workshop Held at Rajshahi University, Bangladesh, 28 Oct.-1 Nov. 1996. Vol. 1. ,Physics Department Rajshahi University, 1997.
190. M. A. Omar, *Elementary solid state physics: principles and applications* ,Pearson Education India, 1975.
191. D. S. Ginley and C. Bright, *Transparent conducting oxides*. MRS bulletin, 2000. **25**(8): p. 15.
192. N. Bogoroditsky, V. Pasynkor, and T. BM, *Electrical Engineering* Materials, Mir Publishers, Moscow, 1979.
193. A. Efros and B. Shklovskii, *Critical behaviour of conductivity and dielectric constant near the metal-non-metal transition threshold.* Physica status solidi (b), 1976. **76**(2): p. 475.
194. B. Sharma and R. Purohit, *Semiconductor heterojunctions*. Vol. 5. ,Elsevier, 2015.
195. T. Tsurumi, S. Nishizawa, N. Ohashi, and T. Ohgaki, *Electric properties of zinc oxide epitaxial films grown by ion-beam sputtering with oxygen-radical irradiation.* Japanese journal of applied physics, 1999. **38**(6R): p. 3682.
196. B. G. Streetman and S. Banerjee, *Solid state electronic device,* Prentice-Hall of India, 2001.
197. P. Kireev, *Semiconductor Physics in Russian.* Vysshaya Shkola, Moscow, 1969.
198. G. B. Armen, *Hall Effect Experiment.* Department of Physics and Astronomy, 2007. **401**: p. 37996.
199. H. D. Young, R. A. Freedman, T. Sandin, and A. L. Ford, *University physics*. Vol. 9. ,Addison-Wesley Reading, MA, 1996.
200. Y. Kang, K. Krishnaswamy, H. Peelaers, and C. G. Van de Walle, *Fundamental limits on the electron mobility ofβ-Ga_2O_3.* Journal of Physics: Condensed Matter, 2017. **29**(23): p. 234001.
201. T. Seiyama, *Chemical Sensor Technology: Volume 2*. Vol. 2. ,Elsevier, 2013.
202. A. Hulanicki, S. Glab, and F. Ingman, *Chemical sensors: definitions and classification.* Pure and Applied Chemistry, 1991. **63**(9): p. 1247.
203. K. Karki, K. Gnanasekar, and B. Rambabu, *Nanostructured Semiconductor Oxide Powders and thin Films for Gas Sensors*. Appl. Sur. Sci,2002.
204. D. Bandgar, S. Navale, G. Khuspe, S. Pawar, R. Mulik, and V. Patil, *Novel route for fabrication of nanostructured α-Fe_2O_3 gas sensor.* Materials science in semiconductor processing, 2014. **17**: p. 67.
205. E. Scerri, *The periodic table: its story and its significance* ,Oxford University Press, 2019.

206. G. E. Patil, D. Kajale, D. Chavan, N. Pawar, P. Ahire, S. Shinde, V. Gaikwad, and G. Jain, *Synthesis, characterization and gas sensing performance of SnO_2 thin films prepared by spray pyrolysis.* Bulletin of Materials Science, 2011. **34**(1): p. 1.
207. R. H. Bari, S. Patil, and A. Bari, *Synthesis, Characterization and Gas Sensing Performance of Sol-gel Prepared Nanocrystalline SnO_2 Thin Films.* International Journal on Smart Sensing & Intelligent Systems, 2014. **7**(2):p.1.
208. M. Mahabole, R. Aiyer, C. Ramakrishna, B. Sreedhar, and R. Khairnar, *Synthesis, characterization and gas sensing property of hydroxyapatite ceramic.* Bulletin of Materials Science, 2005. **28**(6): p. 535.
209. X. Song, L. Gao, and S. Mathur, *Synthesis, Characterization, and Gas Sensing Properties of Porous Nickel Oxide Nanotubes.* The Journal of Physical Chemistry C, 2011. **115**(44): p. 21730.
210. S. Bagga, *Gas sensor-studies on sensor film deposition, ASIC design and testing*. 2009.
211. G. Korotcenkov, *Gas response control through structural and chemical modification of metal oxide films: state of the art and approaches.* Sensors and Actuators B: Chemical, 2005. **107**(1): p. 209.
212. T. Miller, S. Bakrania, C. Perez, and M. Wooldridge, *Nanostructured tin dioxide materials for gas sensor applications.* Functional Nanomaterials, 2006. **30**: p. 453.
213. R. Mishra, S. K. Mishra, and S. Prakash, *Optical and Gas Sensing Characteristics of Tin Oxide Nano-Crystalline Thin Film.* Journal of Ovonic Research, 2009. **5**(4):p.1.
214. V. Mishra and R. Agarwal, *Sensitivity, response and recovery time of SnO2 based thick-film sensor array for H_2, CO, CH_4 and LPG.* Microelectronics Journal, 1998. **29**(11): p. 861.
215. R. Moos, K. Sahner, M. Fleischer, U. Guth, N. Barsan, and U. Weimar, *Solid state gas sensor research in Germany–a status report.* Sensors, 2009. **9**(6): p. 4323.
216. P. Meakin and R. Jullien, *Restructuring effects in the rain model for random deposition*. journal de Physique, 1987. **48**(10): p. 1651.
217. J. Welton-Holzer, G. McCarthy, and I. Grant-in-Aid, *North Dakota State University*. Fargo, North Dakota, USA, ICDD Grant-in-Aid, 1989.

218. H. Swanson, R. Fuyat, and G. Ugrinic, *US Natl. Bur. Stand. Circ., 1953.* International Centre for Diffraction Data, Powder Diffraction File, Entry, 1996: p. 5.
219. R. Datta and R. Roy, *Reinvestigation of Order-Disorder in Gallate Spinels*. Journal of the American Ceramic Society, 1968. **51**(5): p. 297.
220. W. G. Lee, Y. Cho, and S. W. Kang, *Effect of Ionic Radius in Metal Nitrate on Pore Generation of Cellulose Acetate in Polymer Nanocomposite.* Polymers, 2020. **12**(4): p. 981.
221. J. C. Slater, *Atomic radii in crystals.* The Journal of Chemical Physics, 1964. **41**(10): p. 3199.
222. B. Zheng, J. Lian, L. Zhao, and Q. Jiang, *Optical and electrical properties of Sn-doped CdO thin films obtained by pulse laser deposition.* Vacuum, 2011. **85**(9): p. 861.
223. B. Streetman, *Solid State Electronic Devices (Prentice Hall, India,* 2000.
224. Y. Yang, S. Jin, J. E. Medvedeva, J. R. Ireland, A. W. Metz, J. Ni, M. C. Hersam, A. J. Freeman, and T. J. Marks, *CdO as the Archetypical Transparent Conducting Oxide. Systematics of Dopant Ionic Radius and Electronic Structure Effects on Charge Transport and Band Structure.* Journal of the American Chemical Society, 2005. **127**(24): p. 8796.
225. H. Li, J. Wang, H. Liu, C. Yang, H. Xu, X. Li, and H. Cui, *Sol–gel preparation of transparent zinc oxide films with highly preferential crystal orientation.* Vacuum, 2004. **77**(1): p. 57.
226. Z. Galazka, *β-Ga_2O_3 for wide-bandgap electronics and optoelectronics.* Semiconductor Science and Technology, 2018. **33**(11): p. 113001.
227. K. Karthik, S. Dhanuskodi, C. Gobinath, S. Prabukumar, and S. Sivaramakrishnan, *Multifunctional properties of CdO nanostructures Synthesised through microwave assisted hydrothermal method.* Materials Research Innovations, 2019. **23**(5): p. 310.
228. D. J. Seo, *Structural and optical properties of CdO films deposited by spray pyrolysis.* Journal of the Korean Physical Society, 2004. **45**(6): p. 1575.
229. Z. Jiang, Z. Wu, C. Ma, J. Deng, H. Zhang, Y. Xu, J. Ye, Z. Fang, G. Zhang, J. Kang, and T.-Y. Zhang, *P-type β-Ga_2O_3 metal-semiconductor-metal solar-blind photodetectors with extremely high responsivity and gain-bandwidth product.* Materials Today Physics, 2020. **14**: p. 100226.

230. E. Chikoidze, A. Fellous, A. Perez-Tomas, G. Sauthier, T. Tchelidze, C. Ton-That, T. T. Huynh, M. Phillips, S. Russell, M. Jennings, B. Berini, F. Jomard, and Y. Dumont, *P-type β-gallium oxide: A new perspective for power and optoelectronic devices.* Materials Today Physics, 2017. **3**: p. 118.
231. B. Karunagaran, P. Uthirakumar, S. Chung, S. Velumani, and E.-K. Suh, *TiO_2 thin film gas sensor for monitoring ammonia.* Materials Characterization, 2007. **58**(8-9): p. 680.
232. G. Korotcenkov, *Metal oxides for solid-state gas sensors: What determines our choice?* Materials Science and Engineering: B, 2007. **139**(1): p. 1.
233. A. Garde, *LPG and NH_3 Sensing Properties of SnO_2 Thick Film Resistors Prepared by Screen Printing Technique.* Sensors & Transducers, 2010. **122**(11): p. 128.
234. S. Vanalakar, G. Agawane, S. Shin, M. Suryawanshi, K. Gurav, K. Jeon, P. Patil, C. Jeong, J. Kim, and J. Kim, *A review on pulsed laser deposited CZTS thin films for solar cell applications.* Journal of Alloys and Compounds, 2015. **619**: p. 109.

الخلاصة

تم تحضير الأغشية الرقيقة للمركبات Ga_2O_3 و CdO و $CdGa_2O_4$ باستخدام تقنية الترسيب بالليزر النبضي ، وهي طريقة أثبتت كفاءتها في تحضير الأغشية الرقيقة. تم استخدام ليزر Nd-YAG بطاقة 500 ملي جول ، عدد النبضات (1000 نبضة) ، التردد (6 هرتز) ، الطول الموجي (1064 نانومتر) والضغط(10^{-4}mbar) للترسيب على ركائز من الكوارتز.

تم فحص التركيب البلوري للأغشية المحضرة بطريقة حيود الأشعة السينية (XRD) وأظهرت النتائج أن جميع الأغشية المحضرة متعددة التبلور في الطور المكعب لـ CdO و $CdGa_2O_4$ و monoclinic لـGa_2O_3 و هناك نقصان في الحجم البلوري للجسيمات النانوية ، وانخفاض في الإجهاد وكثافة الانخلاعات عند زيادة تركيز CdO و هذا مؤشر على تحسن الخصائص التركيبية للأغشية المحضرة. تمت دراسة الطبوغرافية السطحية للأغشية المحضرة باستخدام مجهر القوة الذرية (AFM) لقد لوحظ أن الحجم الحبيبي يتناقص مع زيادة تركيزCdO هناك أيضًا انخفاض في معدل خشونة السطح ومعدل الجذر التربيعي (RMS) عن طريق زيادة تركيزCdO . اما نتائج المجهر الالكتروني الماسح (FESEM) ومشتت الطاقة في التحليل الطيفي للأشعة السينية (EDX) ، اظهرت الصور أن شكل الحبيبات شبه كروي لجميع الأفلام. في حين أن الأغشية 25%wt, 0% and 50%wtهي شكل شبه كروي مع وجود ثقب مع زيادة تركيز أكسيد الكادميوم ، يمكن ملاحظة أن الثقوب الموجودة في الحبيبات تختفي وتتجمع لتشكل حبيبات بلورية أكثر كثافة

تمت دراسة الخواص البصرية للأغشية المحضرة بسمك (205 ± 5) نانومتر باستخدام قياسات النفاذية الضوئية في المنطقة الطيفية (200-900) نانومتر. لوحظ أن الانتقال المباشر المسموح به والزيادة في تركيز CdO تؤدي إلى انخفاض فجوة الطاقة الضوئية لأغشية Ga_2O_3 $_{(1-X)}$ $CdO_{(X)}$ من 4.19 eVإلى4.65eV وتم حساب الثوابت البصرية مثل معامل الانكسار ومعامل الخمود وثابت العزل الكهربائي لجميع الأغشية المحضرة.

تم دراسة الخواص الكهربائية مثل موصلية التيار المستمر وتأثير هول. أظهرت النتائج أن الأغشية المحضرة كانت من النوع p لـلعينات Ga_2O_3 و 25%wt تصبح من النوع n عند زيادة CdO وجد أن المقاومة والمقاومية تزداد مع زيادة درجة الحرارة للأغشية 0% و 25%wt و العكس صحيح للأغشية الأخرى. كما تقل الموصلية مع زيادة درجة الحرارة لأغشية 0% و 25%wt والعكس صحيح بالنسبة للأغشية الأخرى.

الخلاصة

تم قياسات خواص الاستشعار للأغشية الرقيقة لغازات NO_2 و NH_3 أن جميع العينات تعمل في درجة حرارة تشغيل الغرفة عندما يضاف CdO إلىGa_2O_3 ، والحساسية القصوى لمستشعر الغاز تحت الاختبار تصل إلى 60 جزء في المليون لـ NO_2 وهي حوالي 61.7٪ عند 300 درجة مئوية بالنسبة لمركب75%wt ، بينما يحتوي المركب بنسبة 50%wt على أقل حساسية بنسبة 0.8٪ تجاه NO_2 وعند استخدام NH_3 كغاز فحص ، يمكن أن تصل الحساسية القصوى لمستشعر الغاز إلى 200 جزء في المليون لـ NH_3 إلى 48.2٪ لـ Ga_2O_3 النقي ، وتكون درجة حرارة الاستشعار المثلى للمستشعر المركب حوالي (200-300) درجة مئوية . بالإضافة إلى نقصان زمن الاستجابة و زمن الاسترداد عند زيادة درجة الحرارة ، بمعنى آخر ، سرعة الاستجابة ة لغاز NO_2 (10.8 ثانية) لعينة 75%wt عند 250 درجة مئوية و (9 ثانية) لغاز NH_3 للعينة Ga_2O_3 النقي عند 250 درجة مئوية لغاز.

جمهورية العراق
وزارة التعليم العـالي والبحث العلـمي
جامـــعة بـــابـــل
كليـــة العلـوم للبنات
قســـم فيزيـــاء الليزر

تحضير و توصيف $Ga_2O_{3\,(1-X)}CdO_{(X)}$ ذات التراكيب النانوية باستخدام الترسيب بالليزر النبضي للتطبيقات التحسسية

أطروحة

مقدمة الى مجلس كلية العلوم للبنات في جامعة بابل

كجزء من متطلبات نيل درجة الدكتوراه فلسفة في العلوم/ فيزياء الليزر وتطبيقاته

من قبل

عقيل ابراهيم فارس

بكالوريوس في علوم الفيزياء (جامعة بابل - **2009**)
ماجستير في علوم الفيزياء (جامعة بابل - **2017**)

بأشراف

أ.م. د.جنان علي عبد
كلية العلوم للبنات/ قسم فيزياء الليزر

أ.د. فيصل علي مصطفى
كلية الحلة الجامعة / قسم تقنيات الاشعة والسونار

1442 هـ **2021 م**